NUMERICAL AND EXPERIMENTAL ANALYSIS OF INDENTATION

A THESIS SUBMITTED TO
THE GRADUATE SCHOOL OF NATURAL AND APPLIED SCIENCES
OF
MIDDLE EAST TECHNICAL UNIVERSITY

BY

ERGE KORAY

IN PARTIAL FULFILLMENT OF THE REQUIREMENTS
FOR
THE DEGREE OF MASTER OF SCIENCE
IN
MECHANICAL ENGINEERING

MARCH 2005

Approval of the Graduate School of Natural and Applied Sciences

_____

Prof. Dr. Canan Özgen
Director

I certify that this thesis satisfies all the requirements as a thesis for the degree of Master of Science.

_____

Prof. Dr. Kemal İder
Head of Department

This is to certify that we have read this thesis and that in our opinion it is fully adequate, in scope and quality, as a thesis for the degree of Master of Science.

_____

Prof. Dr. A. Erman Tekkaya
Supervisor

Examining Committee Members

Prof. Dr. Mehmet Çalışkan (METU, ME) _____

Prof. Dr. A. Erman Tekkaya (METU, ME) _____

Prof. Dr. Yalçın Mengi (METU, ES) _____

Asst. Prof. Dr. Ergin Tönük (METU, ME) _____

Asst. Prof. Dr. Merve Erdal (METU, ME) _____

I hereby declare that all information in this document has been obtained and presented in accordance with academic rules and ethical conduct. I also declare that, as required by these rules and conduct, I have fully cited and referenced all material and results that are not original to this work.

Erge Koray

ABSTRACT

NUMERICAL AND EXPERIMENTAL ANALYSIS OF INDENTATION

Koray, Erge

M.S., Department of Mechanical Engineering

Supervisor: Prof. Dr.-Ing. A. Erman Tekkaya

March 2005, 116 pages

Indentation tests are widely used with simultaneous measurements of indentation depth and force especially for determining material properties. In this study; numerical and experimental investigation of the force-indentation measurements is presented. For indentation tests on anisotropic metals, a novel indenter which is not self similar is used with three transducers to measure the displacements. It is seen that in order to have high repeatability and accuracy at the tests, workpiece and indenter parameters have crucial importance. These parameters in the indentations are analyzed by finite element methods. Ideal dimensions of the workpiece are determined. It is shown that plane strain conditions can only be achieved by embedded indentations. Effect of surface quality and clamping on repeatability are investigated. It is shown that surface treatments have significant effects on the results. Also it is seen that clamping increases the repeatability drastically. Moreover, indentation tests are conducted to verify the results of numerical simulations. Effect of anisotropy on the force-displacement curves is clearly observed.

Keywords: Indentation Test, Anisotropy, FEM, Compression Test

ÖZ

ÇUKURİZ BASMA YÖNTEMİNİN SAYISAL VE DENEYSEL ANALİZİ

Koray, Erge

Yüksek Lisans., Makina Mühendisliği Bölümü

Tez Yöneticisi: Prof. Dr.-Ing. A. Erman Tekkaya

Mart 2005, 116 sayfa

Çukuriz basma deneyleri, basma derinliğinin ve kuvvetin birlikte kaydedilmesiyle, malzeme özelliklerinin belirlenmesi amacıyla kullanılmaktadırlar. Bu çalışmada, kuvvet-basma ölçümleri sayısal ve deneysel olarak araştırılmıştır. Anizotropik metallerin çukuriz basmalarında, öz benzer olmayan yeni bir zımba, basma miktarının ölçülmesini sağlayan üç ilerleme ölçerle birlikte kullanılmıştır. Yüksek tekrarlanabilirlik ve hassasiyet elde edilebilmesinde numune ve zımba parametrelerinin büyük önemi olduğu görülmüştür. Bu parametreler sonlu elemanlar yöntemleriyle incelenmiştir. İdeal numune ölçüleri belirlenmiştir. Düzeysel genleme durumunun sağlanabilmesinin yalnızca gömülmüş basma yapılarak mümkün olabileceği gösterilmiştir. Yüzey kalitesinin ve sabitlemenin etkileri araştırılmıştır. Yüzey işlemlerinin belirgin etkileri gösterilmiştir. Numunelerin sabitlenmesinin, deneylerin tekrarlanabilirliğini büyük ölçüde arttırdığı gözlemlenmiştir. Ayrıca bu sonuçlar deneylerle kanıtlanmıştır. Anizotropinin kuvvet-ilerleme eğrilerine etkisi açıkca görülmüştür.

Anahtar Kelimeler: Çukuriz Basma Testi, Anizotropi, Sonlu Elemanlar Yöntemi, Basma Testi

To Sarp

ACKNOWLEDGEMENTS

I would like to express my deepest gratitude and appreciation to my supervisor Prof. Dr.-Ing. A. Erman Tekkaya, who inspired, encouraged and supported me for this study.

I would like to thank to my colleagues Nagihan Topcu, Prof. Dr.-Ing. Klaus Pöhlandt, Prof. Dr.-Ing. Reiner Kreibig, Dr.-Ing. Klaus Eberle, Mario Lindner, Michele D'Ottavio and Gian Francesco Ferraris whose help and guidance made great contribution to this work.

This study was carried out at METU by the sponsorship of TÜBİTAK. The support provided by TÜBİTAK is greatly acknowledged.

I am very grateful to Ömer Music and Volkan Güley for their help in preperation of specimens at ORS Bearing Company and to Burak Ay for his help in OSTİM.

My best wishes go to Femlab members; Mete Egemen, Muhsin Öcal, Ahmet Kurt, Kürşad Kayatürk, Halil Bil, Özgür Koçak, Bahadır Koçaker, Murat Özmen, Erkan Önder, Çağrı Kaya, Alper Güner and Koray Demir for enliving my life. I would like to thank my roommate Oya Okman for her patience and support.

The greatest thanks go to my family members; my parents Tarık and Didem, my sister Özge and my uncle Haluk for their endless support and trust throughout my education.

TABLE OF CONTENTS

APPENDICES

LIST OF TABLES

TABLE

LIST OF FIGURES

FIGURE

CHAPTER 1

INTRODUCTION

1.1 Introduction

Cold metal forming is an efficient metal forming process, in which greater stresses than a metal's elastic limit are used to form shapes with high production rates, very small amount of scrap material, and moreover with improved strength and reliability through work hardening and an uninterrupted grain flow. In general, customers prefer these products for their improved yield strengths and texture properties. However, it is not easy to predict the formed texture so the anisotropic properties of the product. There is a strong need in metal forming industry to obtain the yield loci of anisotropic materials as well as the material properties of parts before and after cold working with a reasonable effort and in a reasonable time. Especially by using more precise material data, achieving high accuracies by finite element simulations will be possible.

Usually, simple tension tests, compression tests or biaxial tests are made to estimate the anisotropy of the materials. Also some researchers determine the yield locus of these metals by means of modern methods of parameter identification based on force-displacement curves measured in indentation tests. Both testing and inverse analysis with indentation tests aim to obtain reliable knowledge of data that describes the plastic material behavior.

In this thesis, indentation testing, with a novel indenter, (Figure 1.1) in order to determine the anisotropic parameters by inverse analyses will be investigated.

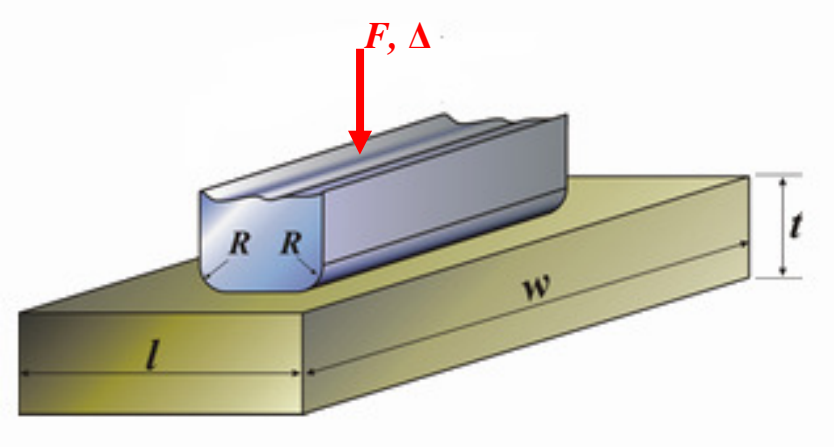

Figure 1.1 Indentation

1.2 Aim and Scope of the Study

To determine anisotropic yield locus by using indentation tests a new indenter which is not self similar is used (Figure 1.2). It is not self similar as it should collect large amount of data, needed for inverse parameter analysis, by passing through different stress-strain states. It is expected that in order to have high repeatability and accuracy at these tests, workpiece and indenter parameters have crucial importance.

In this study, it is aimed first to determine optimum values of these parameters to achieve higher repeatability and accuracy. For this purpose finite element analyses (FEA) are made. Also some other parameters affecting the force-displacement curves to be used in inverse analysis are examined by FEA. Results of these analyses are given in Chapter 4.

Finite element simulations of indentation are performed with isotropic material model with both two dimensional (plane strain) and three dimensional models.

Details of the models used in FEA and comparison of plane strain model and the three dimensional model will be given in Chapter 4.

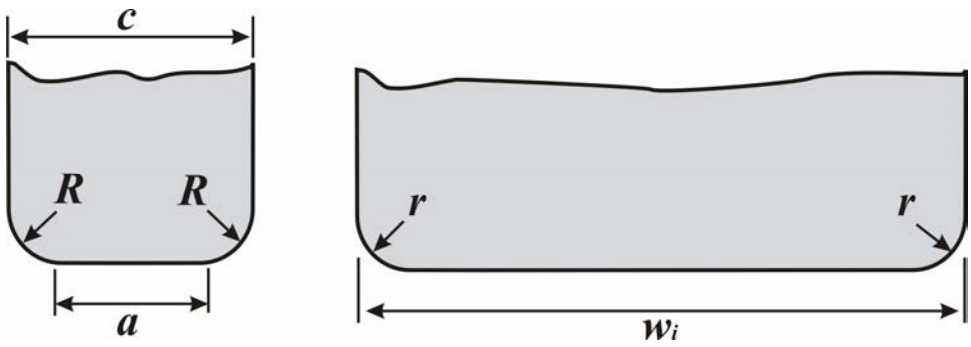

Figure 1.2 Novel indenter geometry

Experiments are made in order to verify finite element simulations and more importantly to obtain force-displacement curves to be used in inverse analysis. Indentation experiment results are given in Chapter 5.

To obtain the material properties of specimens used in experiments, compression tests are conducted. Results of the compression tests will be given in Chapter 6.

These experiment and simulation results are discussed in Chapter 7.

1.3 Joint Research Study and the Partners

This thesis is supported by TÜBİTAK (The Technical and Scientific Research Council of Turkey) and DFG (German Research Foundation) under the contract number MISAG-DFG-1.

Main aim of this joint research study is determining the initial anisotropic yield locus of the test material through inverse analysis of the force-displacement curves obtained in special indentation tests.

In this study, it is assumed that the initial anisotropy is orthogonal, the yield locus is quadratic and that no kinematic hardening exists. With these assumptions the six

independent anisotropy parameters characterizing plastic material behaviour can be deduced from three measured force-displacement curves during indentation on three mutually orthogonal planes by inverse methods. The inverse methods are based on semi-analytical sensitivity computations by means of forward finite element computations.

Thesis author worked in cooperation with two universities from Germany, Stuttgart University and Chemnitz Technical University and a colleague, Nagihan Topcu from Middle East Technical University throughout the study.

The research partners from each university are:

- Ankara / Middle East Technical University: Erge Koray, BSc., (Eng.)
  A. Erman Tekkaya, Prof.,
  Nagihan Topcu, BSc., (Eng.)
- Chemnitz / Chemnitz Technical University : Reiner Kreiβig, Prof.,
  Mario Lindner, Dipl.-Ing.
- Stuttgart / Stuttgart University: Michele D'Ottavio, Dipl.-Ing.
  Klaus Eberle, Dr.-Ing.
  Gian Francesco Ferraris, Ing.
  Bernd Kröplin, Prof.
  Klaus Pöhlandt, Prof.

The joint-research consists of three subgroups:

- **Stuttgart Subgroup (SG1):** *Design and Construction of the Experimental Set-Up and Numerical Optimization of the Global Geometry of the Indenters.* This research is conducted at the University of Stuttgart under the leadership of Prof. Pöhlandt. Main aim of this subgroup is to perform the design and construction of the experimental set-up to be used by Ankara Group.

- **Ankara Subgroup (SG2):** *Numerical Verification of the Experimental Set-Up and Conduction of Experiments.* This research is conducted at the Middle East Technical University under the leadership of Prof. Tekkaya. Here, the indenter manufacturing tolerances are determined by numerical simulation, optimization of the indenter and workpiece parameters are performed and the experiments are conducted.

- **Chemnitz Subgroup (SG3):**: *Parameter Identification by Using Semianalytical Sensitivities.* This research is conducted at the University of Chemnitz under the leadership of Prof. Kreiβig. The basic goal of this subgroup is the identification of the material parameters from the experimental indentation force versus indentation depth measurements.

The cooperation between the research partners can be seen in Figure 1.3. Stuttgart Subgroup designed and constructed the experimental set-up for Ankara Subgroup with its interaction. Furthermore, optimized indenter geometries are supplied to subgroups SG1 and SG3, in which the forward simulation of the indentation process is done.

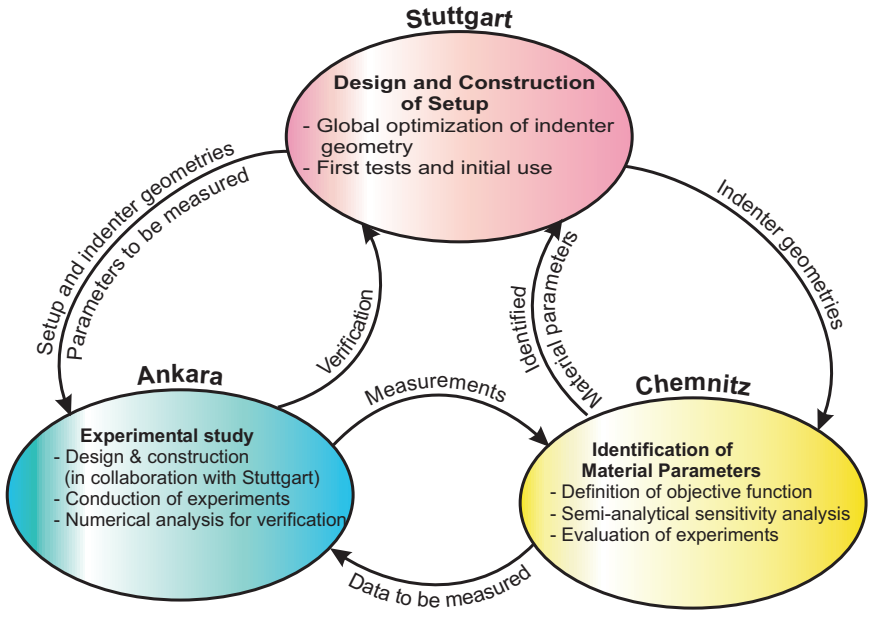

Figure 1.3 Interactions between the three subgroups

Subgroup SG2 supplies subgroups SG1 and SG3 with the measured test results (Figure 1.3). These also include error estimates based on finite element computations for given indenter and workpiece manufacturing tolerances. Subgroup SG3 supplies the two other subgroups with computed sensitivities and with possible modifications of the measurement procedure or even the set-up.

CHAPTER 2

LITERATURE SURVEY

In this chapter literature on various yield criteria are widely discussed. Their advantages and disadvantages are given. Also the mechanical parameters needed for each of them are presented.

Literature on mechanical tests like indentation test and compression test are discussed. From these, compression tests are extensively used for determining the mechanical parameters needed for the anisotropic yield criteria. Correction methods for compression tests are presented.

Literature on inverse analysis methods for parameter identification is also presented. Different inverse analysis applications are discussed.

2.1 Plastic Material Behaviour

In order to describe the plastic behaviour of a material in a general stress state, three elements are needed:

– a yield criterion expressing the relationship between the stress components at the moments when plastic yielding occurs,

– an associated flow rule expressing the relationship between the components of the strain-rate and stress tensors,

– a hardening rule describing the evaluation of the initial yield stress during the forming process [1].

In the following sections both isotropic and anisotropic yield criteria are discussed.

2.2 Yield Criteria

A material's state changes from elastic (recoverable) to elastic-plastic (partly permanent) when a certain stress, yield stress, is reached. A yield criterion, which is in the form of an implicit function ("yield function"):

$$\mathrm{f}(\sigma_{xx},\sigma_{yy},\sigma_{zz},\sigma_{xy},\sigma_{yz},\sigma_{xz},\sigma_Y)=0 \tag{2.1}$$

indicates for which combination of stress components this transition occurs. Here $\sigma_{xx},\sigma_{yy},\sigma_{zz},\sigma_{xy},\sigma_{yz},\sigma_{xz}$ are the stress components and σ_Y is the yield stress obtained from a simple test like tensile test or compression test. Eq. 2.1 can also be written like:

$$\mathrm{f}(\sigma_1,\sigma_2,\sigma_3,\sigma_Y)=0 \tag{2.2}$$

where $\sigma_1,\sigma_2,\sigma_3$ are the principal stresses. Such a relation is the mathematical description of a surface in the three dimensional space of the principal stresses usually called the "yield surface".

For incompressible materials it is in the form of a cylinder, whose cross section depends on the criterion used. All the points located inside of the surface are related to an elastic state of the material. The points on the surface are related to the plastic state. Points at the outside have no physical meaning.

In one dimension yielding occurs when the uniaxial stress reaches the yielding stress. However, in case of a multiaxial stress it is more difficult to define a criterion for the transition from elastic to the plastic state. This problem is solved

with phenomenological (approximating the experimental data by analytical functions) theories called yield criteria.

2.2.1 Isotropic Yield Criteria

In the following sections the most common isotropic yield criteria by Tresca and von Mises are discussed.

2.2.1.1 Tresca Yield Criterion

This criterion was proposed by Tresca in 1864 [2]. According to Tresca, yielding occurs when maximum shear stress $\tau_{\max}$ reaches a critical value.

$$\frac{\sigma_{\max} - \sigma_{\min}}{2} = k \tag{2.3}$$

where $\sigma_{\max}$ and $\sigma_{\min}$ are maximum and minimum principal stresses, respectively and k is the yield stress in shear. The yield stress k in shear is not independent of the yield stress σ_Y in uniaxial tension. To compute their relation, apply the Tresca criterion to uniaxial tension. For this case, $\sigma_1 \neq 0$ and $\sigma_2 = \sigma_3 = 0$. So it can be written that:

$$\tau_{\max} = \frac{\sigma_{\max} - \sigma_{\min}}{2} = \frac{\sigma_1 - 0}{2} = \frac{\sigma_1}{2} = k \tag{2.4}$$

From which it can be concluded that in uniaxial tension yielding occurs when $\sigma_1 = 2 \cdot k$, i.e. for the Tresca yield criterion:

$$k = \frac{\sigma_Y}{2} \tag{2.5}$$

Using Eq. 2.5, Tresca yield criterion can be written as:

$$\sigma_{\max} - \sigma_{\min} = \sigma_Y \tag{2.6}$$

Eq. 2.3 represents a hexagon in the plane of the principal stresses σ_1 and σ_2 (Figure 2.1).

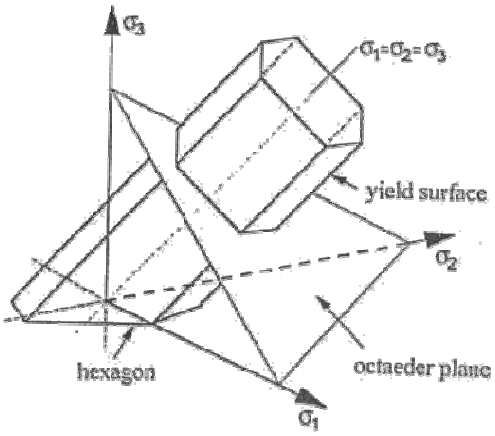

Figure 2.1 Tresca yield surface in stress space [1]

Tresca is a simple criterion which tends to be conservative in design point of view. However, it is not very accurate for some stress states, as it does not take the third principal stress into account. It is also a mathematical difficulty that the yield surface is not smooth.

2.2.1.2 von Mises Yield Criterion

This criterion was proposed by von Mises in 1913 [3] based on the observation that hydrostatic pressure cannot cause plastic deformation.

In terms of principal stresses, the von Mises criterion can be written as:

$$\frac{1}{2}\left[(\sigma_1-\sigma_2)^2+(\sigma_2-\sigma_3)^2+(\sigma_1-\sigma_3)^2\right]=\sigma_Y^2 \qquad (2.7)$$

von Mises criterion can also be written in a general way as follows:

$$\frac{1}{2}\left[(\sigma_x-\sigma_y)^2+(\sigma_y-\sigma_z)^2+(\sigma_z-\sigma_x)^2+3(\tau_{xy}^2+\tau_{yz}^2+\tau_{zx}^2)\right]=\sigma_Y^2 \qquad (2.8)$$

A physical interpretation of the von Mises rule shows that the left side of Eq. 2.8 is proportional to the energy which is stored in the elastically deformed material prior to yielding. This is the energy necessary for elastic volume change. The flow rule says that plastic flow starts when this elastic energy reaches a critical value. That is why the von Mises rule is also called the "distortion energy criterion".

von Mises yield criterion represents an ellipse in the plane of the principal stresses σ_1 and σ_2 (Figure 2.2).

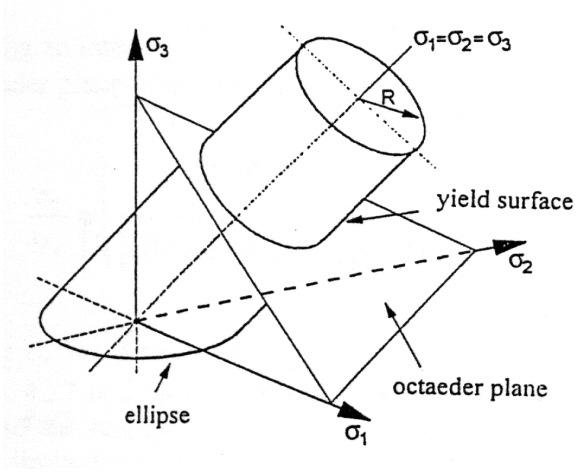

Figure 2.2 von Mises yield surface in the stress space [1]

2.2.2 Anisotropic Yield Criteria

Metals, especially sheet metals, show anisotropic material properties due to the crystallographic texture caused by the forming processes. Anisotropy means showing different behaviours in different directions. For example, elastic modulus, electrical conductivity and the index of refraction of the anisotropic materials may have different values in different directions.

From the standpoint of metal forming, elastic and plastic anisotropy as well as anisotropic strain hardening are important. The causes of mechanical anisotropy lie in crystal anisotropy combined with texture and in structure anisotropy, which is produced by the alignment of certain structure elements like grain boundaries [4].

The amount of plastic anisotropy in the sheet metals is measured by the anisotropy coefficient [5]

$$r = \frac{\varepsilon_2}{\varepsilon_3} \tag{2.9}$$

where ε_2 and ε_3 are the strains in the width and thickness directions respectively. These strains are obtained by standard tensile tests. As *r* depends on the direction, the normal anisotropy can be obtained from the equation

$$r_n = \frac{r_0 + 2 \cdot r_{45} + r_{90}}{4} \tag{2.10}$$

after determining the *r* values in three different directions.

There is a variety of yield criteria, which can express the yield conditions for anisotropic materials. In the following sections some of these are discussed.

2.2.2.1 Hill's Quadratic Yield Criteria (Hill 1948)

In 1948 Hill proposed a yield criterion for anisotropic materials [6]. Although in the following fifty years, more accurate yield criteria are introduced, this criterion became one of the most popular criteria for steel type of metals because of its simplicity and easy implementation to FEM codes.

This criterion is based on the von Mises' isotropic yield criterion (Eq. 2.7). In this model, material is supposed to have anisotropy with three orthogonal symmetry planes.

The yield criterion can be expressed in the following form:

$$\begin{aligned} 2f(\sigma_{ij}) \equiv\ & F(\sigma_y - \sigma_z)^2 + G(\sigma_z - \sigma_x)^2 + H(\sigma_x - \sigma_y)^2 \\ & + 2L\tau_{yz}^2 + 2M\tau_{zx}^2 + 2N\tau_{xy}^2 = 1 \end{aligned} \tag{2.11}$$

Here f is the yield function; F, G, H, L, M and N are constants specific to the anisotropy state of material, and x, y, z are the principal anisotropic axes. It must be noted that for $F=G=H$ and $L=M=N=3F$, Eq. 2.11 reduces to von Mises criterion. In the case of sheet metals x is usually parallel to the rolling direction, y in transverse and z in normal direction.

If the tensile yield stresses in the principal anisotropy directions are denoted by X, Y and Z, it can easily be shown that

$$\frac{1}{X^2} = G + H; \quad \frac{1}{Y^2} = H + F; \quad \frac{1}{Z^2} = F + G \tag{2.12}$$

From this equation, by simple gauss elimination, the coefficients F, G, and H are obtained as functions of the yield stresses in orthogonal directions:

$$F = \frac{1}{2}\left(\frac{1}{Y^2} + \frac{1}{Z^2} - \frac{1}{X^2}\right); \; G = \frac{1}{2}\left(\frac{1}{Z^2} + \frac{1}{X^2} - \frac{1}{Y^2}\right); \; H = \frac{1}{2}\left(\frac{1}{X^2} + \frac{1}{Y^2} - \frac{1}{Z^2}\right) \tag{2.13}$$

If R, S and T are the shear yield stresses associated to the same directions, then

$$L = \frac{1}{2} \cdot \frac{1}{R^2}; \; M = \frac{1}{2} \cdot \frac{1}{S^2}; \; N = \frac{1}{2} \cdot \frac{1}{T^2} \tag{2.14}$$

As a consequence, in order to give a complete description of the anisotropy of the material, six independent yield stresses (X, Y, Z, R, S and T) have to be known as the orientation of the principal anisotropy axes.

For sheet metals, if the principal directions of the stress tensor are coincident with the anisotropic axes ($\sigma_x = \sigma_1, \sigma_y = \sigma_2, \tau_{xy} = 0$) Eq. 2.11 can be written as:

$$\sigma_1^2 - \frac{2r_0}{1+r_0}\sigma_1\sigma_2 + \frac{r_0(1+r_{90})}{r_{90}(1+r_0)}\sigma_2^2 = \sigma_0^2 \tag{2.15}$$

where $\sigma_0 = X$.

This is a simple criterion which requires few tests to determine the coefficients. Three parameters are enough. However, this yield function is only able to describe the plane stress yield locus as a more or less stretched ellipse. This yield locus shape is very often inconsistent with experimental yield loci or those obtained from polycrystal calculations, especially for aluminium alloys. Another important drawback is the failure of Hill's yield criterion in describing the so-called 'anomalous behaviour' often observed in aluminium alloy sheets.

2.2.2.2 Other Anisotropic Yield Criterion

Because of the problems of Hill's quadratic yield function, several scientists have proposed improved yield functions for anisotropic materials. Hill himself proposed several improved non-quadratic yield criteria to overcome the mentioned disadvantages of his classical theory [7 – 9].

Another important research direction in the field of yield function development was initiated by Hosford [10], who introduced a non-quadratic isotropic yield function based on the results of his polycrystal calculations. Hosford's equation was later extended by Barlat et al. [11 – 13], who extended the yield criterion with respect to anisotropy and shear stresses. Later on, Barlat developed a six-component yield function derived from Hosford's yield function by using a linear transformation operating as a weighting of the Cauchy stress tensor [13]. Karafillis and Boyce [14] have generalized the idea of linear stress transformation and suggested a yield function consisting of the sum of two convex functions. Banabic et al. [15 – 19] extended the plane stress yield function introduced by Barlat and Lian [12]. Recently, Barlat et al. [20] extended the concept of linear stress transformation and introduced two linear stress transformations in their new yield criterion.

During the last two decades, many other yield functions have been developed in order to improve agreement with experimental results. A selection is given in the following: Bassani [21] has introduced a non-quadratic yield criterion; Gotoh [22] developed a fourth-degree polynomial yield function, Budiansky [23] suggested a yield function based on a parametric expression in polar coordinates, Cazacu and

Barlat [24] developed a yield function by introducing the so-called generalized invariants in their yield function.

2.2.3 Conclusions about the Yield Criterion

It can be concluded that for isotropic materials von Mises criterion is the most suitable one. However for the anisotropic materials it is hard to select one criterion as all of the mentioned yield criteria are being used.

While selecting an anisotropic yield criteria, mechanical test opportunities the researcher has is very important. Table 2.1 shows the tests needed for some of the criteria. First decision should be if biaxial yield stress (σ_b) can be determined which requires a special setup. Without determining the biaxial yield stress, Hill 1948 yield criterion can be used for simple predictions of the yielding. However it is not suitable for aluminium alloys. For better results Hill 1990, Barlat 1996 and Karafillis - Boyce yield criteria can be used. These can also be used for aluminium alloys.

Finally, yield criteria implemented in different finite element analysis programs can be seen in Table 2.2. It can be concluded that Hill 1948 and Hill 1990 are the most common anisotropic yield criteria used in the commercial programs.

2.3 Indentation Tests

Indentation testing with simultaneous recording of penetration and force is similar to the hardness test which usually uses spherical (known as Brinell or Rockwell) or a square like (known as Vickers) indenters (Figure 2.3). Geometries and imprints of these indenters can be seen in Figure 2.4. However, hardness is the instantaneous response to the indentation with a given constant load. Therefore, by indentation with simultaneous recording (also called impression testing) more information can be obtained.

Table 2.1 Experimental parameters required for anisotropic yield criteria [25]

Yield Criterion	σ_0	σ_{45}	σ_{90}	σ_b	k	r_0	r_{45}	r_{90}
Hill 1948	x					x		x
Hill 1979	x			x		x		
Hill 1990	x	x	x	x	x		x	
Hill 1993	x		x	x		x		x
Hosford 1979	x					x		x
Barlat - Lian 1989	x				x	x		x
Barlat 1991	4 parameters							
Karafillis - Boyce	6 parameters							
Barlat 1994	6 parameters							
Barlat 1996	x	x	x	x		x	x	x

Table 2.2 Yield criteria implemented in FEA software [25]

Software	von Mises	Hill 1948	Hill 1990	Barlat 1991	Barlat 1996	Karafillis - Boyce
ABAQUS	x	x	x	x	x	x
AUTOFORM	x	x	x			
DYNA-3D	x	x	x	x		x
MARC	x	x				
OPTRIS	x	x		x		
PAM-STAMP	x	x	x	x		
SIMEX	x	x	x			
STAM-PACK	x	x	x			

In the indentation tests, deformation zone is very small and the small specimens can be used. These advantages make indentation tests superior to conventional tests like tension tests and compression tests in special applications like surface mechanical characterizations. However, this testing is an empirical method that its results must be compared with the conventional test results like the flow curves obtained.

Knoop hardness testing is similar to the indentation testing that will be analyzed in this thesis. The knoop indenter has one long and one short diagonal that have approximately the ratio of 7:1. This results in a plane strain state in the deformation

zone. The inverse analysis program, developed by the research partners in Chemnitz, that will make anisotropy parameter identifications has also an algorithm to work with force displacement curves obtained from plane strain indentations.

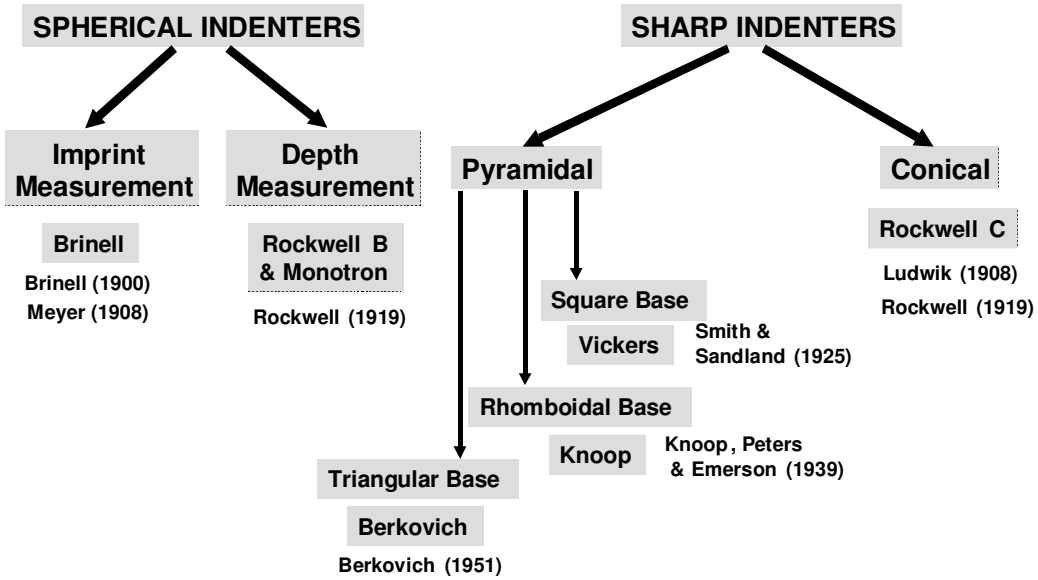

Figure 2.3 Various indenter geometries and the hardness tests they are used in

There has been many researches made in order to measure different material properties of different materials using various indenter geometries. Tabor [26 - 27] explained that there is a close relationship between the flow curves and the hardness measurements. Furthermore, he found that for ductile metals:

$$Hn = 3 \cdot \tilde{\sigma} \tag{2.16}$$

Where Hn is the hardness in the unit of stress and $\tilde{\sigma}$ is the uniaxial flow stress [27]. In his work, Tabor, covered the basics of the indentation tests. Later Tabor's study is further improved by Tekkaya [28 - 30]. Tekkaya analyzed Tabor's experiments by finite element methods and developed correlations for the relationship between the Vickers hardness values and yield strengths. His studies improved the common models' 25% sensitivity to 3%.

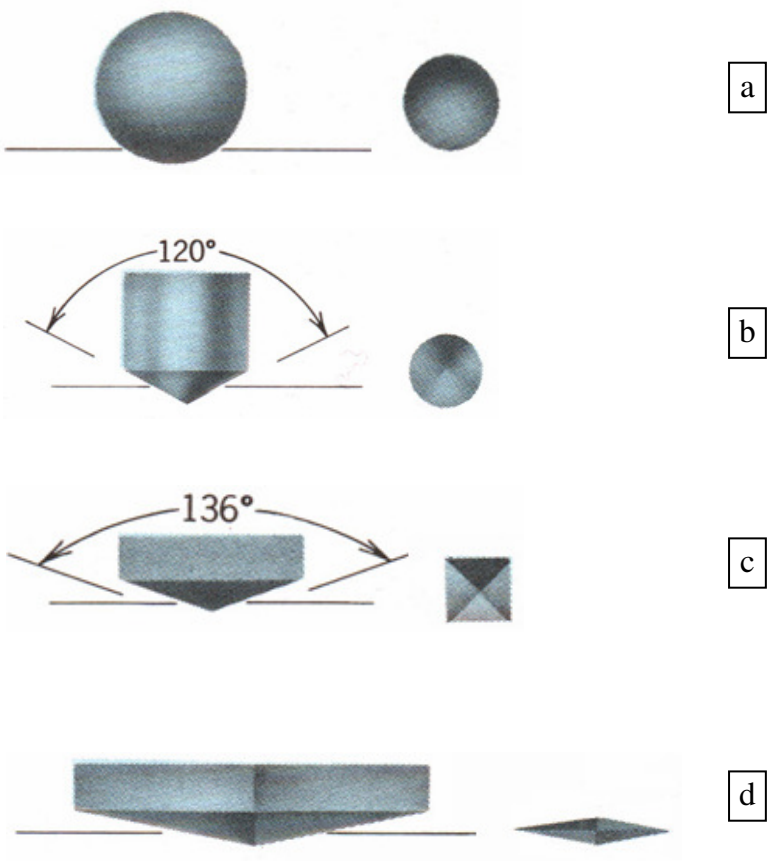

Figure 2.4 Sketches of indenter geometries and their imprints **a)** Spherical, **b)** Conical, **c)** Square Based Pyramidal, **d)** Rhomboidal Based Pyramidal

Recent researches include finite element analysis of indentation and some analytic analysis. In 1996, Chang et al. [31] measured various mechanical properties like flow stress, strength, elastic modulus, strain hardening exponent and strain rate sensitivity of polypropylene copolymer from the force-displacement curves obtained from indentations using a flat indenter (Figure 2.5). Flow curves obtained from indentation tests are compared with the flow curves obtained compression tests. It is seen that they are identical (Figure 2.6 (a)). The effect of diameter is investigated. It is found that diameter of the flat indenter does not effect true stress against normalized displacement curves (Figure 2.6 (b)).

Taljat et al. [32] analyzed spherical indentation using a commercial finite element program. At end of finite element analysis, some equations that relate flow

propertied to the indentation parameters are developed. Effect of indenter diameter is also analyzed and the importance of measuring the correct diameter is emphasized. Furthermore, in some of the analysis, indenter is also modelled as an elastic body. Although the indenter's elastic modulus is taken to be at least three times higher than the elastic modulus of the material, a significant difference in force-displacement curves, obtained from finite element analysis results and experimental results, is observed.

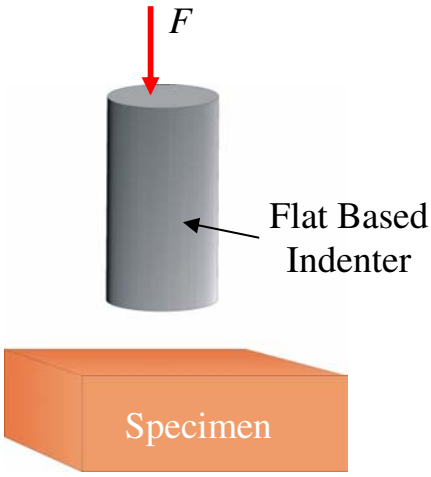

Figure 2.5 Sketch of indentation with a flat based indenter

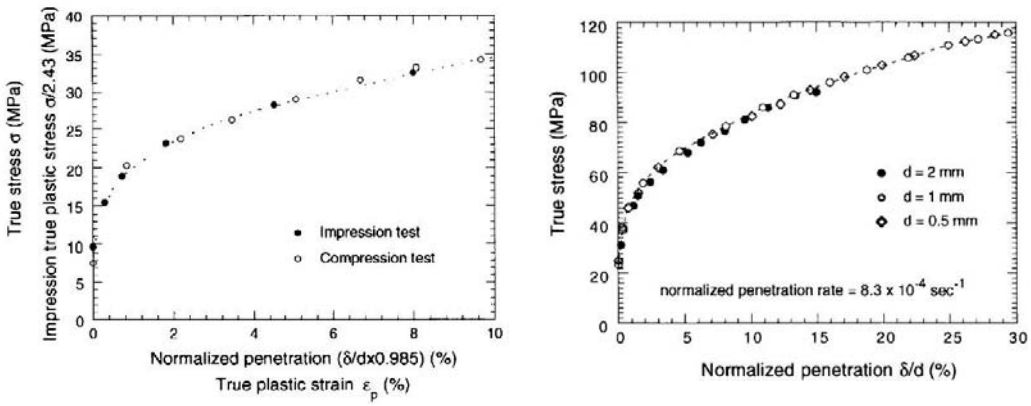

(a) **(b)**

Figure 2.6 a) Comparison of flow curves obtained from indentation tests and compression tests, **b)** effect of diameter [32]

In 2001, Riccardi et al. [33] measured the yield and ultimate tensile stresses by making indentation test with a flat indenter. In the study small diameter (1 mm) indenters are used in order to reduce the volume of material used in the test. For this purpose also 0.8 and 0.7 mm diameter indenters are tested and they gave identical results with the 1 mm diameter indenter. It is proved that this small diameter flat indenter test can be applied to irradiated or in service materials and also to metal welds in order to determine mechanical properties.

Scibetta et al. analyzed the availability of making indentation tests using a flat punch in order to obtain tensile properties [34]. An original method is developed, which enables to estimate the ultimate tensile strength and the yield strength from the indentation test. It is seen that main effect of radius of the flat indenter on the results is the reduction of repeatability. Also flat and spherical indenters are compared and seen that elastic part is more easily figured out with flat indenters (Figure 2.7).

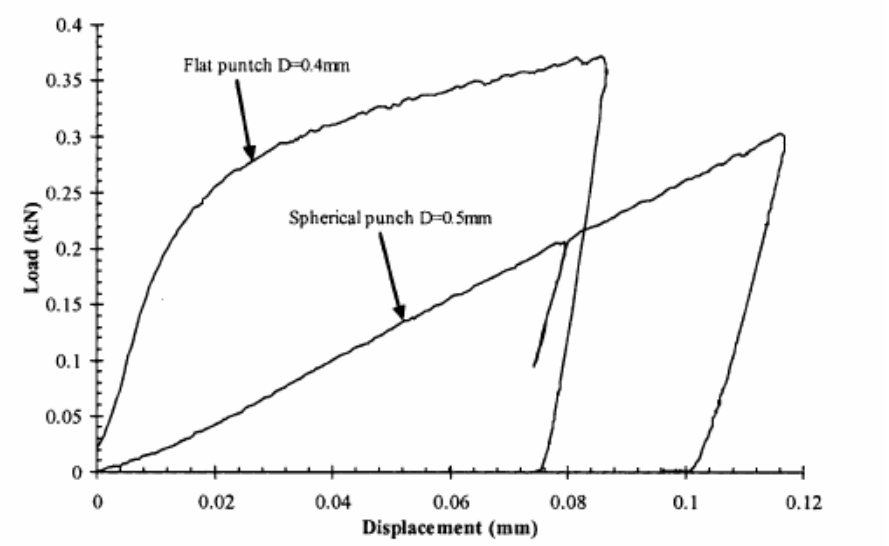

Figure 2.7 Comparison of flat and spherical indenters [34]

As the deformation zone is localized, indentation tests can be used to analyze thin films with small penetrations. In the last decade, as the testing instruments has enabled depths of indentation to be measured in sub nanometer resolution,

researches on material characterization of thin films have attracted a high interest. Results of nanoindentation tests provide information on the elastic modulus, hardness, strain-hardening, cracking, phase transformations, creep, fracture toughness, and energy absorption. Since the scale of deformation is very small, the technique is applicable to thin surface films and surface modified layers.

In 2002, Fischer-Cribbs, explained the basics of nanoindentation testing in his book "Nanoindentation" [35]. Besides identifying the methodology of the test and supplying examples, Fischer-Cribbs also emphasizes the factors affecting the nanoindentation. Surface roughness, initial penetration, set-up compliance and specimen preparation effects are analyzed. It is seen that initial penetration and the instrument compliance must be corrected. Surface roughness is also very important for the cases where the contact area is derived from the indentation depth. So the asperity heights and their distribution on the surface must be determined and roughness effect must be corrected.

Yang found that specimen thickness can not be ignored in indentation tests especially for thin films [36]. He has derived an analytical solution of the force-displacement curves for indentation of an elastic layer by a flat indenter. It is found that contact force is inversely proportional to the film thickness. This study is improved with this thesis as the effect of specimen thickness on force displacement curves in elastic-plastic indentation tests is determined. Also in his study, Yang used frictionless contact. In this thesis effect of friction is analyzed in detail.

Fischer-Cripps has conducted nanoindentation tests on functionally graded materials (FGMs), whose elastic moduli change with the depth from the surface, in order to obtain elastic modulus and hardness [37]. It is seen that, for FGMs, at larger depths the calculated and expected moduli are significantly different because of the conventional nanoindentation analysis methods. That makes it clear that there is a need for a consistent theoretical model for FGMs that can also be used for indentation tests.

2.4 Compression Tests

While designing tools and machines, the designer has to know the forces that can be applied to the system, the stresses caused by these forces and the resulting deformations. When metal forming operations are considered, plastic deformations are desired that the designer should know the relationship between the flow stresses and the plastic strains.

There are several methods for determining this relationship. Compression test, tension test, torsion test, bulging test are the most commonly used ones. The choice of the testing method depends on the material to be investigated and the desired plastic strain amounts.

If the flow stresses are needed just for small strain values tension tests are sufficient. Compression tests are chosen as high plastic strains can be reached by them. Moreover the samples and the tools are simple in geometry and the test itself is very simple. However, main problem of the compression test is the friction at the contact surfaces which causes inhomogeneous deformation of the specimen, e.g. bulging.

Compression test can be defined as the upsetting of a prismatic solid (e.g. circular, rectangular) between two parallel surfaces (Figure 2.8). These parallel dies might be lubricated.

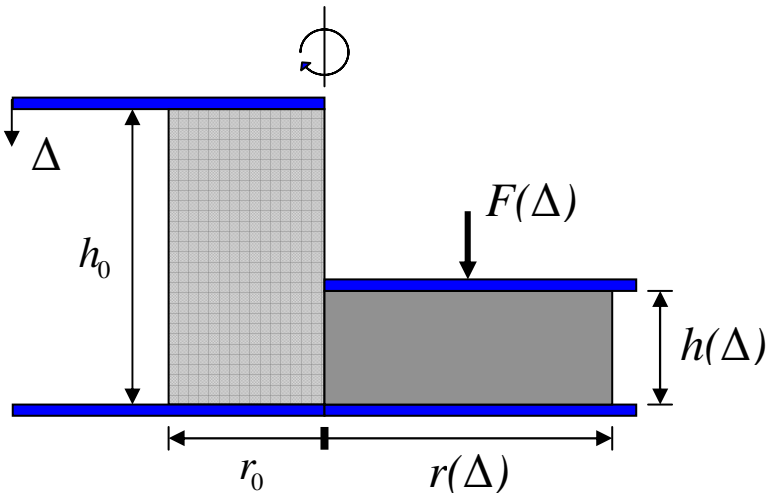

Figure 2.8 Schematic representation of compression test.

The strain is obtained using the equation

$$\varepsilon(\Delta) = \ln \frac{h(\Delta)}{h_0} \tag{2.17}$$

where $h(\Delta)$ is the actual height of the specimen at the force $F(\Delta)$. Also $h(\Delta)$ can be written as:

$$h(\Delta) = h_0 - \Delta \tag{2.18}$$

where Δ is the displacement of the upper die.

Equivalent strain is always positive so it is the negative of the strain calculated by Eq. 2.17:

$$\bar{\varepsilon}(\Delta) = -\varepsilon(\Delta) = \ln \frac{h_0}{h(\Delta)} \tag{2.19}$$

True stress value can be determined by dividing the force by the actual area:

$$\sigma_f(\Delta) = \frac{F(\Delta)}{A(\Delta)} \tag{2.20}$$

where A(Δ) can be expressed as:

$$A(\Delta) = \frac{A_0 \cdot h_0}{h(\Delta)} \tag{2.21}$$

from the volume constancy.

At this point the yield stress can be determined from the true stress-strain graph. The point where the linear part of the stress-strain curve ends is called the proportionality limit and this point shows the transition from the elastic deformations to plastic deformations. Another method to determine the yielding is constructing a line that passes through 0.002 total strain, and whose slope is equal

to elastic modulus. The point where this line intersects the stress-strain curve is accepted as the yielding point by this convention (Figure 2.9).

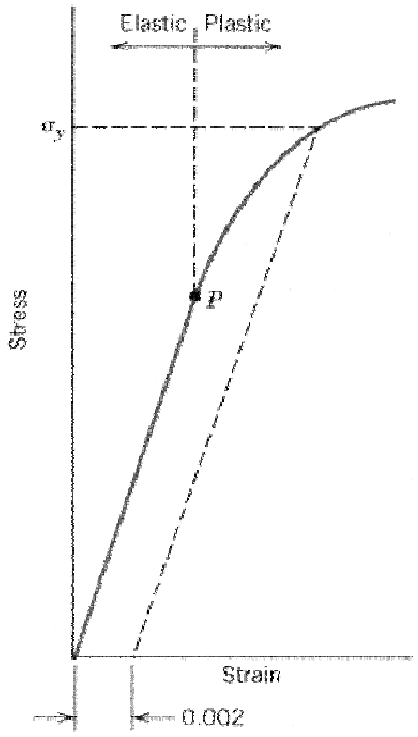

Figure 2.9 Determination of the yielding point [38]

In order to extract plastic strains from Eq. 2.19, elastic strains must be subtracted from the equivalent strain.

$$\varepsilon_{plastic}(\Delta) = \bar{\varepsilon}(\Delta) - \frac{\sigma(\Delta)}{E} \tag{2.19}$$

where the σ(Δ) values start from the yielding stress.

2.4.1 Effect of Friction

The most important problem of compression tests, while determining the flow curves, is the friction between de specimen and the dies. The friction has mainly two effects:

- It causes barrelling. If this happens, the area increase is not same throughout the specimen height. By this way error is allocated in the area calculations while determining the true stresses

- Forces needed for deforming the specimen are also affected by the presence of friction as additional force is needed for the flow of material on the specimen-die interface.

2.5 Inverse Analysis for Parameter Identification

Characterization of materials requires conducting laboratory tests in various strain, strain rate or temperatures that represents the actual cases. Moreover these tests must be simple enough. However, these tests are usually inhomogeneous that it is difficult to interpret them.

In the last decade, finite element methods have been started to be used in identification algorithms with high efficiencies to estimate the material responses to certain boundary conditions.

The finite element simulations are used as a part of an optimization algorithm, so that the material parameters are optimized and these parameters are the input data of the finite element program. Then, the results are checked if the measured responses are obtained. If the results are not similar to the measured response, the inputs (material parameters) are changed and the new ones are input to the FE program. This scheme goes on until the calculated results are close enough to the desired results. This is checked with the objective function, which is tried to be minimized.

For minimizing the objective function, gradient of it must be found. The gradient can be calculated by either finite difference based sensitivity analysis or by using direct differentiation method.

Ghouati et al. proposed a differentiation scheme that combined an optimization algorithm with FEM [39]. The algorithm is based on a Levenberg-Marquardt method. Using this algorithm, the material parameters used in the FE program are tuned until the FE results converge to the observed ones. The scheme is applied in order to calculate the anisotropic elasto-plastic behaviour for aluminium alloys by performing simple tension tests. The approach is also applied to the deep drawing tests. In the identifications, parameters converged at a high speed (Figure 2.10).

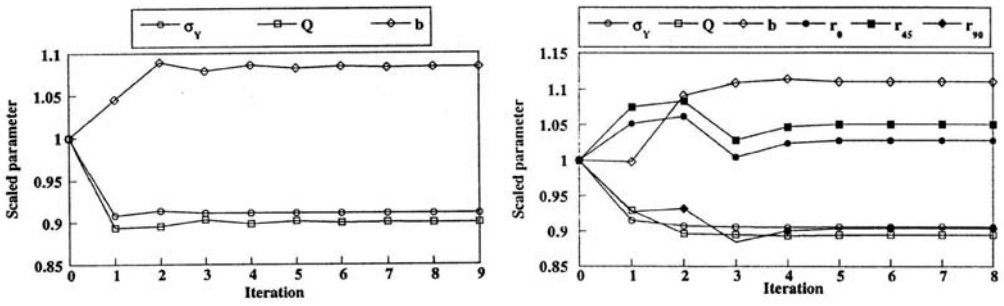

Figure 2.10 Convergence of parameters for **a)** isotropic, **b)** anisotropic cases [39]

Khalfallah et al. presented an inverse identification scheme for determining anisotropic parameters from an inhomogeneous test (plane tensile test) [40]. In this study, four different anisotropic models are used and parameters for each of them are identified. It is seen that using an orthotropic quadratic flow rule is sufficient for identifying under non-associated flow rule assumptions. Also preliminary researches have been done by implementing Barlat yield function into the FE package and satisfactory results have been obtained.

Sasaki et al. has developed a measurement system to investigate the anisotropic mechanical properties of thin films [41]. The approach combines optimization of FEM with nanoindentation tests using spherical indenters. The force displacement curves from the elastic indentation are compared with FE results and then the assumed material properties are modified according to this comparison. In this approach, testing of one sample is enough as the mechanical properties in surface plane are assumed to be isotropic. Just E_1, υ_{12} and E_2, υ_{22} are identified, which are elastic moduli and poisson ratios in thickness direction and on surface plane,

respectively. These tests are conducted on thin Al film on a Si substrate (Figure 2.11). The identified parameters are also verified by X-ray diffraction.

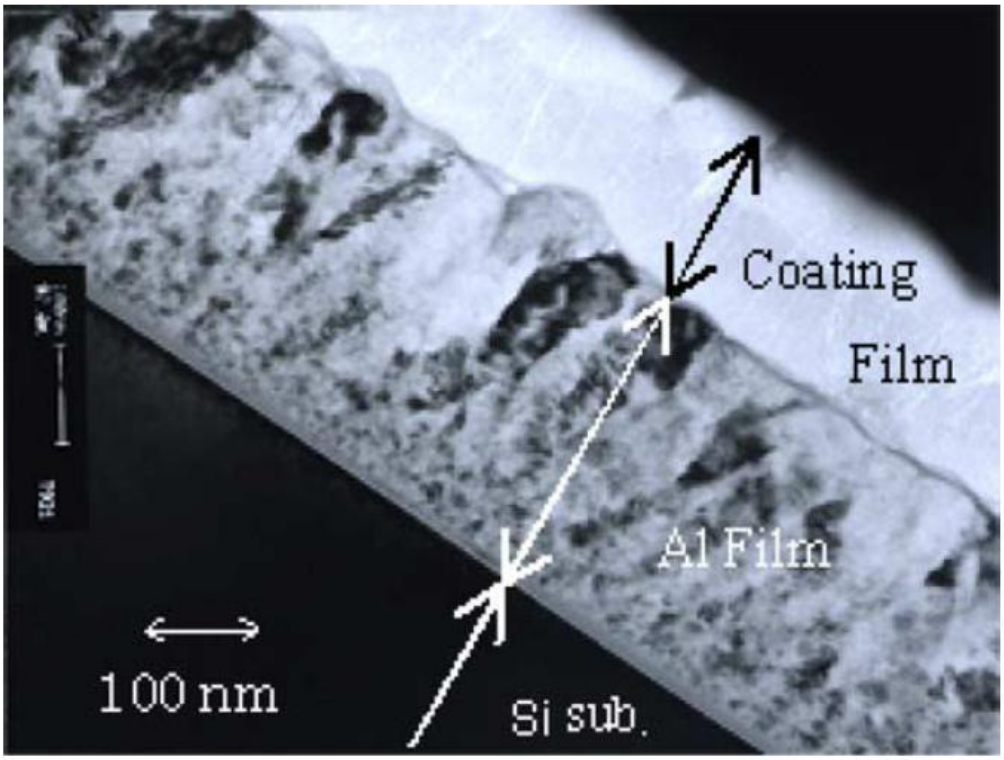

Figure 2.11 cross sectional view of the Al film on Si substrate [41]

CHAPTER 3

EXPERIMENTAL SETUP

In this chapter experimental setup is introduced. The experimental setup consists of three parts:

- Press
- Measurement System
- Indenter

These parts will be explained in the following sections.

3.1 Press

In the experiments Zwick Z020 press is used (Figure 3.1). This is a mechanical press that works on the powerscrews mounted at two sides. It has a maximum capacity of 2 tons. It is controlled by a computer via its own testing program. The press can be used for tensile tests, compression tests and also hysterisis tests. Through the program, the indentation speed, load removal speed, maximum indentation (either by defining maximum load or maximum speed), etc. can be defined. It is possible to direct the press move by 1 μm accuracy.

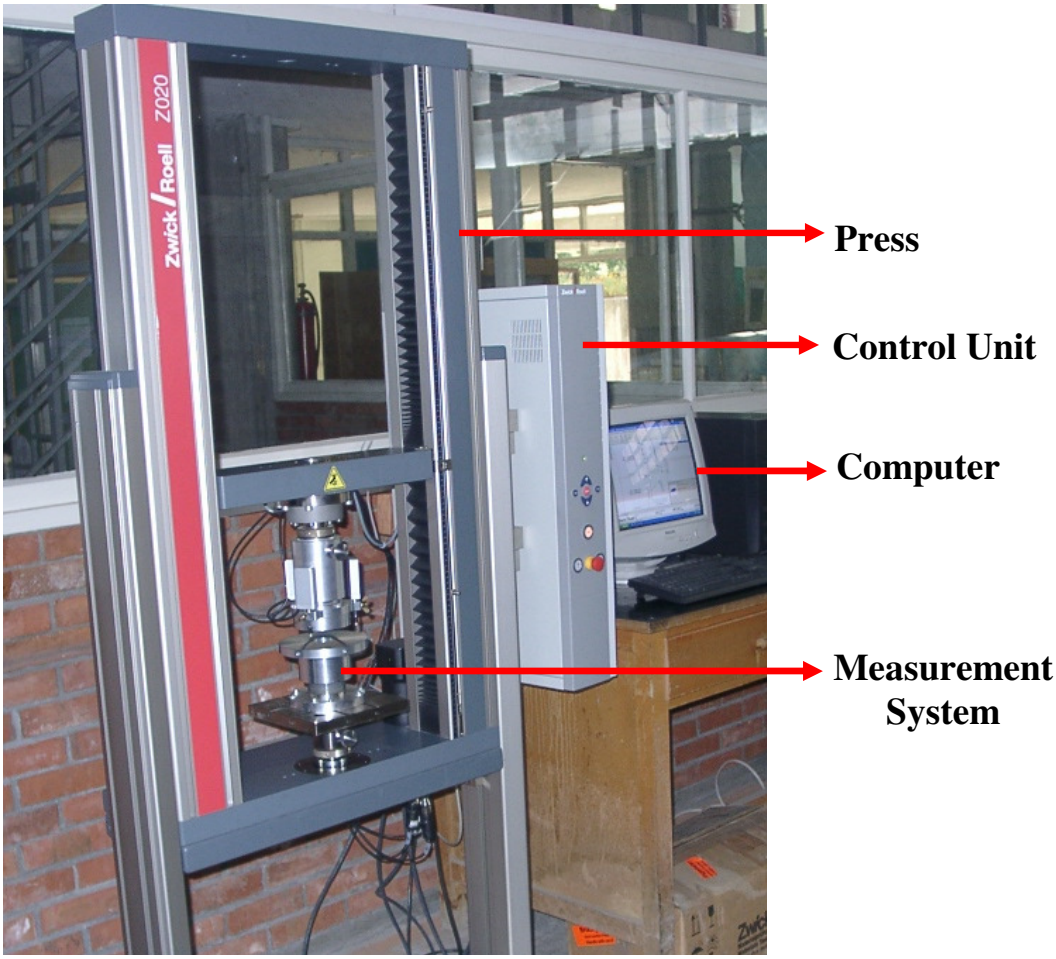

Figure 3.1 Press and the controlling units

3.2 Measurement System

Measurement system used in the experiments is designed and manufactured at the Stuttgart University in Germany by the research partners in SG1. Main aim of this system is measuring the depth of indentation accurately and with high repeatability. In this sense, first decision is whether to use one displacement transducer or more to measure the displacement of the indenter. As measurements are in a very small scale and results can be affected by every unexpected reaction of the system, it is decided to use three transducers 120^{o} apart from each other (Figure 3.2). During the indentations, the measured displacements from each transducer are summed up and

averaged. By this way; tilting of the system, which might occur because of several reasons like unparallel lowering of the press or inclined indentation, are eliminated.

In the experiments, Heidenhain MT1201 transducers are used (Figure 3.3). They have the nominal length of 12 mm, so maximum depth of indentation is limited by this value. In the transducers, there is a ball guided plunger. Accuracy of the transducers is ±0.2 µm.

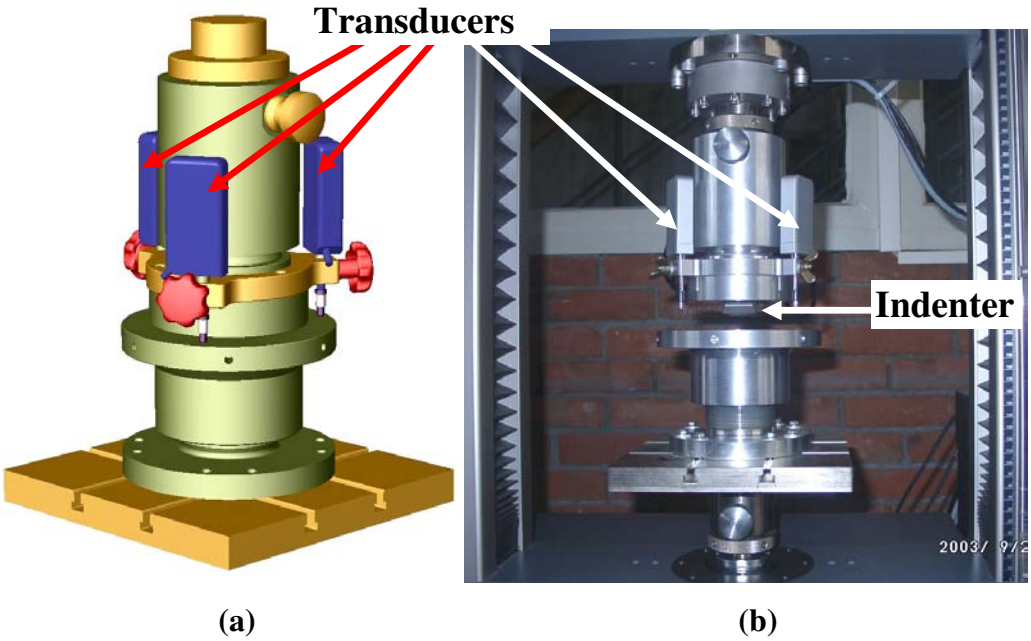

(a) **(b)**

Figure 3.2 Measurement system: **(a)** CAD drawing **(b)** actual picture

Figure 3.3 Displacement transducer

In order to increase the accuracy of the results, the transducers are placed out of the force path. Moreover the parts in the force path are made by steel and hardened steel so that the structural deformations of the system are minimized and plastic deformations of these parts are eliminated. However, there are still elastic deformations of the press and the other steel parts that can influence the results.

In the system, specimens are placed on the anvil and then fixed by the reference plate that moves on the screwed lower support (Figure 3.4). Top surface of this plate works as the reference surface for the transducers.

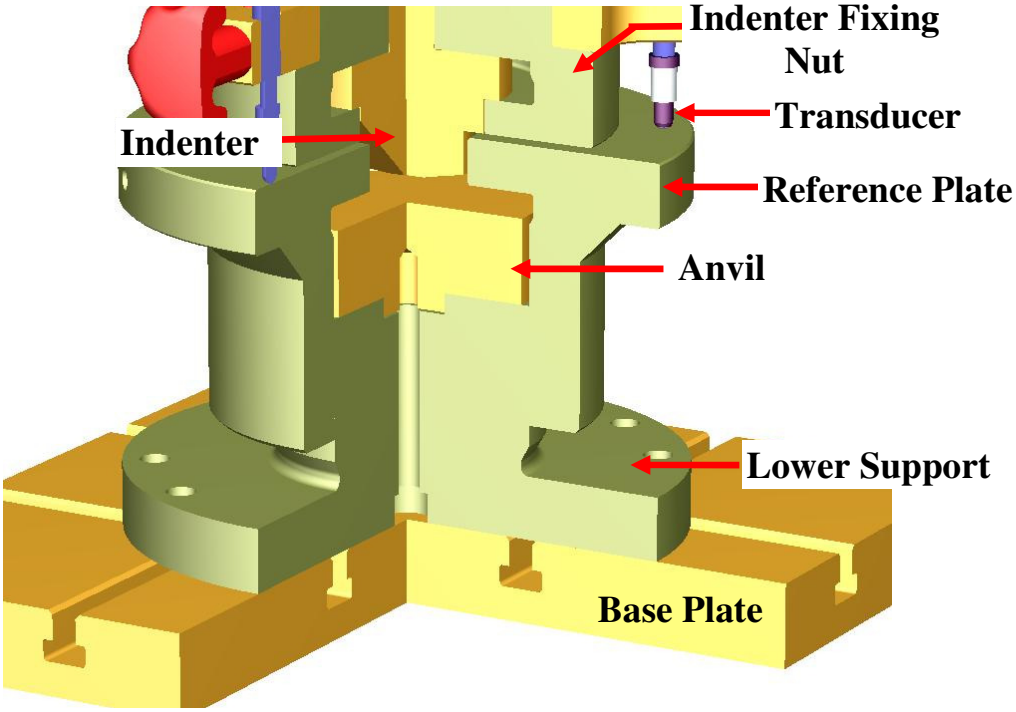

Figure 3.4 Sectional view of the measurement system

3.3 Indenter

Indenters used in the experiments are designed at the Stuttgart University and manufactured by Mössner Company in Germany (Figure 3.5). The indentation is made by the diamond part at the center of the indenter. This diamond part is glued to a hardened steel part and this hardened steel part is embedded in a steel casing

(Figure 3.6). Indenter geometry can be seen in Figures 3.7 and 3.8. Height of the indenter can be adjusted by putting rings (1 mm thick) between the indenter and the indenter fixing nut. Indentation speed is selected to be 1 mm/min.

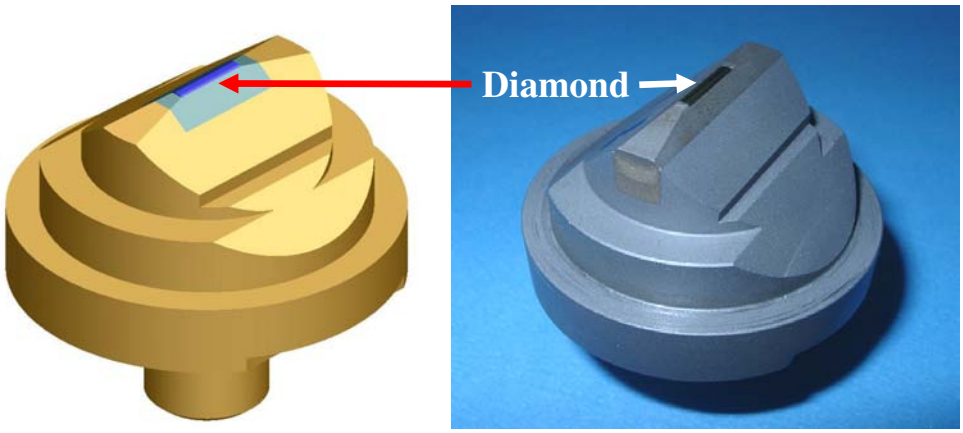

(a) **(b)**

Figure 3.5 Indenter **(a)** CAD drawing, **(b)** actual picture

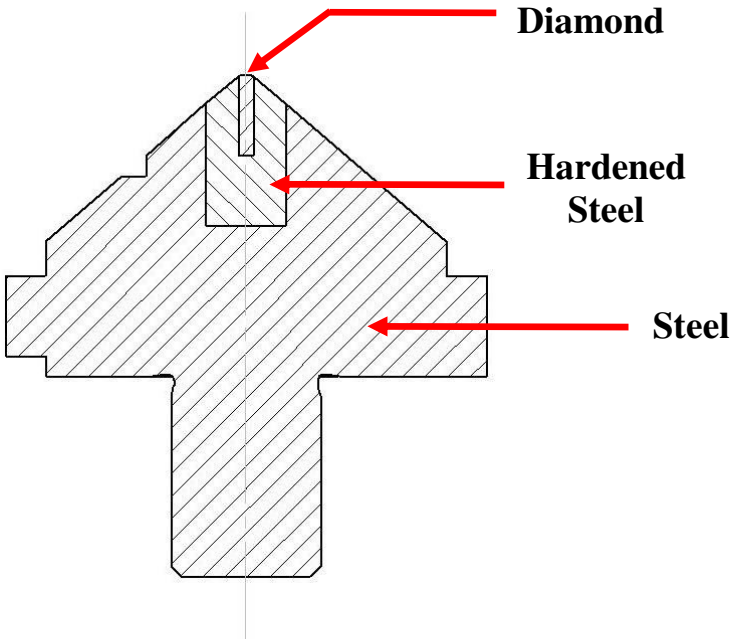

Figure 3.6 Structural details of the indenter

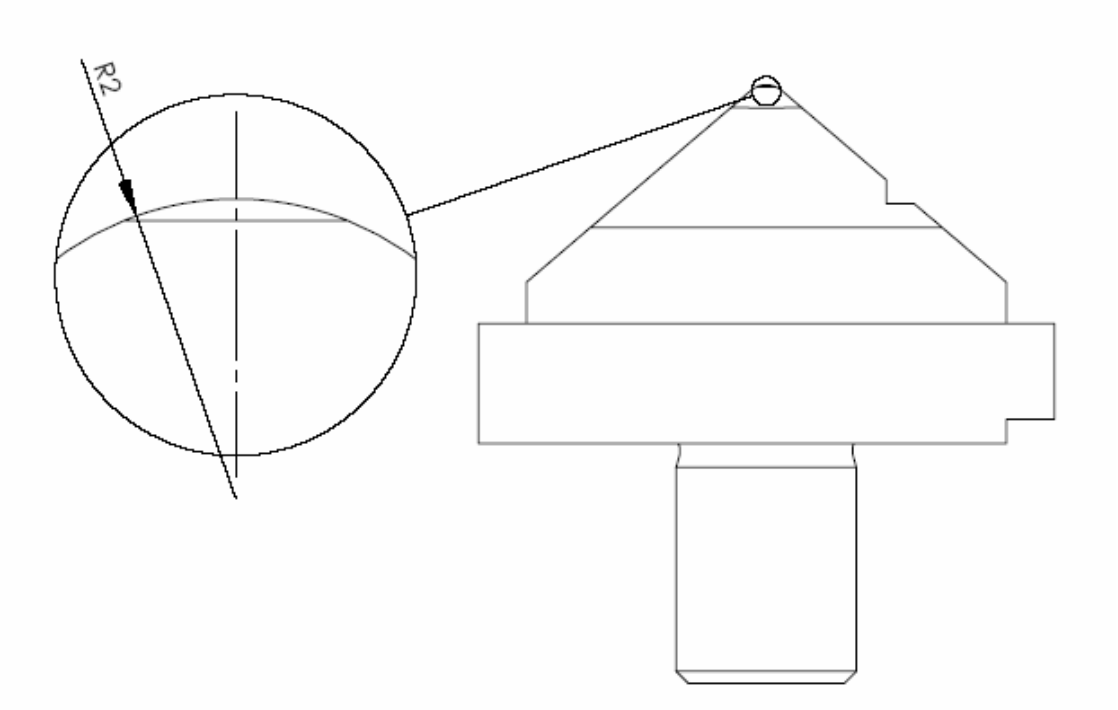

Figure 3.7 Sketch of the indenter geometry (Side view)

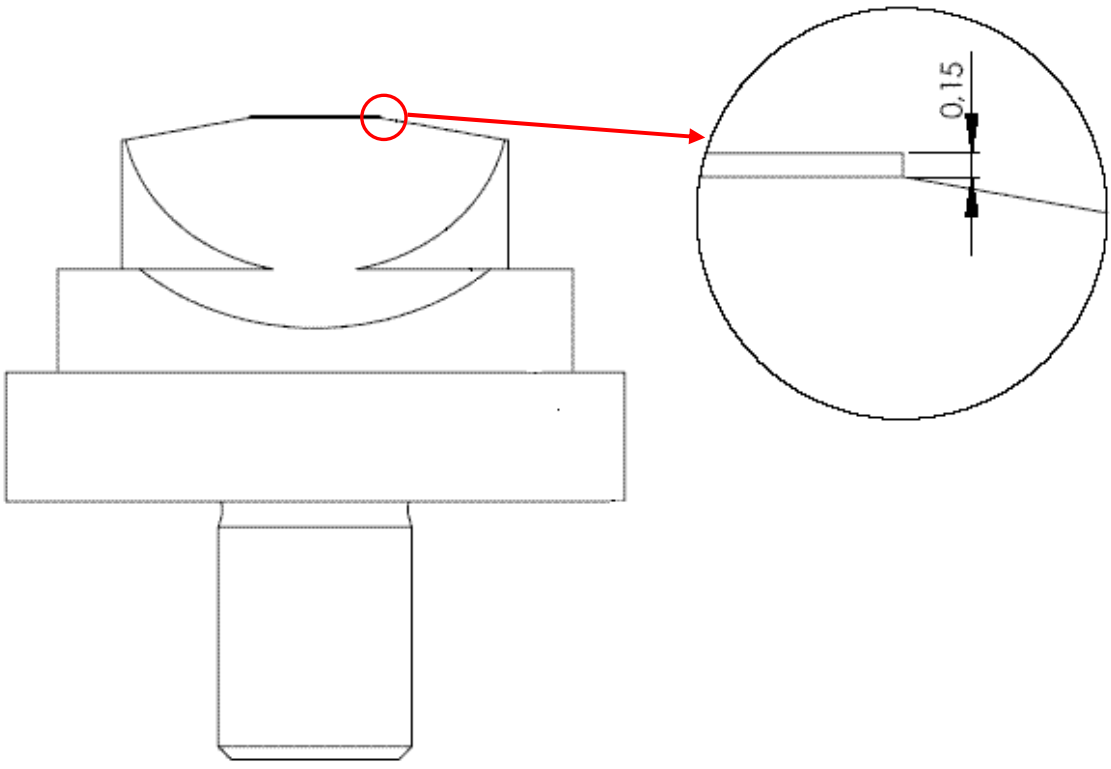

Figure 3.8 Sketch of the indenter geometry (Front view)

CHAPTER 4

NUMERICAL ANALYSIS OF INDENTATION

In this section finite element analysis of indentation will be presented. Firstly the reliable model for analysis will be explained. The geometry, boundary conditions, material properties used in modelling of indentation in two and three dimensions will be shown. Then effects of different parameters like friction, indenter radius, specimen dimensions, etc. are investigated. Results of these analyses will also be presented.

4.1 Modelling of Indentation

Indentation is analyzed with both two and three dimensional models. Main geometry parameters of the indenter are the major radius (R), minor radius (r) and indenter width (w_i), (Figure 4.1). Values of these parameters are given in Table 4.1. Specimen dimensions are the specimen width (w), the specimen length (l) and the specimen thickness (t), (Figure 4.2).

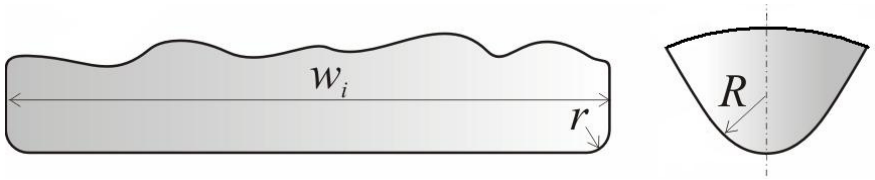

Figure 4.1 Sketch of the indenter

Table 4.1 Indenter geometry parameters

R *(mm)*	r *(mm)*	w_i *(mm)*
2	0.15	10

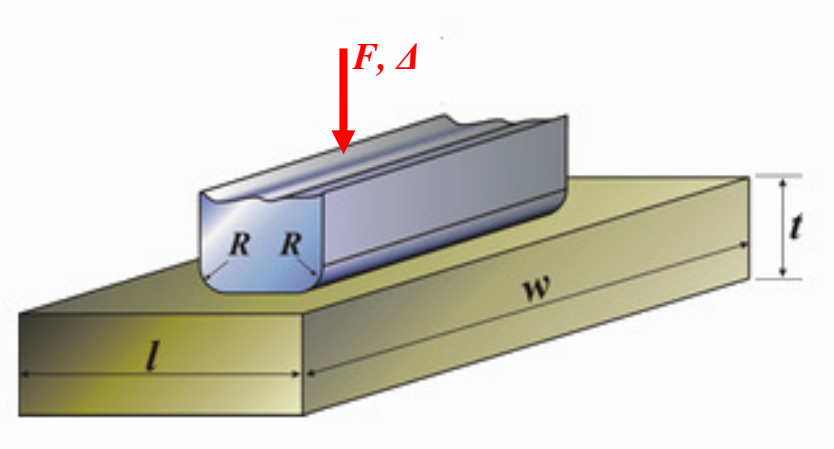

Figure 4.2 Sketch of the indenter and the specimen

4.1.1 Two Dimensional Model

Analyses started with modelling of the indentation in two dimensions with plane strain assumption. In this two dimensional model, effects of indenter parameters and coefficient of Coulomb friction on force-displacement curves are analyzed. Therefore, an isotropic material model is used. In order to reduce computational time by reducing number of elements and the model size, a symmetry axis is implemented (Figure 4.3).

As the deformation zone is very small and concentrated, remeshing is not used. Instead of remeshing, a mesh which is fine at the deformation zone and coarse at the other parts is used. This is managed by using transition elements. By using this mesh, the number of elements is reduced. Convergence analysis of this special mesh is made for another indenter in Chapter 3 of [42]. As this indenter is simpler, contact problems arise in the case of the flat based indenter, it is convenient to use this mesh.

In the analyses, Coulomb friction coefficient (μ) is taken to be 0.1 on the die and indenter surfaces. Effect of friction is analyzed separately and the results will be presented later.

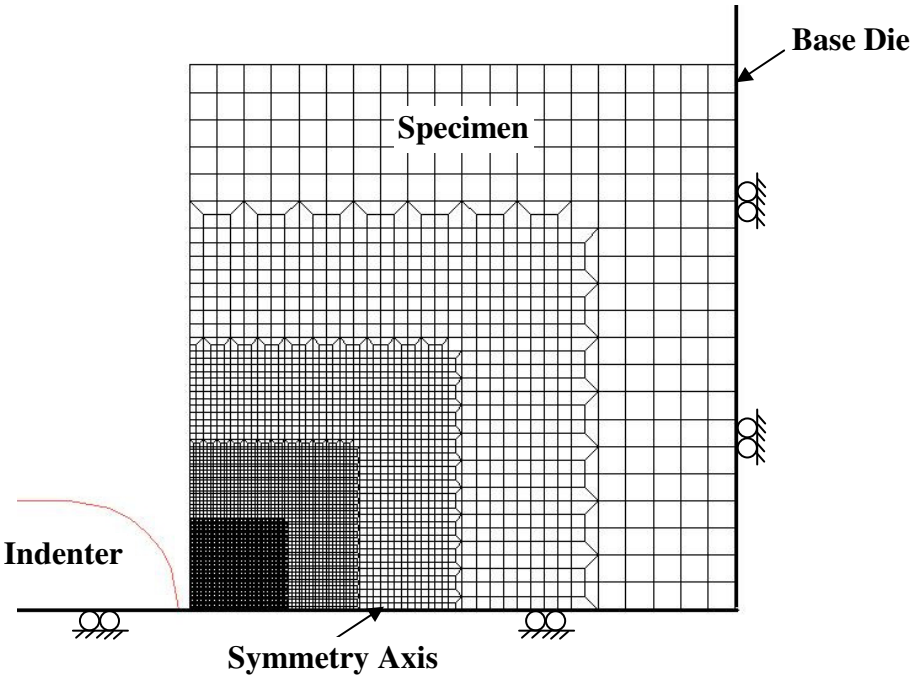

Figure 4.3 Geometry of the indentation in two-dimensional model

Indentation force is limited with the capacity of the real press (2 tons) and as the model is symmetric, maximum force is inputted as the half of this limit (9810 N).

Main data and the assumptions of the two dimensional model are given in Table 4.2.

4.1.2 Three Dimensional Model

Main aim of the three dimensional model is to check the plane strain assumption made in the two dimensional analysis and also to check the effect of specimen dimensions on the force-displacement curves.

Table 4.2 Modelling conditions for the two dimensional model

Problem Types Analyzed:	2-D Plane Strain
Material Law:	Elasto-plastic (isotropic)
Dies and Indenters:	Rigid
Friction Model:	Nodal Stress based Coulomb Law
Indenter Speed:	0.5 mm/s
Finite Element Class:	Quad 4 (bilinear)
Remeshing:	None
Number of Elements:	6319
Minimum Edge Length:	0.03125 mm
Number of Increments:	4000 Fixed Time Steps
Total Loadcase Time:	10 sec
Termination:	Maximum Force (9810 N)

In this model two symmetry axes are used in order to decrease the higher calculation times of the three dimensional analysis. Again remeshing is not allowed. In this case, as it is very difficult to implement transition elements to three dimensions, a biased mesh, which is also fine at the deformation zone and coarse at the other parts, is used (Figure 4.4).

Main problem faced with in the three dimensional modelling of the indentation is the contact with the specimen at the minor radius (r). It is seen that material escapes into the indenter when the elements are not fine enough (Figure 4.5).

However the element size for avoiding this is not feasible to use, as the total number of elements increases in a great amount. This problem is solved by using fine elements aligned with the minor radius. Initial mesh and the modified mesh that solves the contact problem can be seen in Figure 4.6.

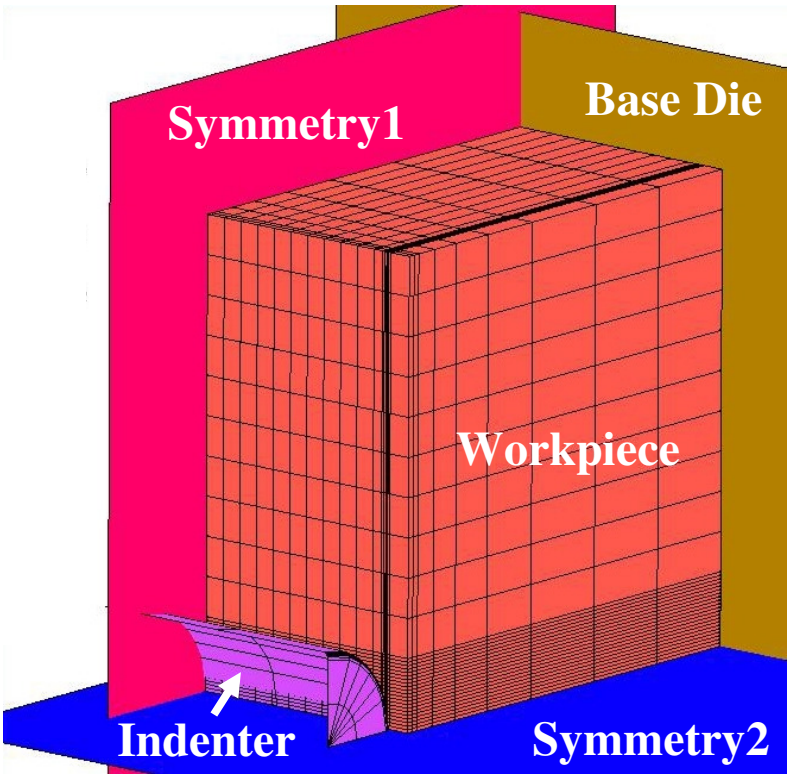

Figure 4.4 Geometry of the three dimensional indentation model

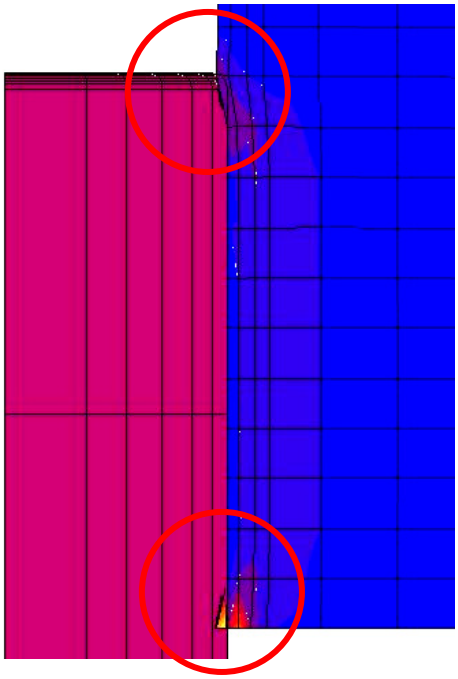

Figure 4.5 Contact problems with the initial mesh

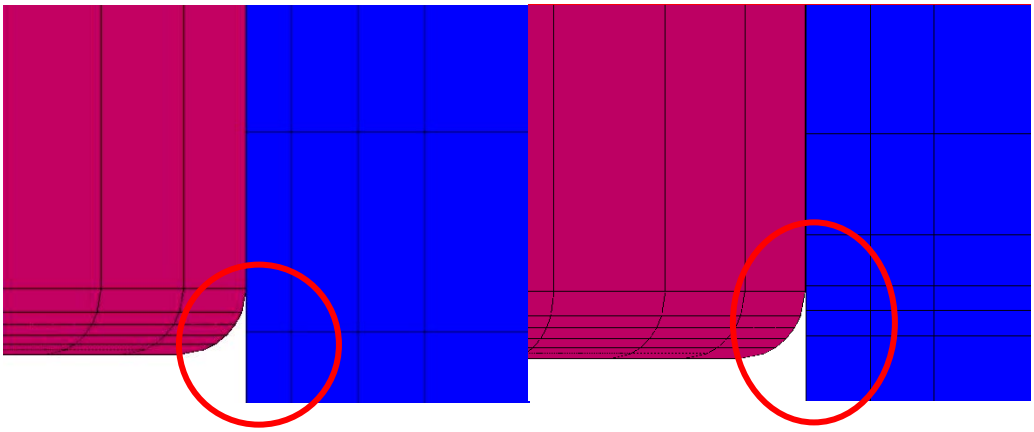

Figure 4.6 Refinement of the mesh

Main assumptions of the three dimensional model are given in Table 4.3:

Table 4.3 Modelling conditions for the three dimensional model

Problem Types Analyzed:	3 - D
Material Law:	Elasto-plastic (isotropic)
Dies and Indenters:	Rigid
Friction Model:	Nodal Stress based Coulomb Law
Indenter Speed:	0.5 mm/s
Finite Element Class:	Hex 8
Remeshing:	None
Number of Elements:	4743
Minimum Edge Length:	0.05625 mm
Number of Increments:	500 Fixed Time Steps
Total Loadcase Time:	1.5 sec
Termination:	Maximum Force (4905 N)

4.2 Material Properties

While modelling the indentation, material is assumed to exhibit isotropic hardening and yielding. In the simulations elasto-plastic material model is used. True stress versus plastic strain values are used as the flow stress data of the material in the simulations. As the indentations are made at room temperature, flow curves at the

room temperature are enough (Figure 4.7). In the simulation C15 is used as the material, and the flow curves are supplied by the research partners in Stuttgart, from their compression tests. Strain rates in the simulations are always less than 8.0 1/s.

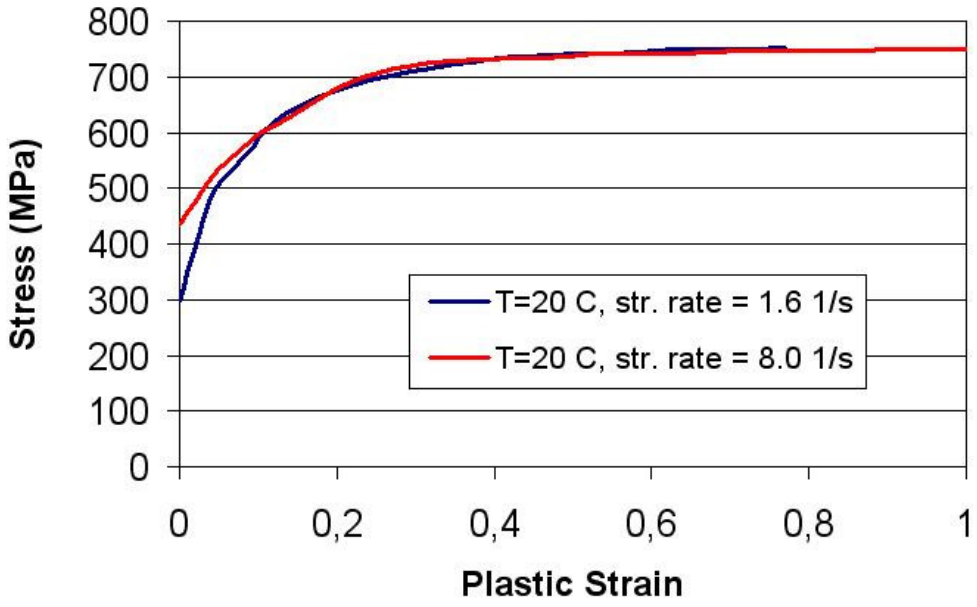

Figure 4.7 Flow curve of C15 at room temperature for different strain rates

4.3 Two Dimensional Simulation Results

Two dimensional simulations are mainly concentrated on the indenter and setup parameters. Influence of friction and radius on the force-displacement curves is investigated. Also effect of the fixing plate (reference plate) on the results is supplied.

4.3.1 Effect of Indenter Radius

In this analysis, major radius (R) has been given four different values; 1 mm, 2 mm, 3 mm and 4 mm. The simulations are conducted up to the highest force limit of the available press (2 tons). Naturally, the maximum indentation depths varied with radii.

Force-displacement curves for each radius can be seen in Figure 4.8. This figure points out that by using indenters with small radii, more indentation into the material is possible as expected.

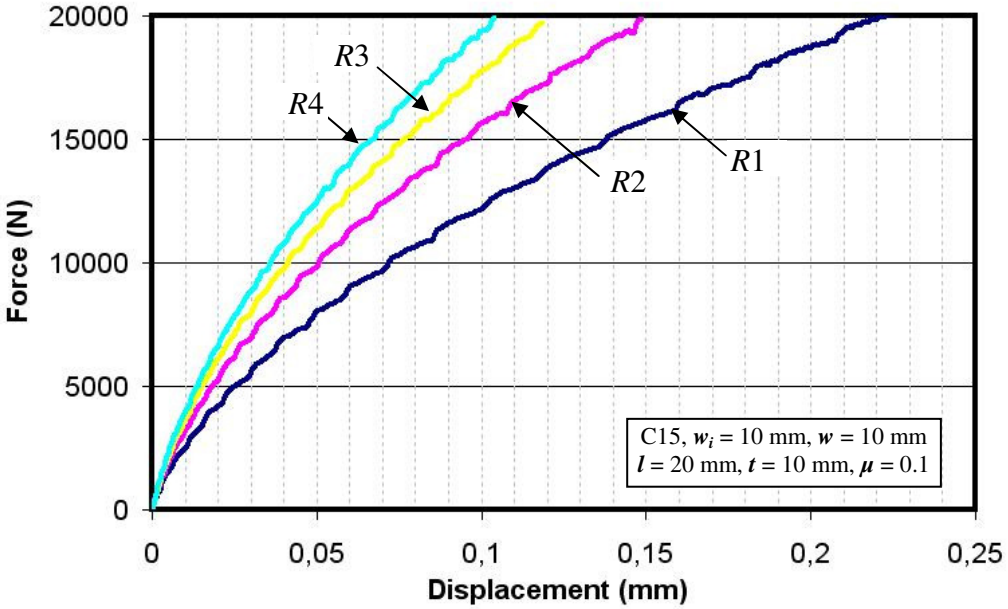

Figure 4.8 Force-displacement curves for indentations with different indenter radii

However, higher indentation depths also bring the problem of higher plastic strains, which is not desired as the initial plastic anisotropy is investigated. It is aimed to reach plastic strain values of 0.1 in the deformation zone. In Figure 4.9, plastic strain distributions for each indenter can be seen. Indenter with major radius 2 mm seems to be the most appropriate one as the indentation depth is reasonably high and the plastic strain values are mostly between 0.15 and 0.10.

4.3.2 Effect of Friction

Friction can also be a big problem as it is hardly controlled by the experimenter. Finite element simulations are carried to check whether with different friction coefficients force-displacement curves vary (Figure 4.10). In the simulations three different Coulomb friction coefficients (μ) (0.05, 0.1, and 0.15) are used besides the frictionless case. It is seen that effect of friction on the force-displacement curves is

very small. This is a big advantage for the tests as it would not be necessary to control the friction.

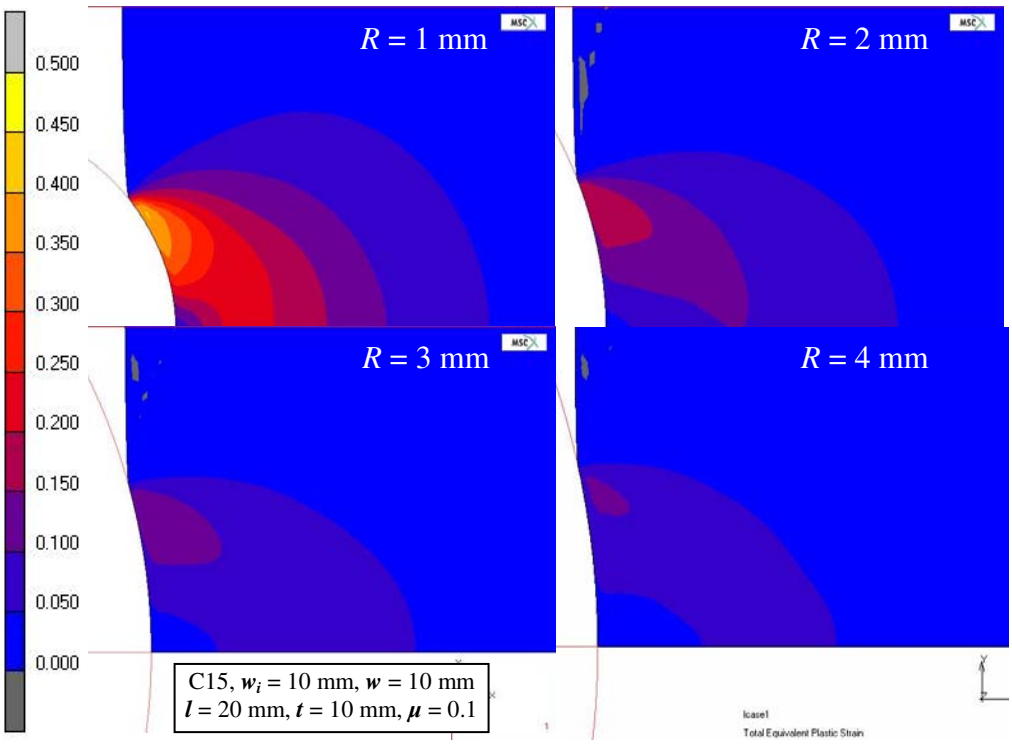

Figure 4.9 Total equivalent plastic strain distributions for indentations with different indenter radii

4.3.3 Effect of Compression

While fixing the specimen with the reference plate, some force is applied to the ends of the specimen. Effect of these small elastic deformations must also be checked and if it effects the force-displacement curves, this fixing should be eliminated.

Finite element simulations are carried to see at which distance to the indenter (ψ), reference plate starts to contribute to the force-displacement curves. For this reason a simple model is prepared (Figure 4.11). This new model has an additional contact surface, which compresses the specimen slightly (0.01 mm).

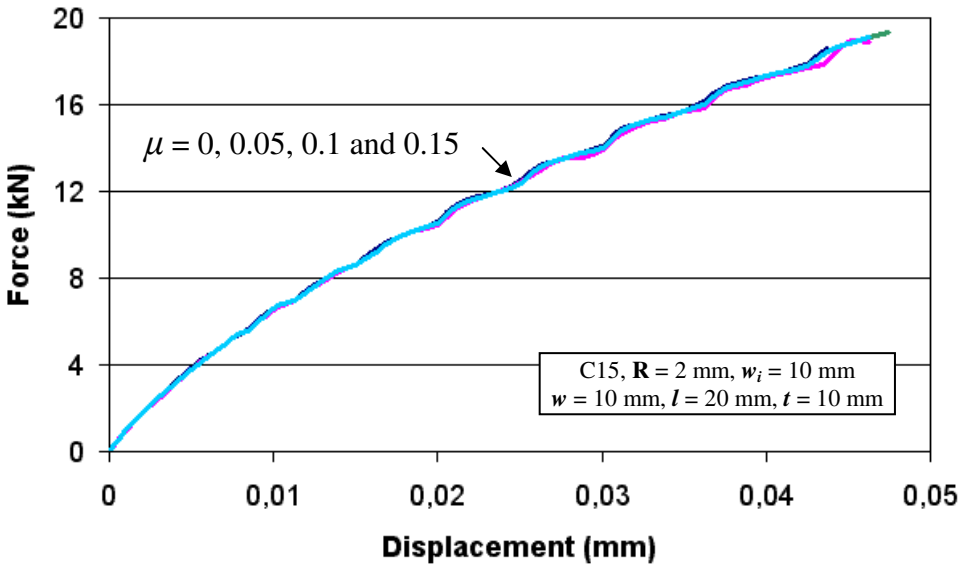

Figure 4.10 Force-displacement curves for indentations with different Coulomb friction coefficients

Figure 4.12 shows the force-displacement curves obtained from the simulations. It is seen that for the cases that $\psi \geq 10$ mm, force-displacement curves are identical with the ones obtained from the not compressed indentations. In the real setup, ψ is equal to 16 mm, so the compression will not affect the repeatability and the accuracy of the experiments.

4.3.4 Effect Length-Limitation

It is also desired to check whether force-displacement curves are affected when the movement of the specimen in the length direction is avoided. For this purpose a model is developed in which a die is implemented at the top (Figure 4.13). This limitation in the length direction changed the forces significantly (Figure 4.14). Therefore during the experiments, this effect should also be considered.

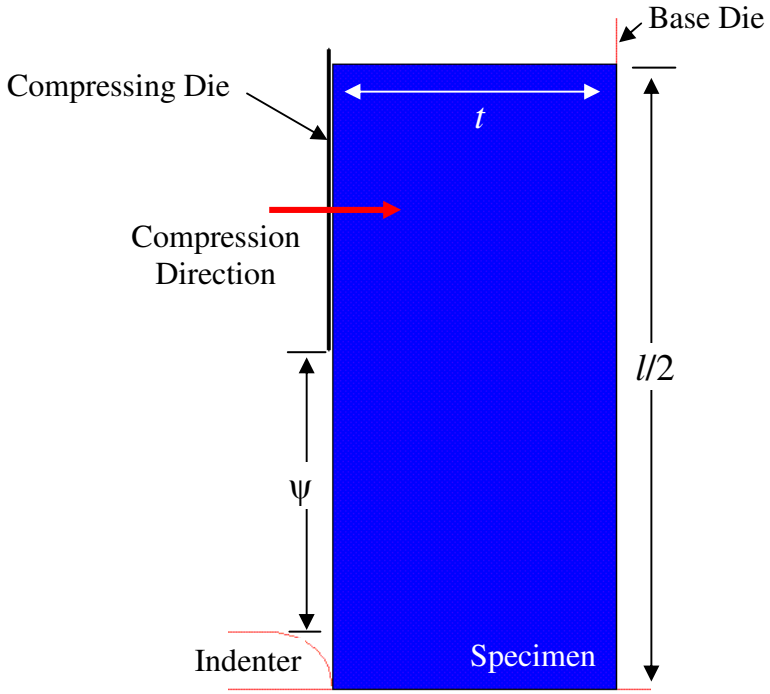

Figure 4.11 Finite element model used in the compression effect analysis

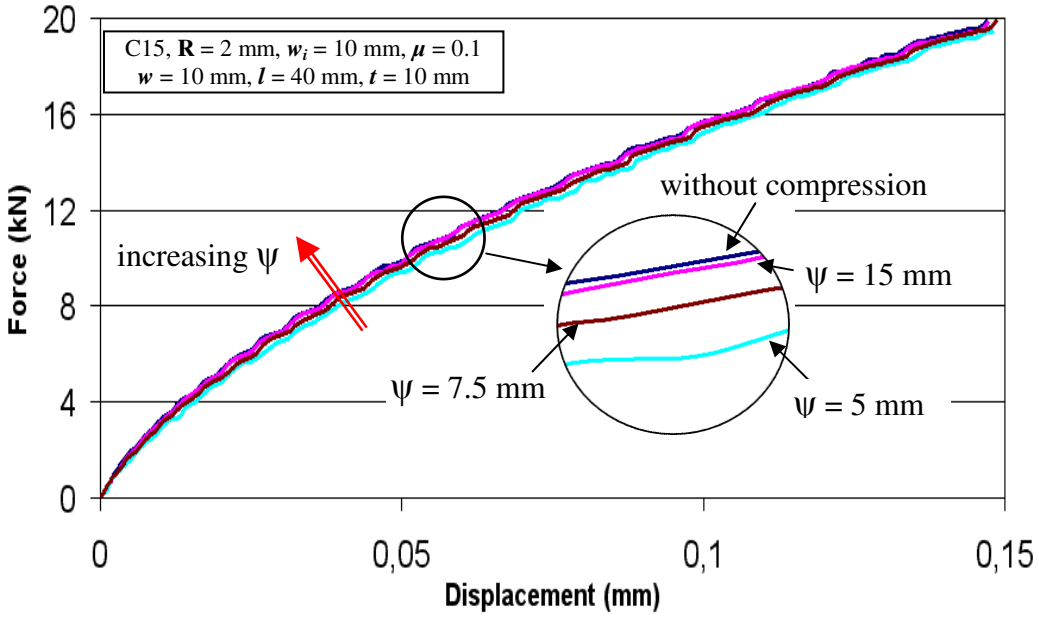

Figure 4.12 Force-displacement curves for indentations with compression

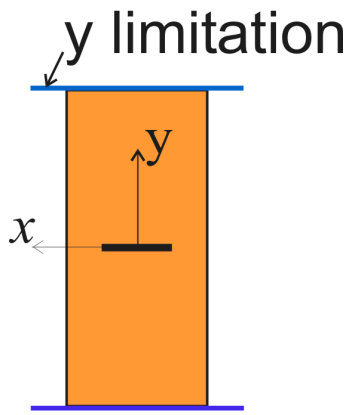

Figure 4.13 Sketch of the model with length-limitation

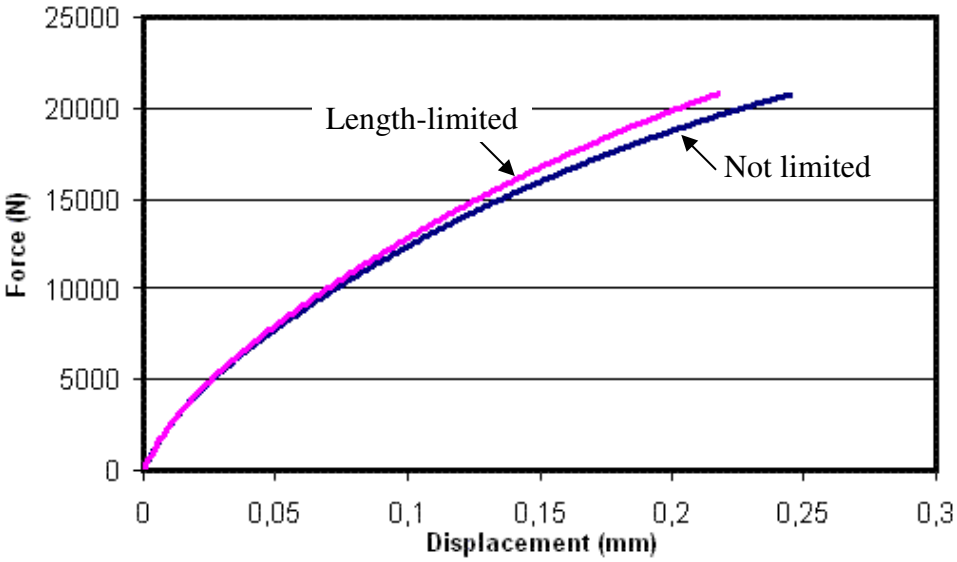

Figure 4.14 Effect of boundary conditions on the force-displacement curves

4.4 Three-Dimensional Simulation Results

Three-dimensional finite element analyses are performed to investigate the effect of specimen parameters on the indentation results.

4.4.1 Plane Strain Assumption Verification

The first study made in three dimensions is the verification of plane strain assumption in the two-dimensional analysis.

In Figure 4.15, it is seen that this assumption is not valid. For specimens with widths smaller than the indenter width, simulation results are smaller than the two dimensional analyses results.

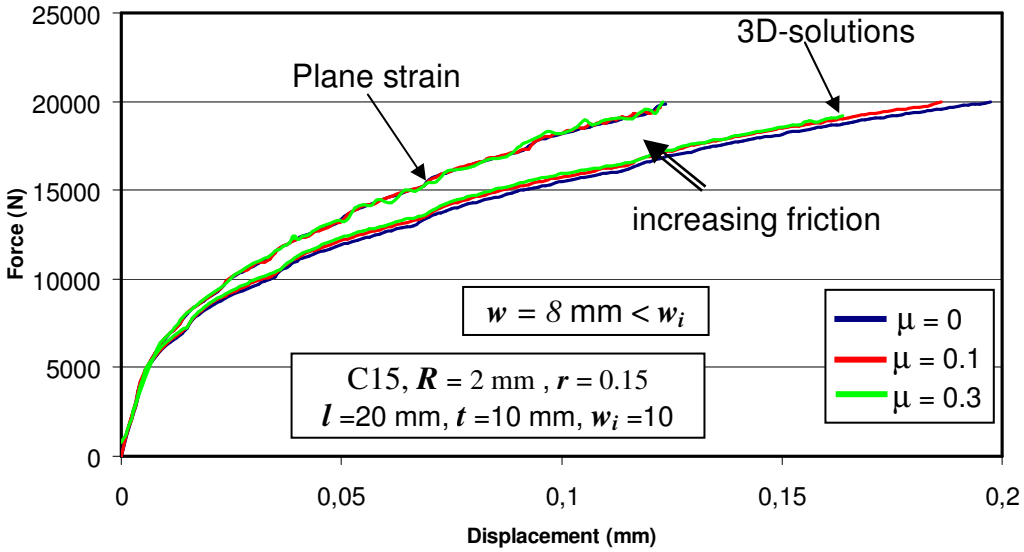

Figure 4.15 Comparison of 3-D results with plane-strain solutions and effect of friction

The gap between the 2-D and 3-D results are tried to be eliminated by increasing the friction. Main idea in this was to prevent the flow of material in width direction. However it is seen that the friction, although improving the solutions, has almost no effect on the results and the gap remained.

Moreover, it is seen that the specimen width influence these results. Following this, some analyses are made to investigate the effect of specimen dimensions on force-displacement curves.

In Figure 4.16, effect of width on the force-displacement curves can be seen. In these analyses, width of the indenter is kept constant at its real value of 10 mm and the width of the specimen is increased. In the simulations, specimen with 12 mm width satisfied the plane strain solution results. However, when the width of the specimens is increased more at 15 mm of specimen width saturation in force-displacement curves is obtained (Figure 4.17).

Unfortunately, this saturation value is different than the plane-strain values (Figure 4.18). In Figure 4.18, upper figures give the equivalent plastic strain distributions for plane strain solutions. Bottom figures give the distributions for 3-D analysis results. The left figure is taken from a section near to the end of the indenter; contrarily the right figure is taken from a section close to the center of the indenter. These figures show that the plane strain assumption is not valid at the ends of the indenter, although it is valid at the center.

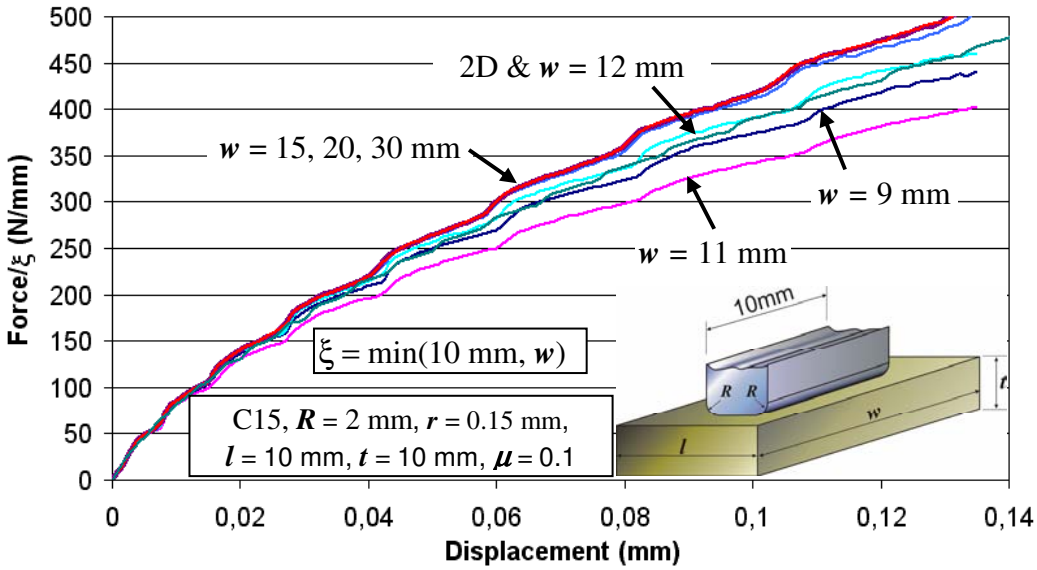

Figure 4.16 Effect of width on force-displacement curves and saturation

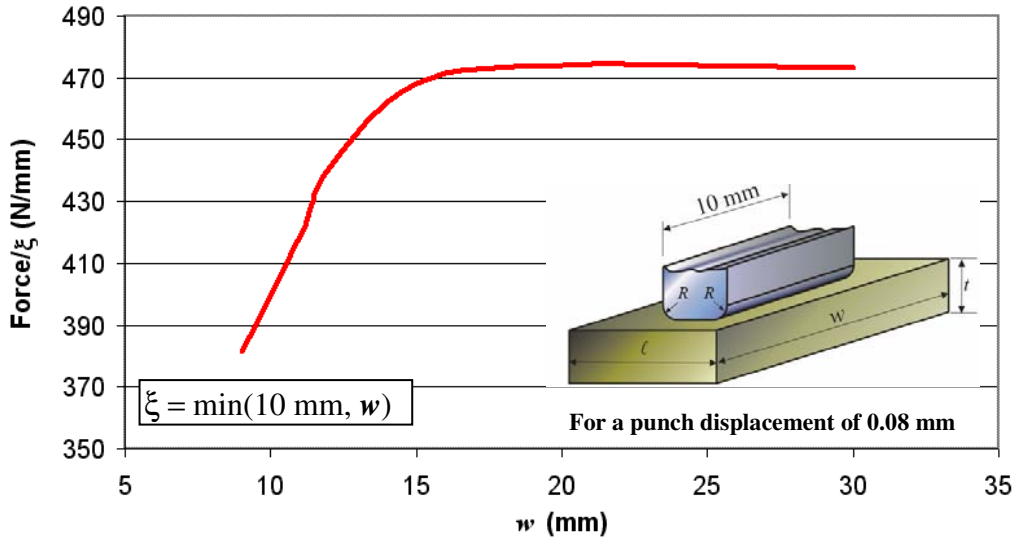

Figure 4.17 Saturation of forces

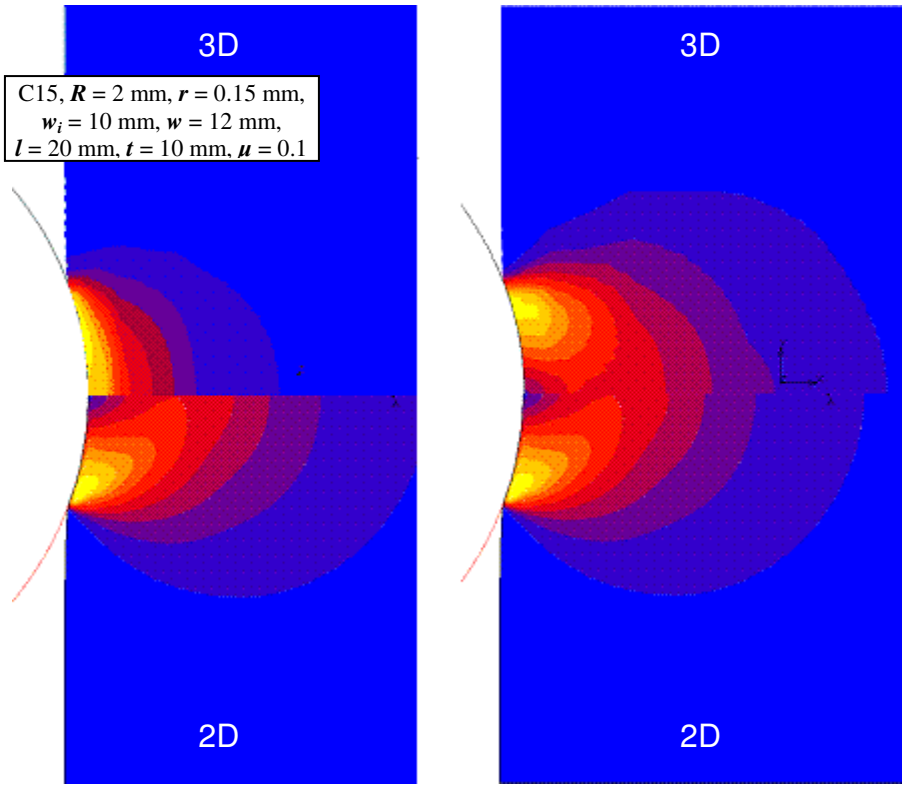

(**a**) (**b**)

Figure 4.18- Verification of plane-strain conditions at the **a)** end, **b)** middle of the specimen

When the specimen width is higher than a certain value, the incompatibility at the ends is stuck in a certain volume and then by increasing width values the force-displacement curves do not change. However, in specimens with width smaller than a certain value, the ratio of the plane strain region to the total deformed region is very small. So when width of the specimens are changed, this ratio also changes significantly that the force-displacement curves also change. In the light of these observations, it is decided to

- use specimens with widths, which will give force-displacement curves in the saturation region,
- correct the saturated force-displacement curves measured to plane strain values by a correction factor.

4.4.2 Correction of Width Effect

In order to correct the saturation force-displacement curves to plane-strain curves, firstly the behavior of the correction factors are analyzed. The next step was to relate these correction factors to the displacements. Correction factors are obtained by dividing the plane-strain forces by saturation forces.

$$C = \frac{F_{plane\ strain}}{F_{saturation}} \tag{4.1}$$

Then some curves are fitted to these correction points. It is seen that a logarithmic function

$$C(\Delta) = A \cdot \ln(\Delta) + B \tag{4.2}$$

fitted best. This function also has the advantage of less number of parameters compared to the polynomial functions that fit to the points.

In Figure 4.19, it can be seen that the saturation force-displacement curve is successfully corrected to the plane-strain values.

4.4.3 Effect of Specimen Thickness

After seeing the contribution of width of the specimen on the force-displacement curves, it is decided to analyze the effect of other dimensions of the specimen. Firstly effect of thickness of the specimen is investigated.

In these analyses a specimen with the saturation width of 15 mm is taken. Its length (***l***) is assumed to be 20 mm and indentations are simulated with different thicknesses (***t*** = 3.9, 4.9, 6.5, 12 mm).

In Figure 4.20, forces at the elastic region are higher for specimens with smaller thicknesses as they behave stiffer. However, as the indentation goes on and the plastically deformed zone increases, forces decrease. In the specimens with smaller thicknesses this effect is dominant as the plastic zone reaches the bottom surface in

a short time. Hence, after the elastic region, forces become higher for thicker specimens (Figure 4.21).

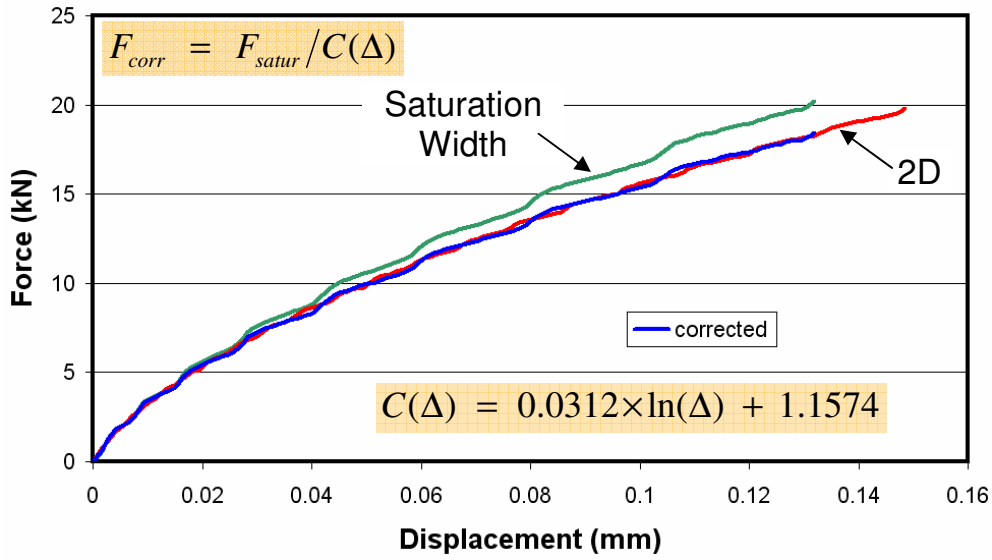

Figure 4.19- Correction of saturation forces to plane-strain forces

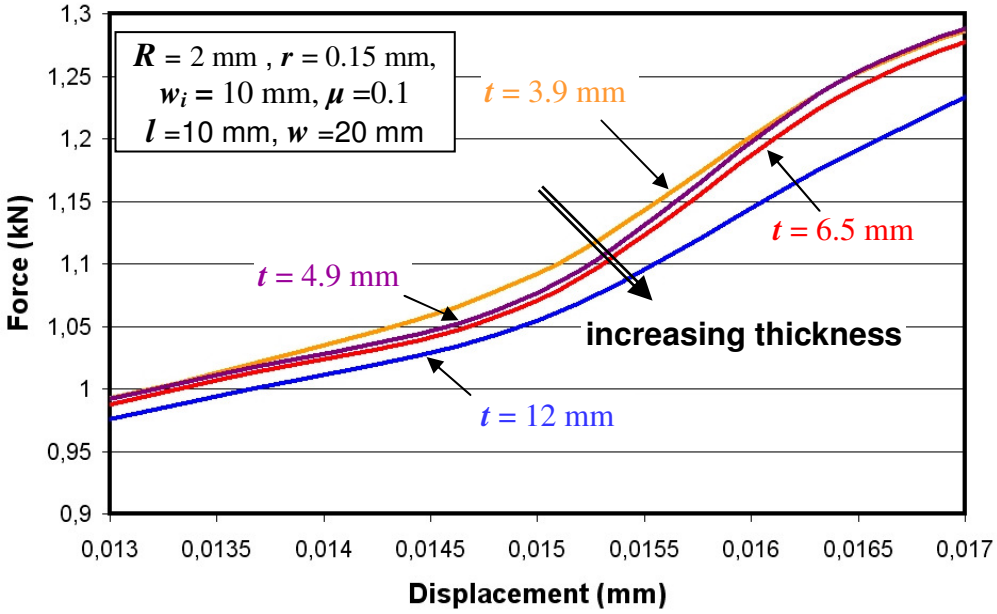

Figure 4.20 Effect of thickness in the elastic zone

However, if the thickness of the specimens is further increased, a saturation zone is reached. Main reason for this is that, when the thicknesses of the specimens are

above some value, the ratio of the thickness of the plastificated zone to the whole thickness becomes smaller and the specimens start to behave similar.

It is decided to use specimens with a thickness of t = 6.5 mm such that force-displacement curves are in the saturation region.

4.4.4 Effect of Specimen Length

For specimen length analysis the specimen width (w) is taken as 15 mm and the specimen thickness (t) is taken as 10 mm. Length of the specimens are changed between 12 mm and 44 mm.

Results of the analysis are given in Figure 4.22. In the elastic region the forces are the same for all specimens. However, when the boundary of the plastic zone propagates in the length direction and reaches the side of the specimen, forces decrease. So, for shorter specimens forces are lower. (Figure 4.22)

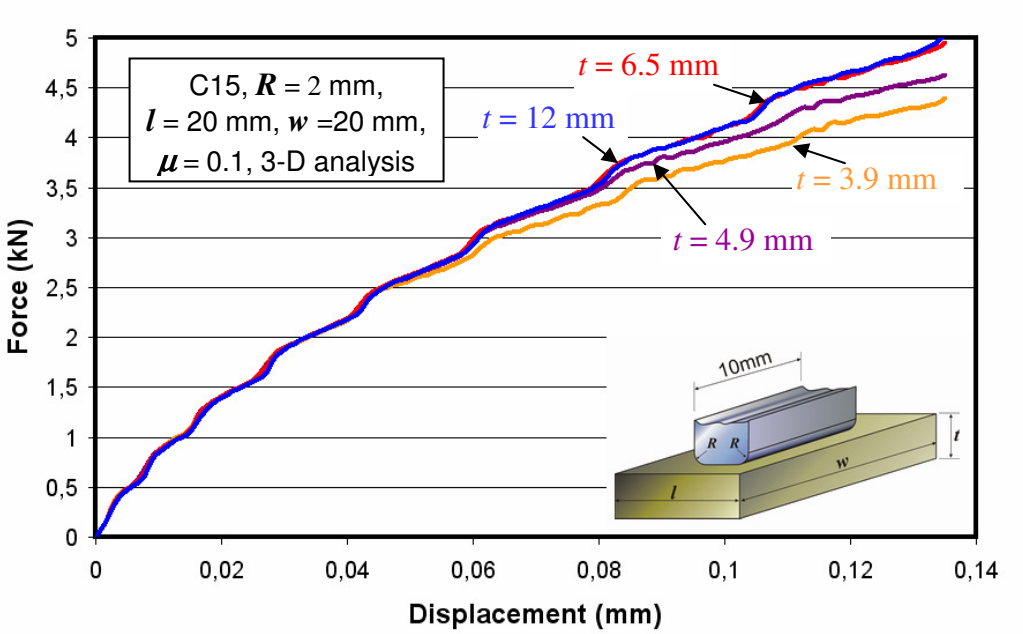

Figure 4.21 Effect of specimen thickness on force displacement curves

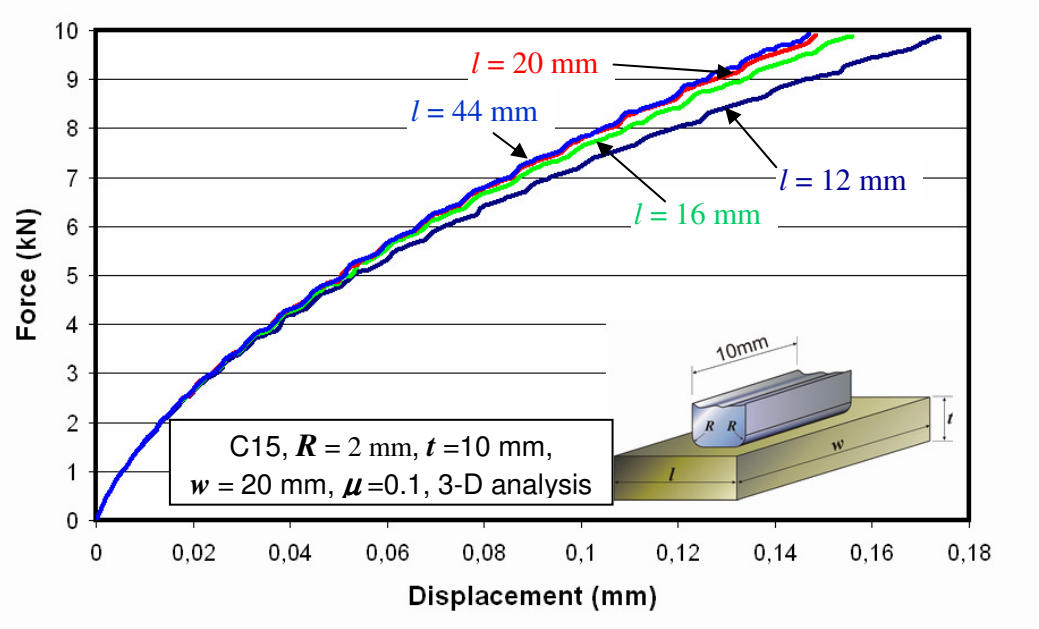

Figure 4.22 Effect of specimen length on force displacement curves

The saturation zone is also observed in this analysis. For specimens with lengths above a certain value, the forces do not change by further increase of the specimen lengths. The reason for this is that the ratio of the plastificated zone length to the whole length of the specimen does not change significantly after a certain specimen length.

It is concluded that using a minimum specimen length (***l***) of 20 mm will provide saturation force-displacement curves and this would help achieving better repeatability in the experiment results.

4.5 Ideal Specimen Dimensions

After determining the suitable range for the specimen dimensions, market is investigated for a cold rolled metal plate that can be used to obtain specimens with such dimensions. The most important criterion in the selection of the specimen dimensions is satisfying the plane strain assumption, which is the hearth of the inverse analysis program. The research partners at the Stuttgart University found a St37 plate with 18 mm thickness. As the specimens will be ground, thickness of the

specimens are agreed to be 16 mm. The specimens to be used in experiments are decided to have the dimensions given in Figure 4.23.

w = 20 mm,

l = 45 mm,

t = 16 mm

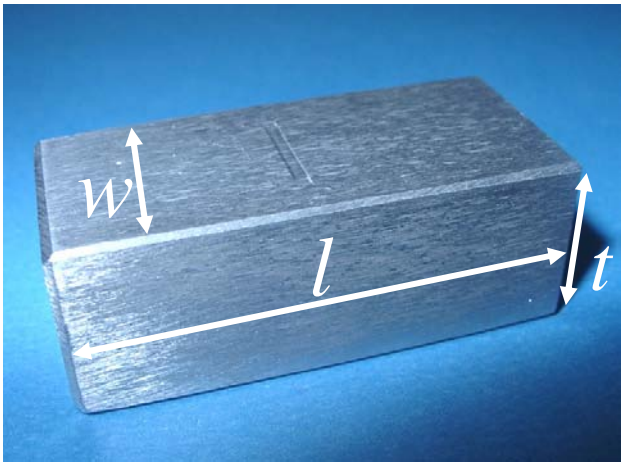

Figure 4.23 Ideal dimensions of the specimen

Here, width is decided to be a little larger than the saturation width (w = 15 mm) in order to avoid the problems that might arise because of centering errors of the specimen. By this way, specimen might be put 2.5 mm away from the center and the plane strain assumption will still be satisfied.

In the selection of the thickness value, the third indentation, which is made on the thickness plane, plays an important role. It is also desired to have a plane strain indentation at this direction so the thickness should be larger than the saturation width of 15 mm. However, desire for high thicknesses decreases the possibility of finding a cold rolled plate and also high anisotropy, since the thick plates are mostly hot rolled. So, the thickness value is selected just above the saturation width. Considering this, the experimenter should be careful with the centering of the specimen.

Length of the specimen could be any value above 30 mm (because of the compression effect considerations). It is selected to be 45 mm in order to increase the grip of the reference plate and by this way the repeatability.

CHAPTER 5

THE INDENTATION TESTS

In this chapter, the materials used in the indentations, the specimens and the indentation results are supplied and these results are evaluated. Firstly the preliminary experiments which emphasize the abilities of the setup and the repeatability of the testing method are presented. Then the actual test results are shown. Performed compression tests for the evaluation of mechanical properties of the materials used in the experiments are given in the Chapter 6.

5.1 Specimens

Materials to be examined are wanted to have high plastic anisotropy. For this reason cold rolled sheets are searched in the market. Another criterion to be taken into account is to find thick plates in order to be able to make indentations also in the thickness direction.

Since Hill 1948 anisotropic yield criterion is implemented, the inverse analysis program can not be used for parameter identification of aluminum specimens. However, some preliminary experiments are made with aluminum plates (Al2014) as it is easier to find cold rolled thick plates of aluminum than steel. Also a thin aluminum plate (Al5086), whose anisotropy is certain, is used to check the capability of the method of determining anisotropy.

Material designations are given according to DIN norms and American standards in Table 5.1. The compositions of these materials are given in Table 5.2. Through out this study materials will be called as St37, Al2014 and Al5086. In Table 5.3, ideal dimensions and the mechanical properties of these can be found. Actual dimensions of the specimens are given in Appendix B. Flow curves of the materials are going to be determined in Chapter 6 by compression tests.

A coding system is developed in order to distinguish different specimens. This includes the material of the system, orientation of the specimen and the number of the specimen (Figure 5.1).

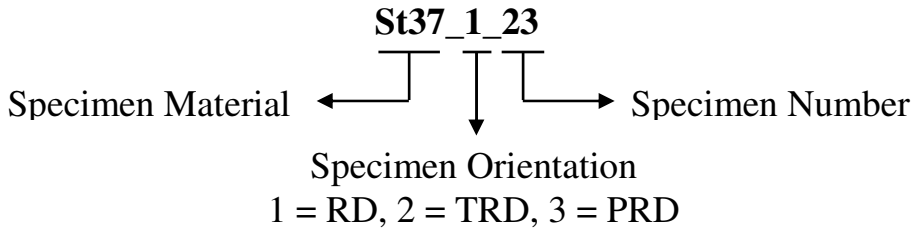

Figure 5.1 Specimen coding

5.1.1 St37 Specimens

Indentation tests are started with the St37 specimens prepared in Stuttgart with the dimensions specified in Sections 4.4 and 4.5. Figure 5.2 shows a specimen with indentations on the surface. The length of indentations is 10 mm whereas width of the specimens is about 20 mm.

The specimens from the St37 plate are made in three orthogonal directions; in the rolling direction (RD), transverse to rolling direction (TRD) and perpendicular to the rolling direction (PRD), (Figure 5.3).

These specimens are made in three different surface qualities (Figure 5.4). First one is the raw material, which is just cut to the required width and length but the indentation surface is not machined. The second one is the milled specimens which are the raw specimens that are milled so that the required thickness is reached.

Third one is the ground specimens, whose surface quality is superior to the milled ones and the indentation surface is parallel to the base of the indenter.

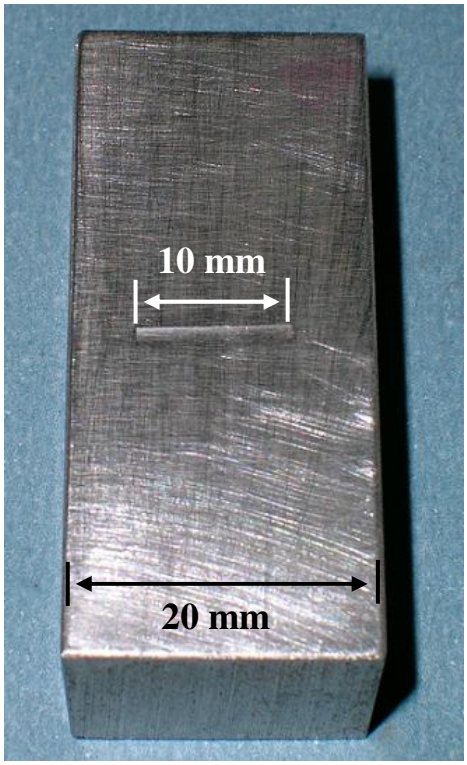

Figure 5.2 An indented St37 specimen

While conducting the indentation test, it is also wanted to learn the flow properties of the St37 plate used. For this reason, steel strips are prepared from the same plate, the indentation specimens are made of, in three directions. Then these strips are cut into square prismatic compression specimens in the Machine Shop in the Department of Mechanical Engineering, METU (Figure 5.5). Some of these steel strips are also turned to have circular compression specimens. Details of the compression test specimens are given in Chapter 6.

Table 5.1 Materials investigated in the study

Materials	DIN	AISI
Steel (St37)	St37	A283B
Aluminum (Al2014)	AlCuSiMn	2014
Aluminum (Al5086)	AlMg4Mn	5086

Table 5.2 Chemical compositions of materials [43]

Chemical Composition % (max. unless noted)												
	C	**Mn**	**P**	**S**	**Si**	**N**	**Cu**	**Zn**	**Mg**	**Ti**	**Fe**	**Cr**
St37	0.09	0.60	0.009	0.016	0.19	0.009	-	-	-	-	-	-
Al2014	-	0.40 - 1.20	-	-	0.50 -0.10	-	3.90 - 5.00	0.25	0.2 - 0.8	0.15	.0.70	
Al5086	-	0.20 – 0.70	-	-	0.40	-	0.1	0.25	3.5 - 4.5	0.15	0.50	0.05 - 0.25

Table 5.3 Dimensions and the mechanical properties of the specimens (Al5086 [43], Al2014 [44], St37 [45])

	***w* (mm)**	***t* (mm)**	***l* (mm)**	**Young's Modulus - E (GPa)**	**Initial Yield Stress - σ_{Y0} (MPa)**	**Poisson's Ratio - υ**
St37	20	16	45	200	270	0.3
Al2014	20	20	45	72.4	290	0.33
Al5086	20	3	45	71	207	0.33

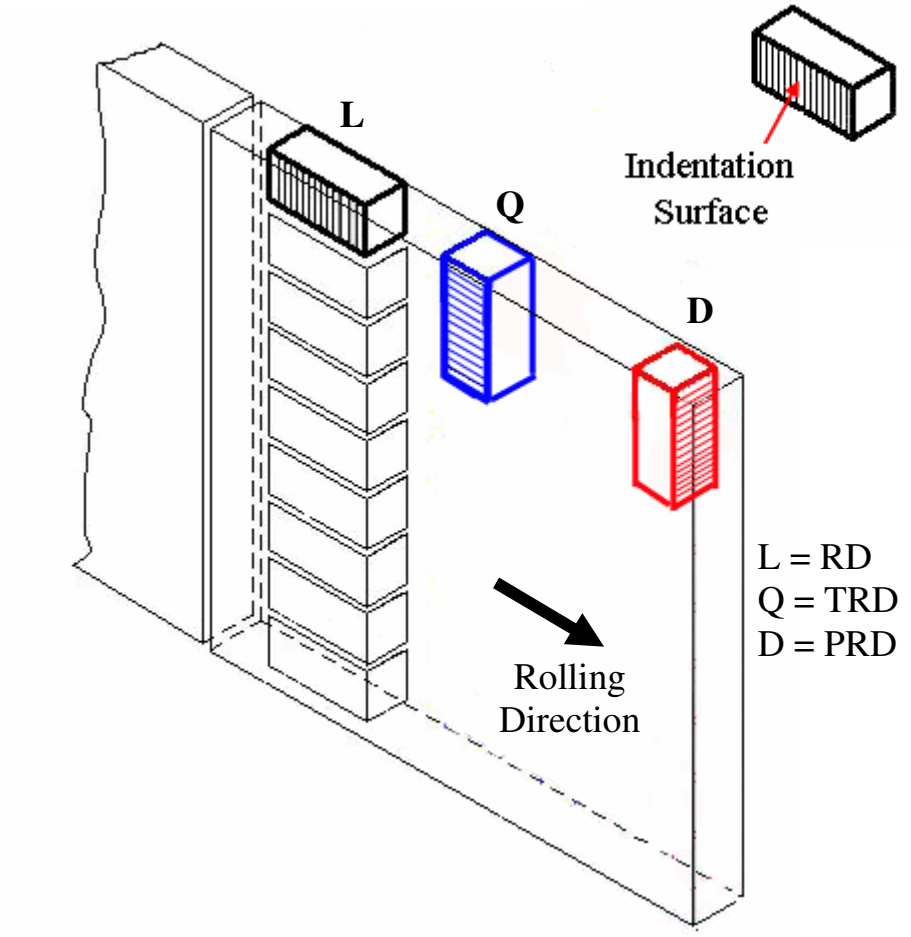

Figure 5.3 Orientations of the specimens in the original plate

5.1.2 Al5086 Specimens

Main aim of these Al5086 specimens is to investigate significant difference between the force displacement curves obtained from indentations at two orthogonal directions, RD and TRD. As these specimens are very thin (t = 3 mm), third indentation in PRD is not possible (Figure 5.6). The plate found is a cold rolled one. By looking at the surface the rolling direction is easily determined.

Before starting the indentation tests, tensile tests are conducted to have an idea about the anisotropy of the plate (Figure 5.7). It is clearly seen that anisotropy exists in the material. This anisotropy is tried to be verified by the indentation tests.

Figure 5.4 Surface conditions of specimens **a)** raw, **b)** milled and **c)** ground

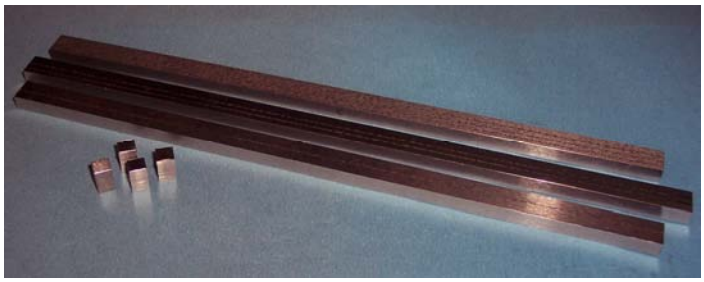

Figure 5.5 Steel strips and compression test specimens (St37)

Figure 5.6 An Al5086 specimen

Specimens are prepared in the Machine Shop in the Department of Mechanical Engineering, METU. Main problem with the specimens prepared is that while cutting the specimens from the plate, parts are bent (Figure 5.8). In order to flatten them, specimens are compressed between two flat dies up to 10000 N. Actually this force will not plastically deform the specimens throughout. However, as the specimens are bent, initial contact area is very small (Figure 5.9) and just at the

bent zone plastic deformation takes place such that the compressed specimens are flat enough.

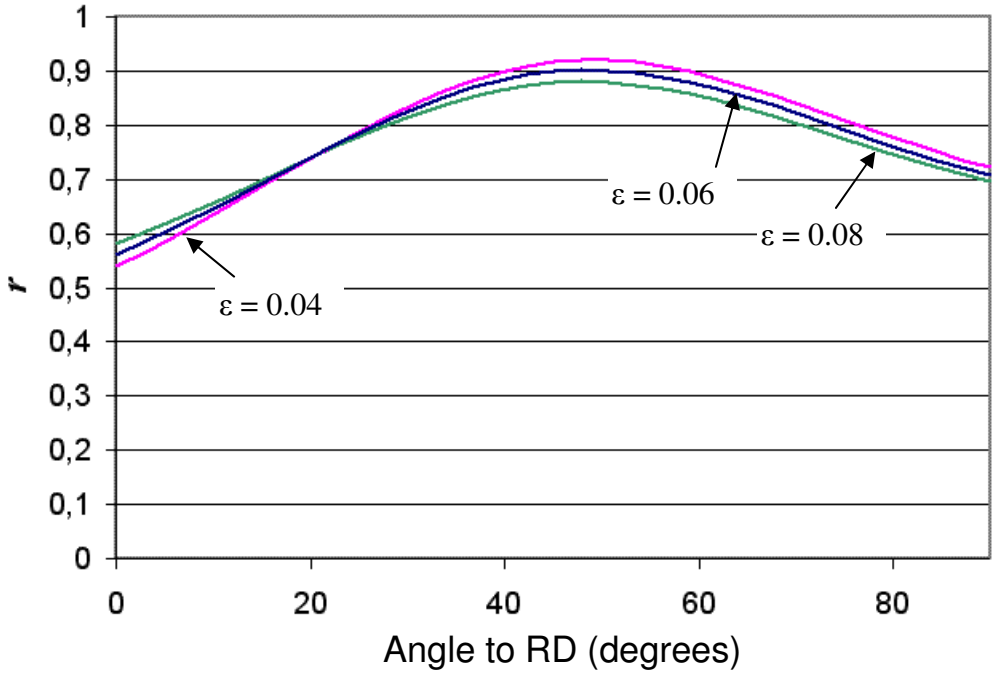

Figure 5.7 Anisotropy coefficient *r* values with respect to material orientation curves for different strain values [42]

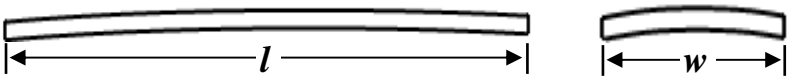

Figure 5.8 Sketch of the bent specimens

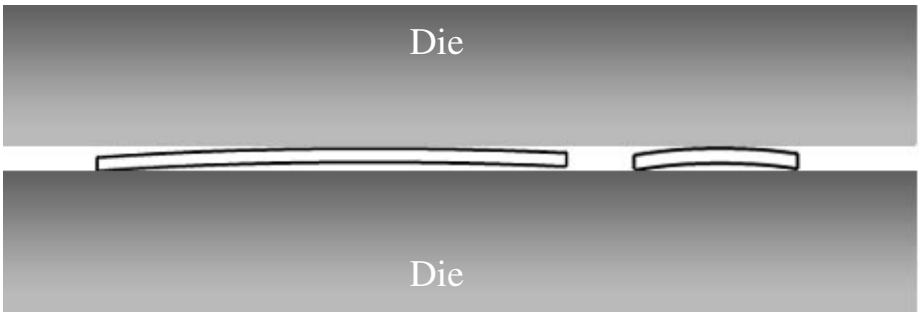

Figure 5.9 Sketch of the compression of the bent specimens

5.2 Preliminary Test Results

The first experiments made aimed to gather experience with the experimental setup and the measurement system. In these experiments, ground specimens are used. Some of the indentations are made with another indenter geometry ($R0.68$) given in Chapter 6 of [42] and the rest are made with the indenter geometry ($R2$) given in Chapter 3. In order to reach the highest accuracy and repeatability, some investigations are made.

5.2.1 Parallelity Problem and Positioning of the Specimens

Finite element simulations in Chapter 4 of [42] show that inclined indentating introduces a significant amount of error into the results. Therefore, the parallelity between the indenter and the specimens must be guaranteed before starting the experiments.

To achieve parallelity, firstly the indenter is moved down to a position that it almost touches the base anvil. Then a light source is placed behind the system and the light passing through the gap between the anvil and the indenter is observed. The base anvil is adjusted so that the gap thickness is the same along the indenter width (Figure 5.10). By this way the parallelity between the indenter and the anvil is achieved. However, as this procedure depends on naked eye observations it includes some error in the parallelity (~10 μm).

Another problem that arises with the parallelity is that, this method tries to achieve parallelity between the base anvil and the indenter. So the specimens must have two perfectly parallel surfaces at the bottom and at the top. However, the ground specimens have parallelity deviations up to 8 μm. This means that even if the base anvil and the indenter are adjusted perfectly, the specimens will introduce some error into the results.

This total parallelilty error of approximately 18 μm (10 μm from adjustments and 8 μm specimens) corresponds to 0.1˚ inclination between the indenter and the specimen.

Base anvil is centered after the parallelity adjustments. For this purpose, a special tool (Figure 5.11) is used. This tool has a chamfered end. Before lowering the tool the base anvil is a little bit loosened. When the tool is lowered slowly, the chamfered end adjusts the reference plate so that their centers coincide. While the centering tool is inside the reference plate, the base anvil is fixed.

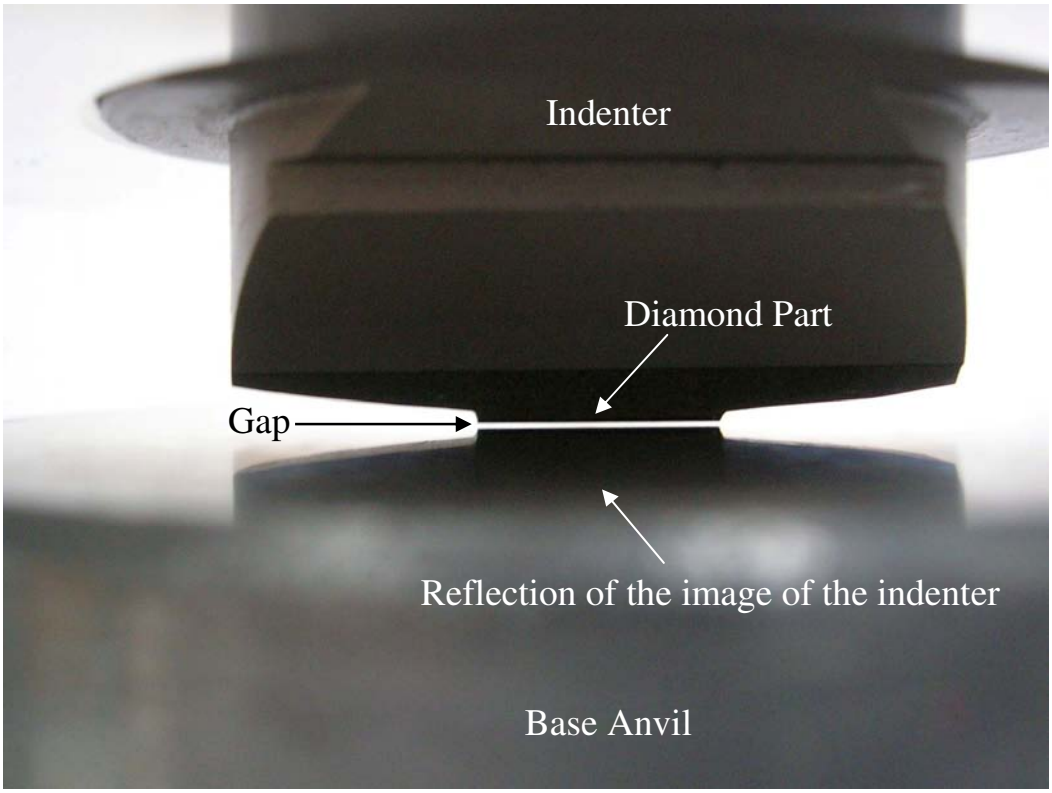

Figure 5.10 The light gap between the indenter and the base anvil during the parallelity adjustments

After fixing the base anvil, specimens are placed on to it and they are confined there by fixing the reference plate on top of them. At this point it is very important to clamp the specimens at the right orientation as the results depend on the rolling direction. While fixing the reference plate, sometimes specimens tend to turn.

Specimens are adjusted so that their clamped orientations will be correct (centered both horizontally and vertically), (Figure 5.12).

Figure 5.11 Centering tool

5.2.2 Contact Detection

As the specimen heights vary although they are ground, is not easy to determine the moment the indenter will contact the specimen.

With the first specimens preloads are used in order to detect the contact. This reduces the work that will be done while evaluating the experimental data. As the system reaches the preload, sensors are zeroed. Then just averaging the measurements of the three sensors are left to the experimenter. However, as the experimental results before reaching the preload are not recorded and the effect of these ignored values on the displacement values is not known, it is decided to go on with the raw data without using the preload option of the system. By this way, it is

made easier to have investigations, like contact point detection investigation, on the experimental data.

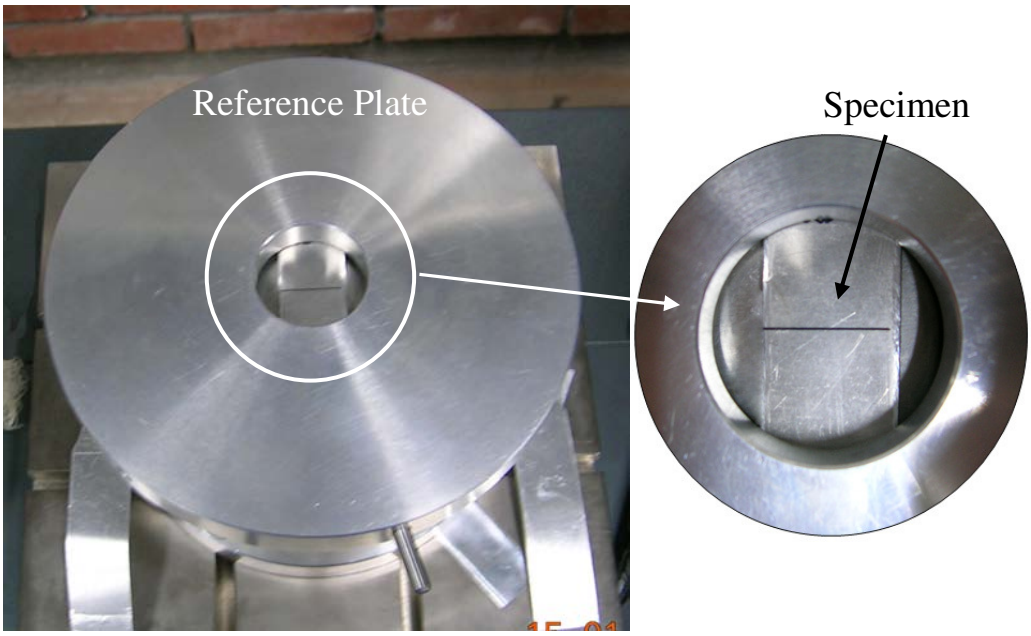

Figure 5.12 A clamped specimen

At the first systematic experiments, some basic concepts like;

- detection of the "zero point" of force-displacement curves,
- effect of surface quality
- effect of fixing of the specimens
- repeatability,

are investigated.

5.2.2.1 Detection of the "Zero Point"

Numerous experiments were performed in order to determine the "zero point" of the force-displacement curves. In Figure 5.13, beginning of a common force-displacement curve is given. As it can be seen from the Figure, first there is a

fluctuating region where the force fluctuates while the indenter is moving down. Then at some point the force increases steadily. This point is accepted as the dummy "zero point".

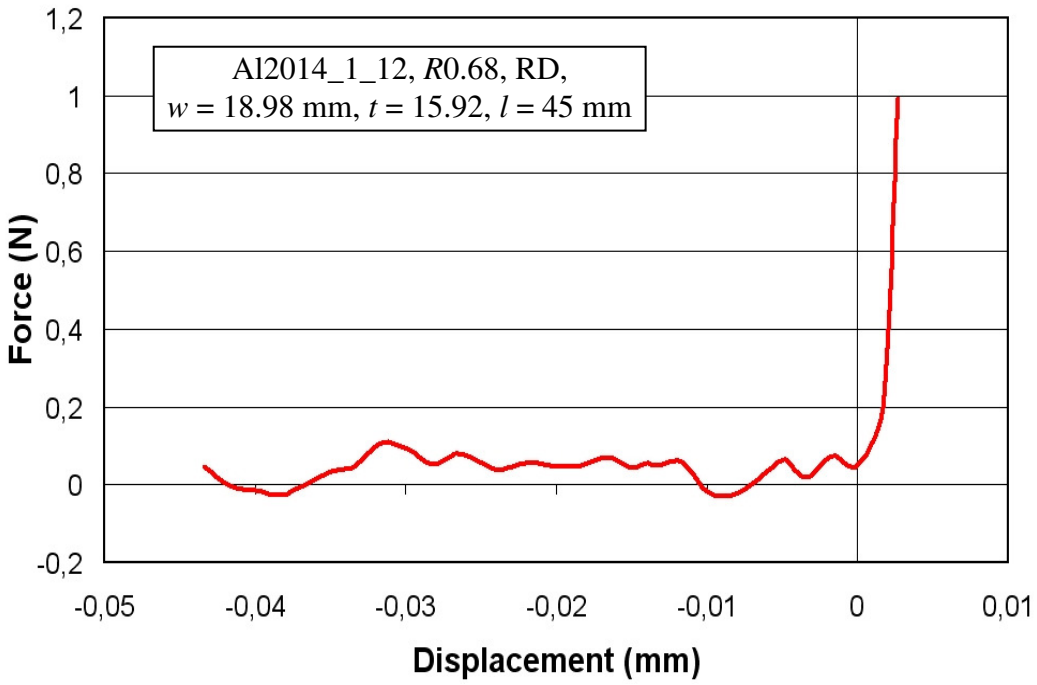

Figure 5.13 Beginning of an indentation

The beginning of the force- displacement curves are not like the ones obtained from the finite element simulations (Figure 5.14). One of the main reasons for this part is the flattening of the asperities. Another reason is that indenter is not perfectly parallel to the specimen. Although some careful precautions are taken, the grinding operation itself involves some errors as mentioned before.

When the force-displacement curves of indentations are investigated on a larger scale, Figure 5.15 is obtained. The importance of the effect of the starting region on the overall results can be easily seen in this scale. It may be said that the length of this nonlinear region changes with the amount of nonparallelity and the maximum value is determined by the surface asperities.

The unloading part of force-displacement curves can also be seen in Figure 5.15. This nonlinearity is impressive. This is mainly caused by the nonlinear contact release of the indenter radii and it is also seen in the finite element simulations.

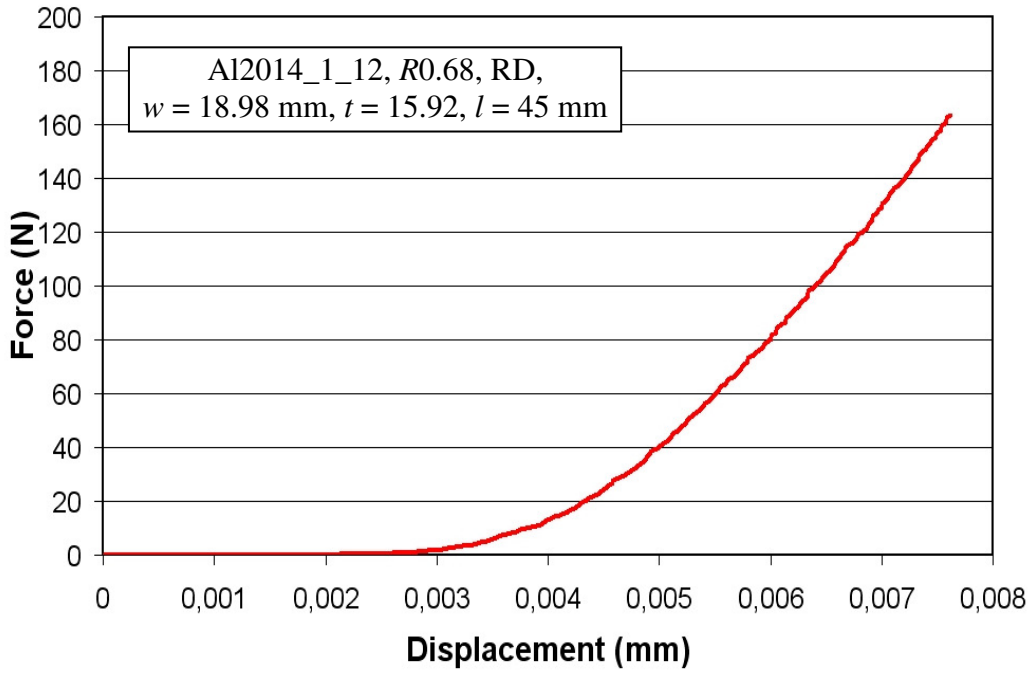

Figure 5.14 Beginning of an indentation after zeroing on a larger scale

5.2.2.2 Extrapolation Method

After trying various methods, it is decided to extrapolate the linear region to determine the "zero point". In this method, firstly the linear region is found. Then the slope of this region is calculated. Using this slope, the linear region is extrapolated and intersected with the displacement axis (Figure 5.16).

At this point, the nonlinear portion of the force-displacement curve is eliminated. Then this intersection point is moved to the zero point and the real curve is obtained (Figure 5.17).

In (Figure 5.18), 3 methods, dummy zero point, 20N preload and extrapolation methods are compared. It can be seen that with the extrapolation method, nearly the entire nonlinear region is eliminated.

Also extrapolation method improves the repeatability of the indentation experiments. In (Figure 5.19), some experiment results evaluated with different methods are compared. It is obvious that repeatability of the results after extrapolation method is higher.

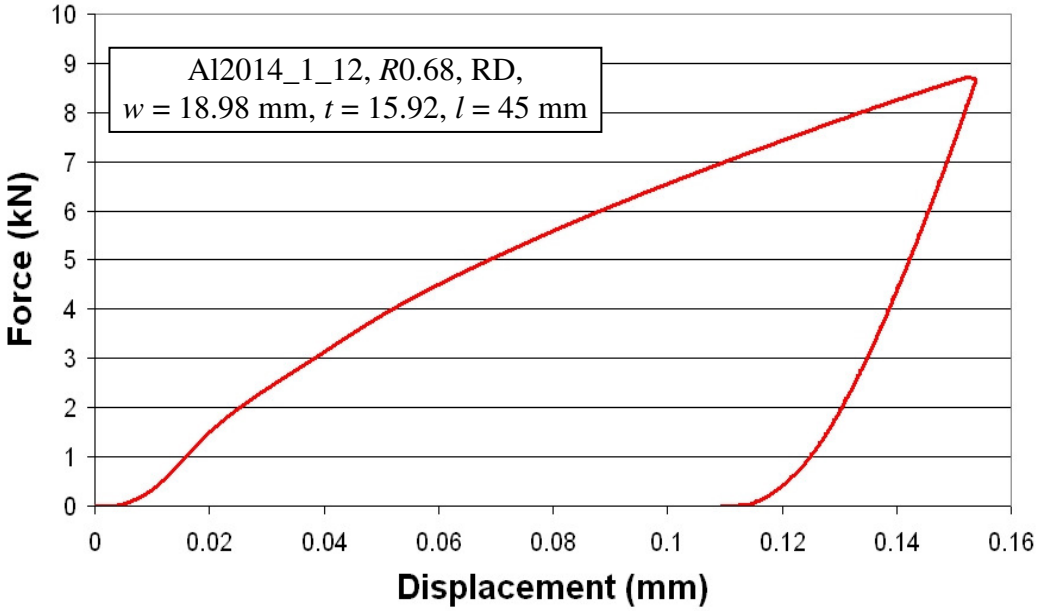

Figure 5.15 Overall indentation force-displacement curve

5.2.2.3 Effect of Surface Quality

St37 specimens are prepared in three different surface qualities (raw, milled and ground materials) as mentioned before. This gives the chance of comparing the effect of surface treatment on the results, especially on the repeatability of the results.

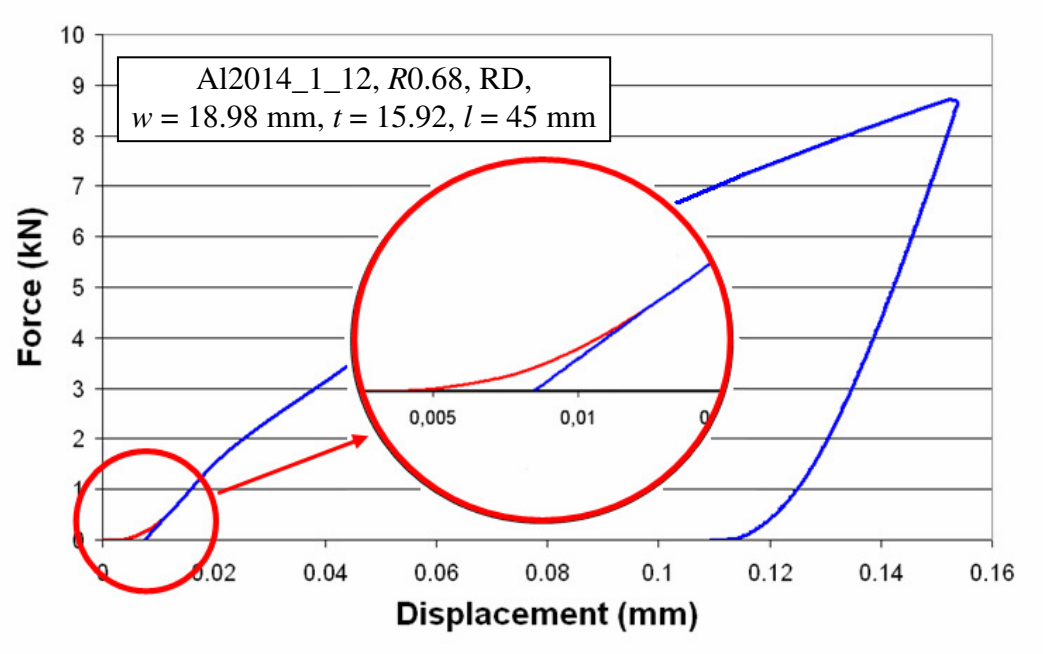

Figure 5.16 Extrapolation of the straight region

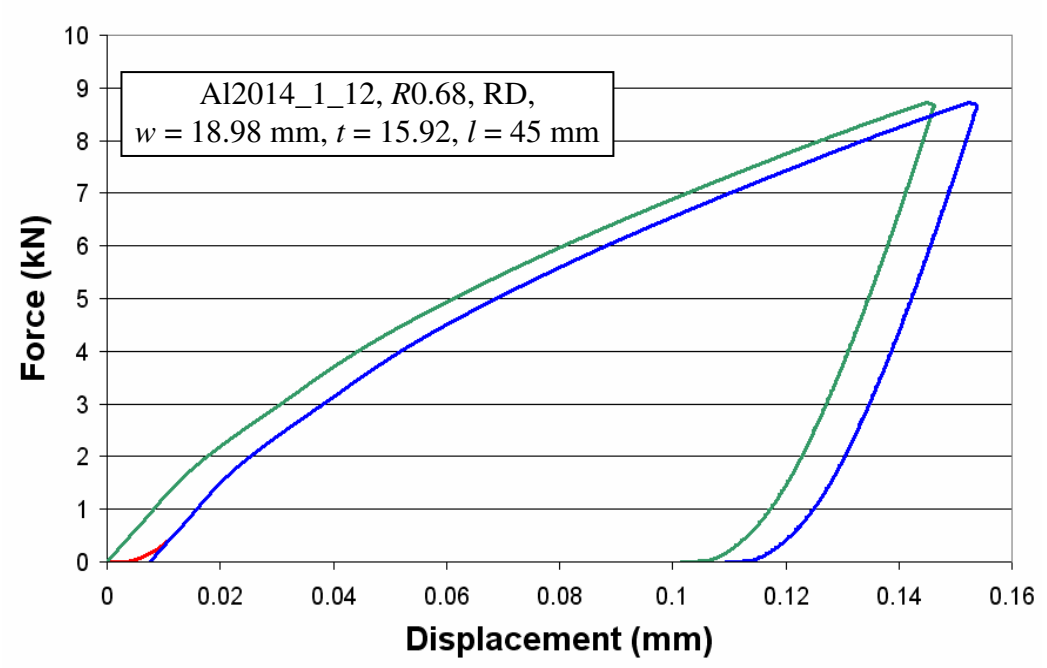

Figure 5.17 Shifting of the extrapolated curve to the zero displacement point

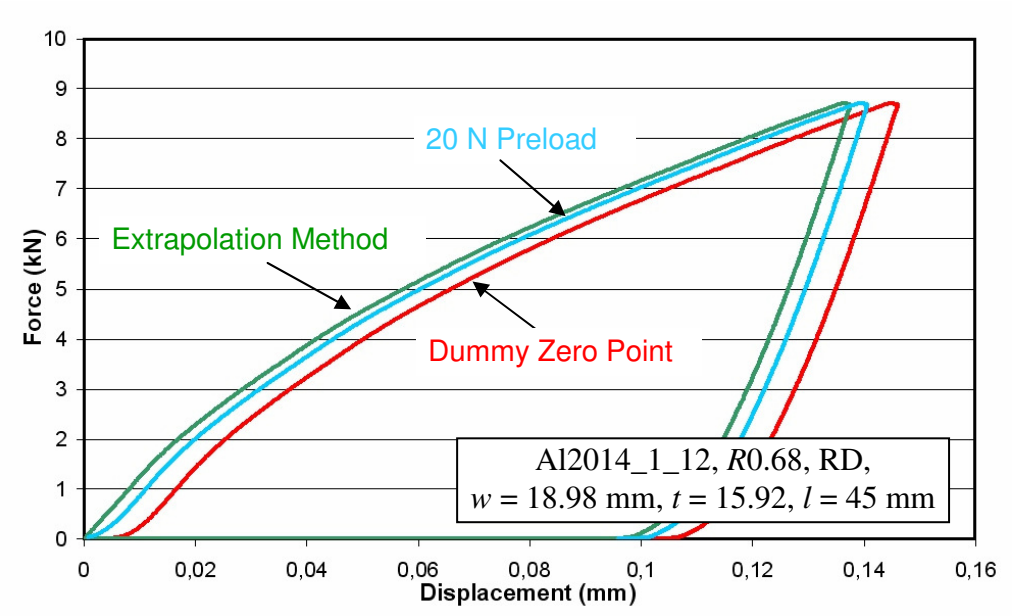

Figure 5.18 Comparison of different zeroing methods

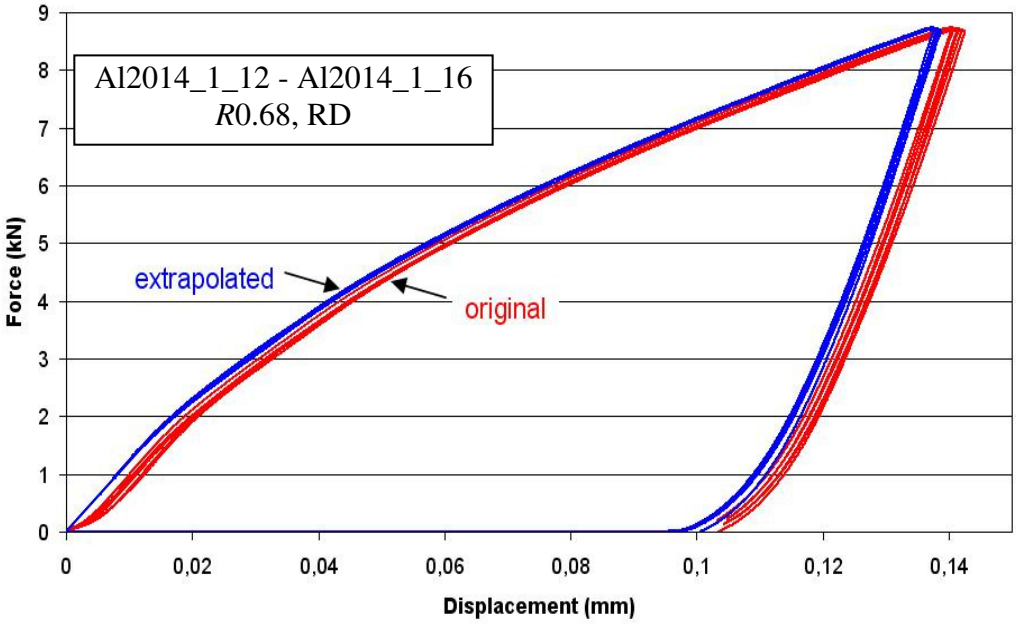

Figure 5.19 Comparison of repeatability of original curves with extrapolated curves

After completing the indentation tests on these three types of specimens, relative difference (δ_F) of the force-displacement curves are plotted (Figure 5.20). It is seen that indentations on the ground specimens have the highest repeatability (lowest spread). Therefore, it is decided to compare the results of other specimens with the ground ones.

$$\delta_F = \frac{F_{\max} - F_{\min}}{F_{\max}} \tag{5.1}$$

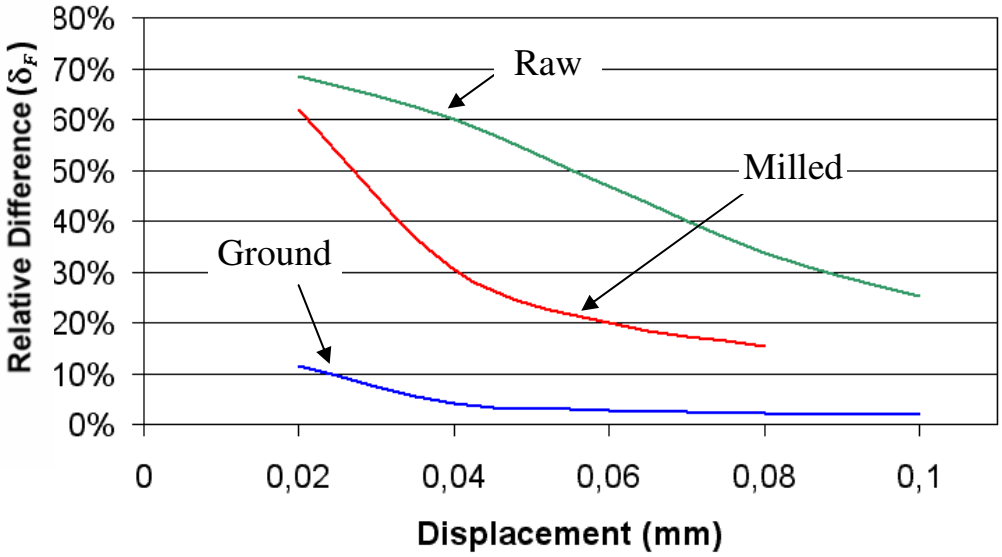

Figure 5.20 Relative difference curves for force-displacement curves obtained from indentations on specimens with different surface qualities

Force displacement curves obtained from ground specimens are given in Figure 5.21. High repeatability of the results can easily be seen. The main parameter that influences the repeatability of the results is actually the thickness difference (Δt) of the specimen (Figure 5.22). As Δt increases, the spread of the results increases so the repeatability decreases. Δt values for the ground specimens are very low (<10 μm).

This effect can be seen in the raw specimens easily (Figure 5.23). In these specimens Δt goes up to 70-80 μm. As Δt increases, the nonlinear zone at the

beginning also increases and the force-displacement curves vary from each other. The most flat specimens supply results similar to the ground specimen results (Figure 5.24).

Another parameter that defines this nonlinear part is also the amount of asperities on the indentation surface. As it can be seen in Figure 5.4 (a), on the raw specimen asperities can be seen by the naked eye. Also on the milled specimens, Figure 5.4 (b), milling traces exist that affects the results.

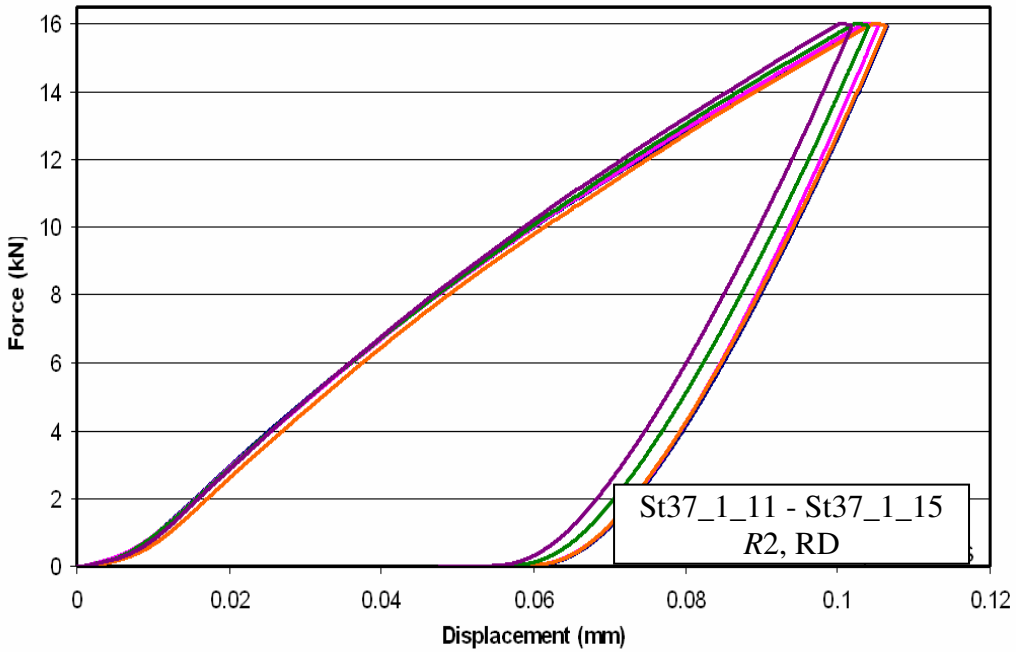

Figure 5.21 Force-displacement curves obtained from indentations on ground specimens in rolling direction (RD)

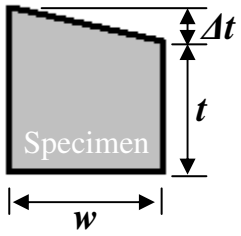

Figure 5.22 Sketch of an inclined specimen

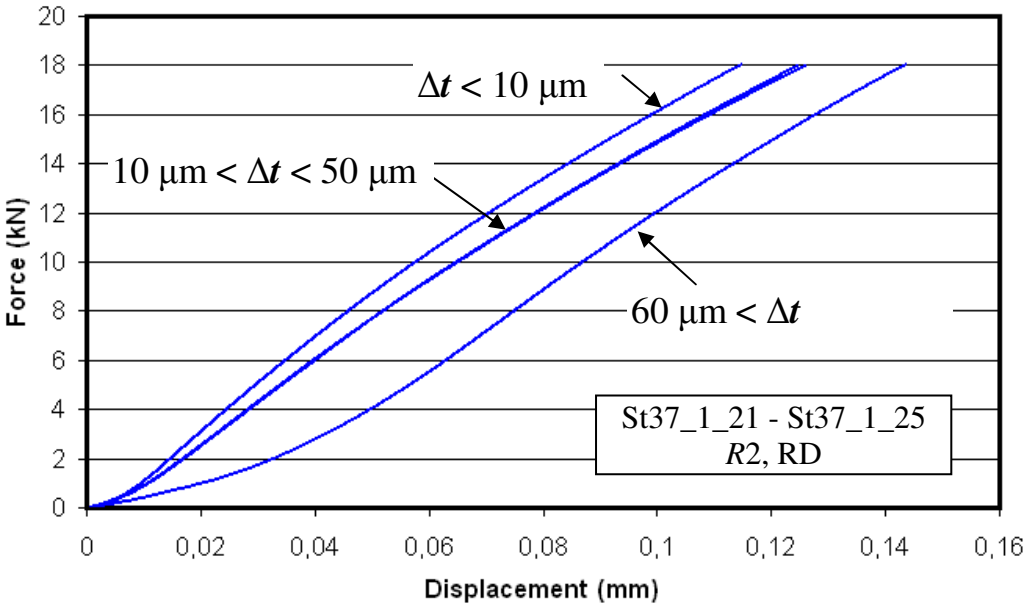

Figure 5.23 Effect of Δt on force-displacement curves obtained from indentations on raw specimens in RD

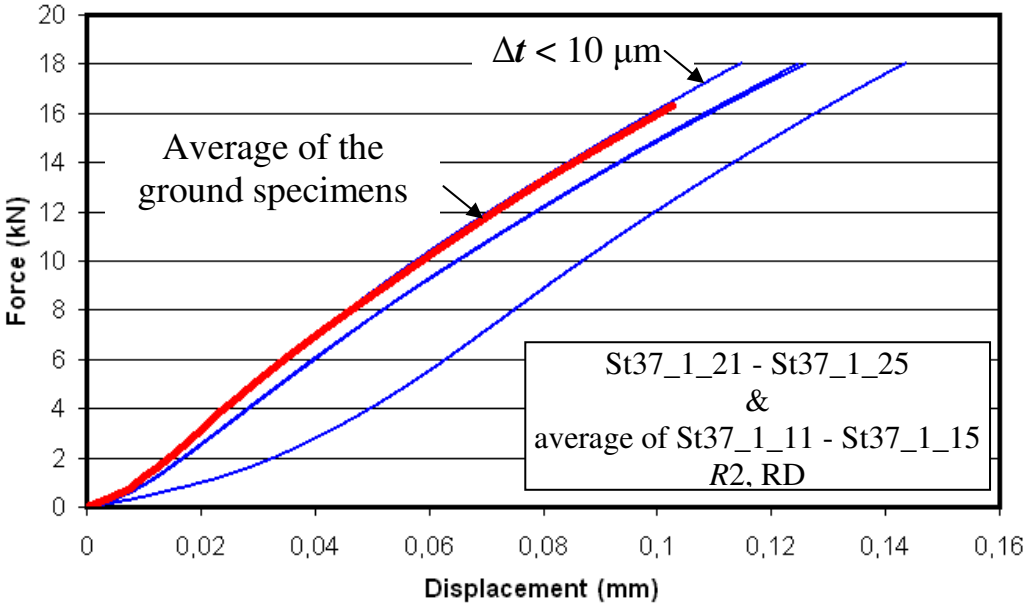

Figure 5.24 Comparison of the force-displacement curves obtained from raw specimens with the average of the ground specimens

Although the parallelity of the milled specimens are much higher than the raw specimens, still the spread can be seen that the repeatability of the results are not sufficient (Figure 5.25). Again the most parallel one gives the same result with ground ones give (Figure 5.26).

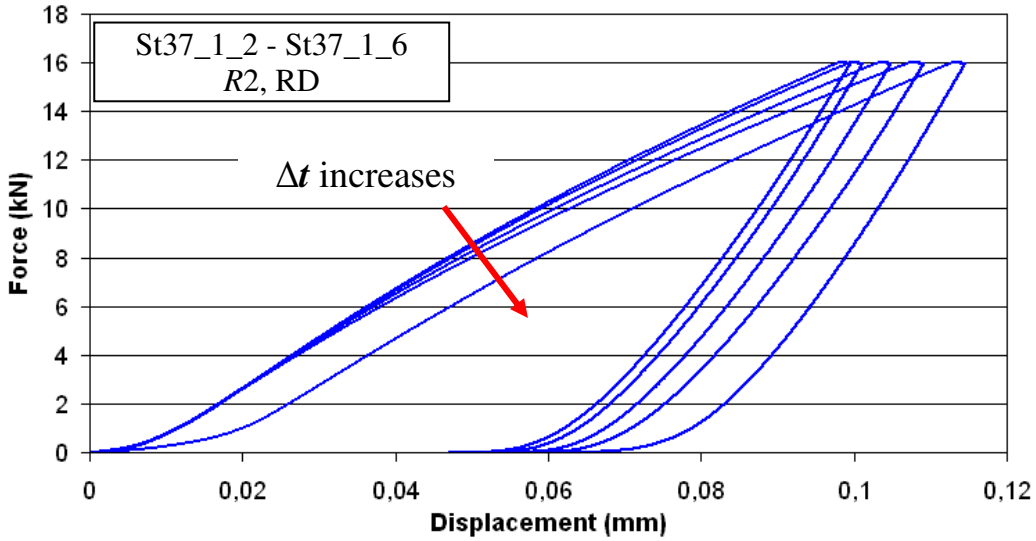

Figure 5.25 Repeatability of the indentation tests on the milled specimens

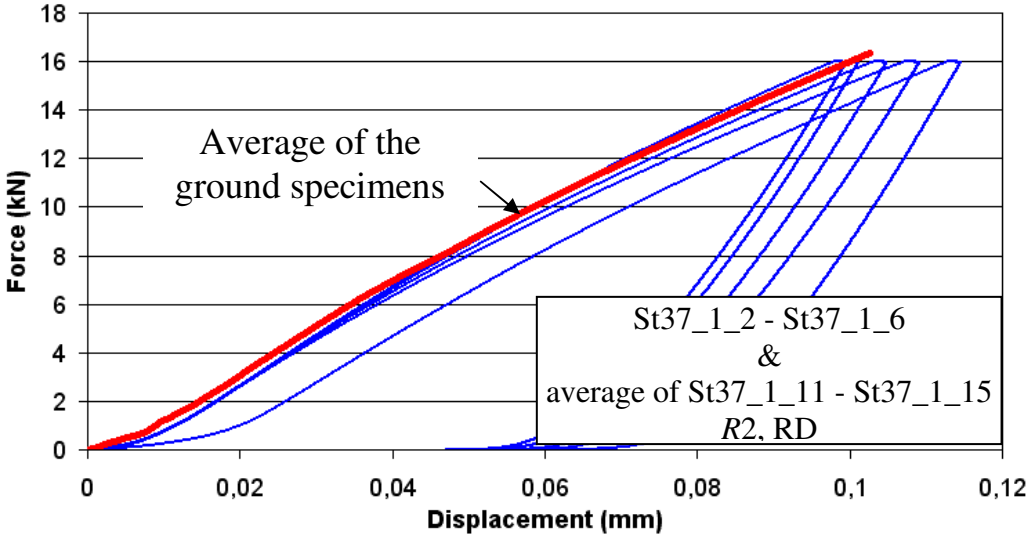

Figure 5.26 Comparison of the force-displacement curves obtained from milled specimens with the average of the ground specimens

Finally, it can be concluded that using ground specimens in the real indentation tests will be a good choice as the repeatability is higher and the results are more accurate with the ground specimens.

5.2.2.4 Effect of Clamping of the Specimens

Effect of compression is analysed by the finite element simulations in Section 4.3.3. However compressing the specimens has another effect in the real tests that it fixes the specimens.

In order to analyze this fixing, some indentation tests are conducted on specimens, which are not clamped by the reference plate. In these tests, reference plate is left a bit higher than the specimens so that the specimens are let free to move on the base anvil during the indentation.

Results of these tests are given in Figure 5.27. Although, in the finite element simulations compression do not affect the results, in the real experiments the influence is obvious. This is most probably because of the non perfect contact of the indenter to the specimen. It is seen that the compression increases the repeatability significantly. As the indenter does not enter the specimen exactly perpendicular, it tries to slide it on the base anvil. When the specimens are clamped by the indenter, this sliding is not possible so that results are more reliable.

5.2.2.5 Conclusion of the Preliminary Tests

At the end of the preliminary tests, basics of the experimental setup and the testing method are taken in. Before starting the real indentation tests to capture anisotropic behaviour of the materials, it is better to conclude what has been done and what has been decided.

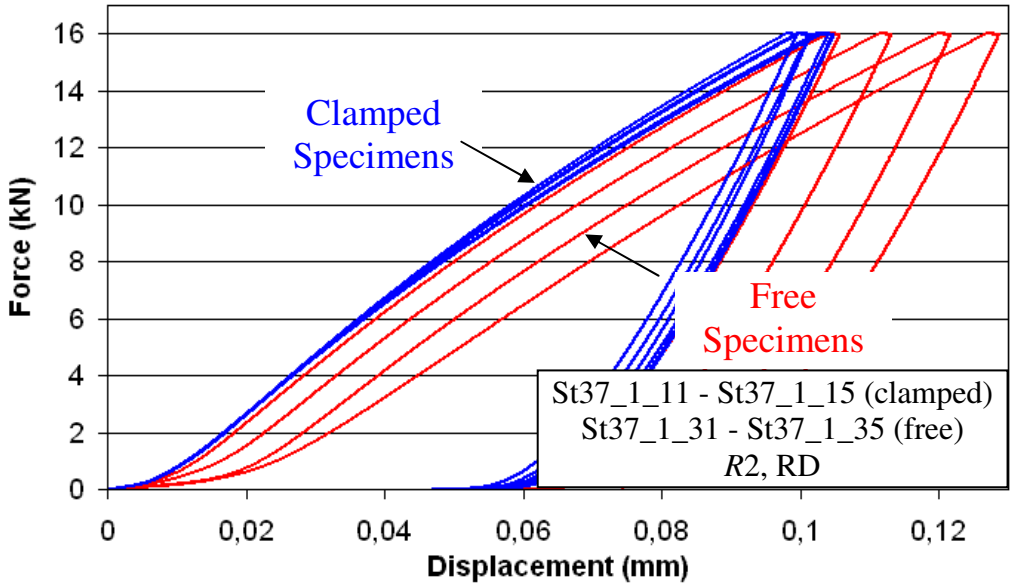

Figure 5.27 Comparison of the force-displacement curves obtained from the indentation tests with fixed specimens and with free specimens

During the preliminary tests, it is concluded that extrapolation method is the most suitable method for having high repeatability. However, after seeing the effect of fixing of the specimens on the results, it is better to go on with the raw data. Main reason for this is that effect of anisotropy on the nonlinear beginning is actually not known. By wiping out this part, the anisotropy influence might have been also ignored. Moreover, the inverse analysis program written by the research partners at Chemnitz uses the derivative of the force-displacement curves in the plastic deformation part. This means that the beginning of the curves would not affect the anisotropy coefficients found by the program as long as those parts remain elastic and the indentation results have high repeatability and accuracy.

In addition to this, ground specimens are going to be used in the experiments and specimen orientations will be adjusted carefully before starting the indentations.

5.3 Indentation Tests

The experiments to determine the anisotropy effect are performed on St37 and Al5086 specimens. Results of these tests are presented in the following sections. Also width and thickness effects seen in finite element simulations in Chapter 4 are verified by experiments.

5.3.1 Indentations on St37 Specimens

Indention tests on St37 specimens are made in three orthogonal directions (RD, TRD and PRD). Ground specimens are used in these tests. Results of these can be seen in Figures 5.20, 5.27 and 5.28. Four or five specimens are used for each direction and then, an average of these tests is taken to be able to compare force-displacement curves in the three orthogonal directions (Figure 5.30).

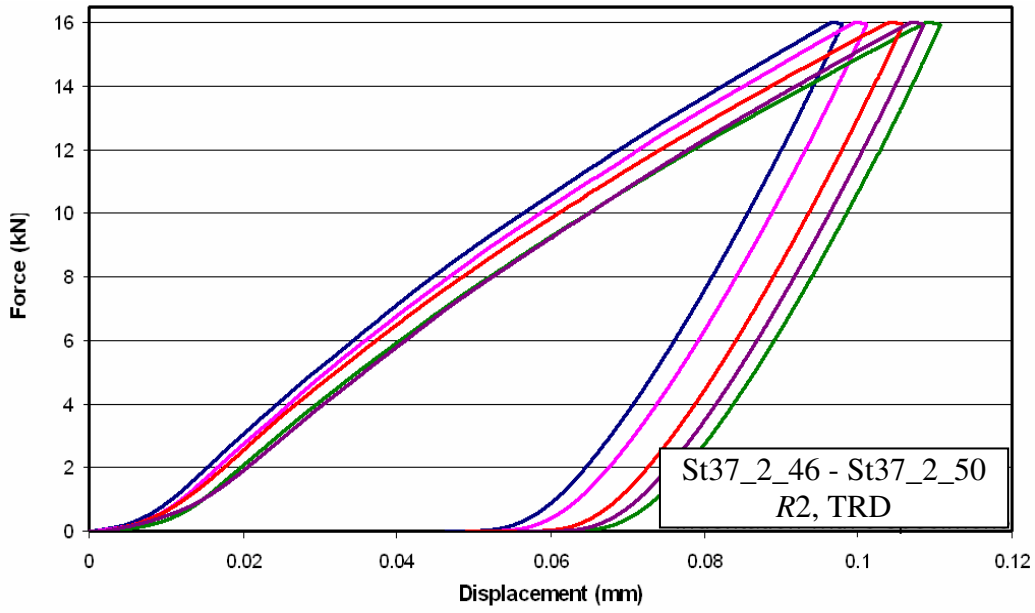

Figure 5.28 Force-displacement curves obtained from indentations on St37 specimens in transverse to rolling direction (TRD)

Repeatabilities of the curves are high except the curves obtained from the specimens in TRD. Most probably, the surface conditions of the specimens in that direction are not perfect and this causes the spread.

Some difference between the curves can be observed but it is not significant. Relative difference (δ_F) of the force-displacement curves in RD and TRD can be seen in Figure 5.31. The difference that should be looked at is after 20 μm, up to which flattening of the asperities or the inclined surface effects ends. It can be seen that difference between the curves is less than 10 percent and vanishes very quickly.

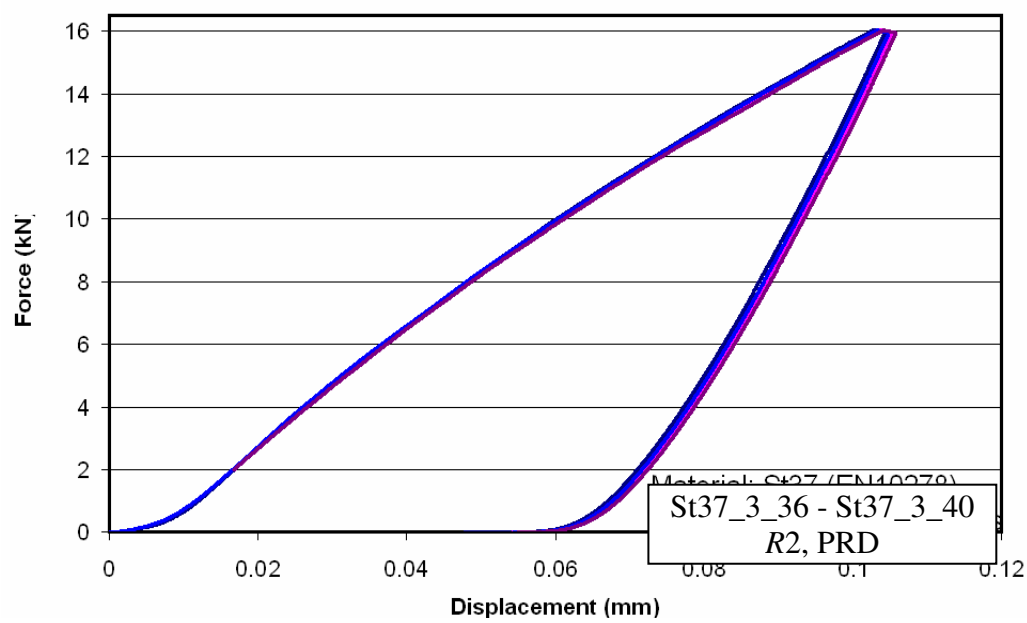

Figure 5.29 Force-displacement curves obtained from indentations on St37 specimens in perpendicular to rolling direction (PRD)

Not seeing a significant difference might have two reasons. Either the material is not highly anisotropic or the experimental method is not capable of capturing the anisotropy. So it is decided to determine the flow curves of the material in the orthogonal directions in order to determine the amount of anisotropy. For this purpose the available setup is used to conduct compression tests. Results of these tests are presented in Chapter 6.

5.3.2 Indentations on Al5086 Specimens

Completing the indentations on St37 specimens and observing no significant difference, it is decided to conduct indentations on a thin plate where the anisotropy

might be higher. By this way the ability of the experimental procedure to determine the anisotropy effect on the force displacement curves will be verified.

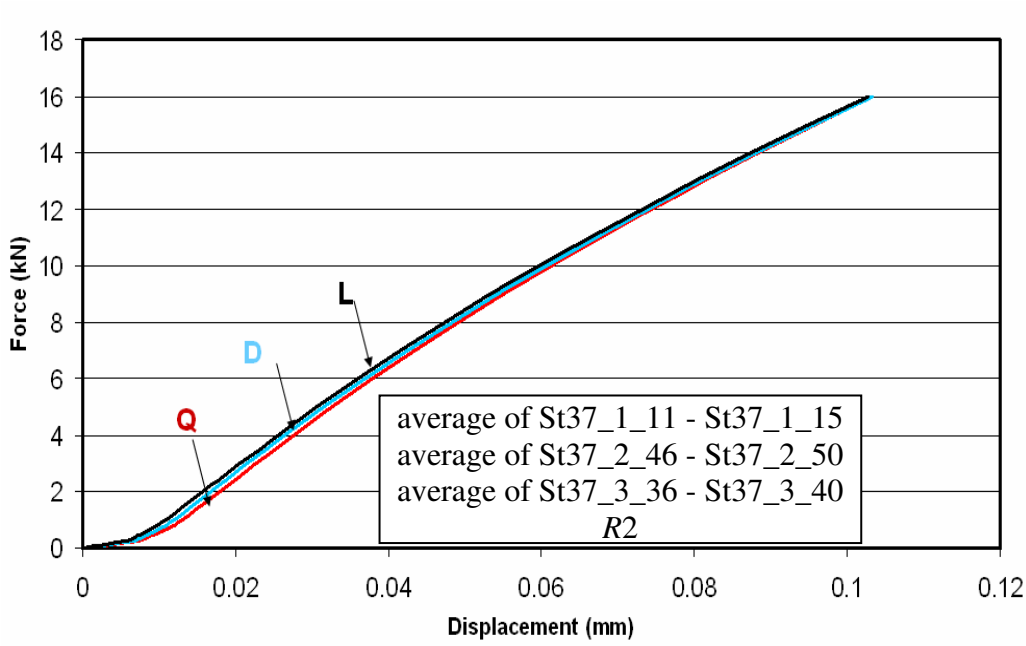

Figure 5.30 Comparison of force-displacement curves obtained from indentations on St37 specimens in three orthogonal directions

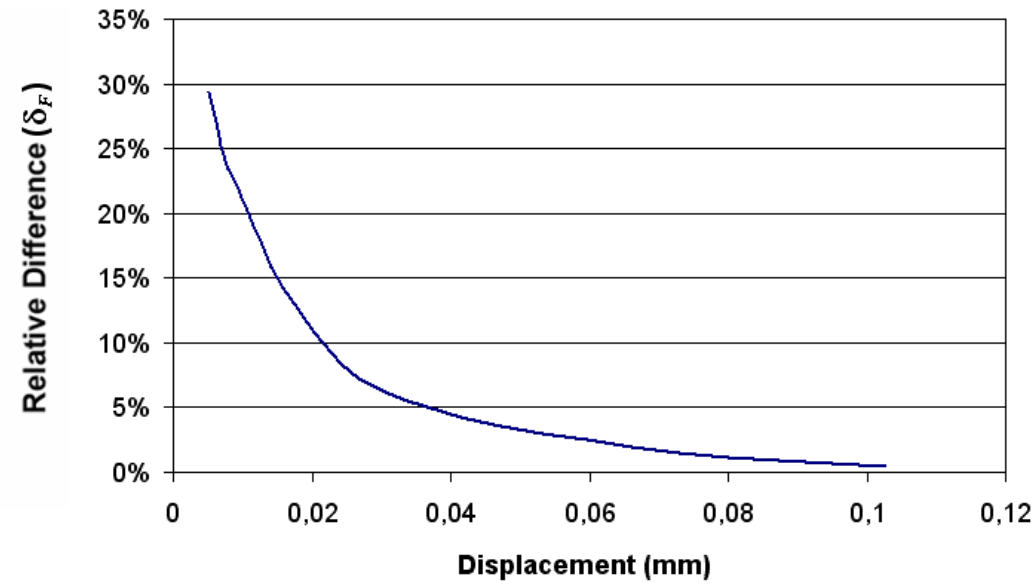

Figure 5.31 Relative difference of force-displacement curves obtained from indentations on St37 specimens in RD and TRD

For this reason an Al5086 plate is bought and as it can be seen in Figure 5.7, it turned out to be anisotropic. After making sure that anisotropy exists on the material, indentation tests are made in two orthogonal directions (RD and TRD).

For these tests, four or five specimens are used in each direction. Results of these indentations can be seen in Figure 5.32 and 5.33. Then averages of these tests are compared (Figure 5.34).

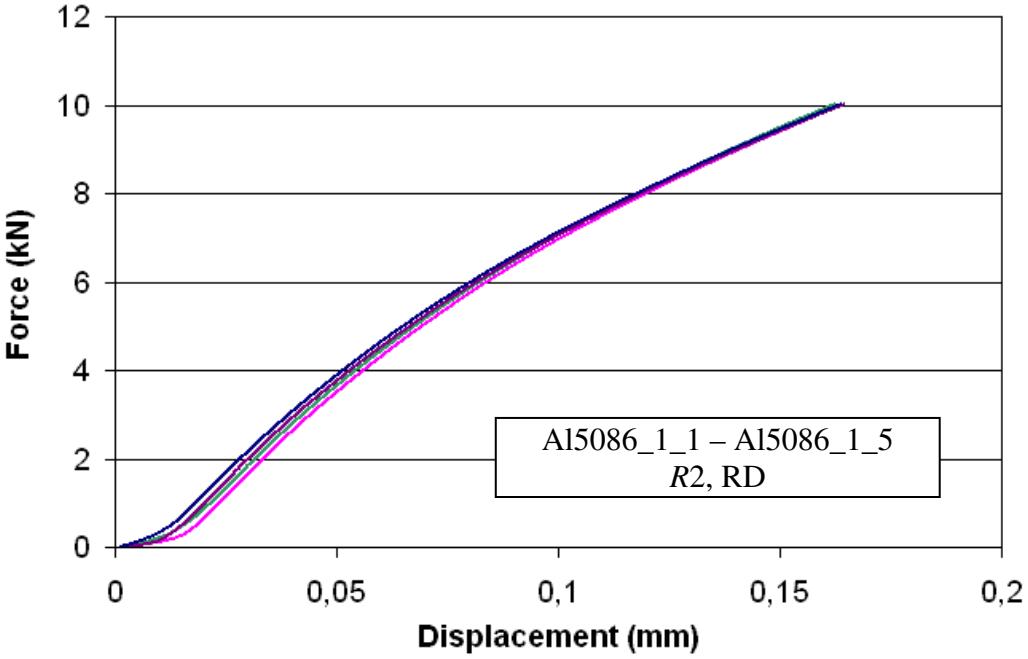

Figure 5.32 Force-displacement curves obtained from indentations on Al5086 specimens in rolling direction (RD)

It can be seen in Figure 5.34 that in Al5086 anisotropy effect is obvious. Figure 5.35 shows the relative difference (δ_F) between the force-displacement curves in RD and TRD. It is seen that the difference between the curves is less than 40 percent but always more than 5 percent after 20 μm of indentation.

5.3.3 Conclusions on Indentation Tests

Although in St37 specimens, anisotropy is hardly seen, it is obvious that experimental method works as it is successful in detecting the anisotropy in the

Al5086 specimens. Most probably the problem with the St37 specimens is that anisotropy is not really present in them.

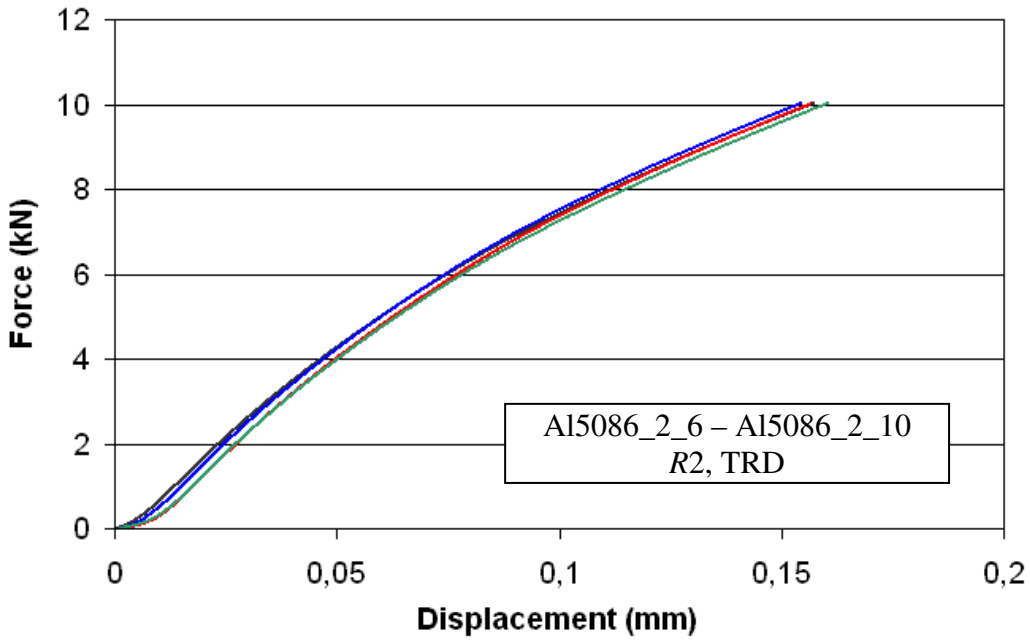

Figure 5.33 Force-displacement curves obtained from indentations on Al5086 specimens in transverse to rolling direction (TRD)

It is not possible to compare the amount of anisotropy in these two materials by using the relative difference graphs since total amount of indentations are different. For the St37 it is possible to indent up to 18000 N but for the Al5086 indentations must stop before reaching 160 μm in order not to damage the diamond tip of the indenter. However, it is possible to compare these graphs by first making the displacements dimensionless (Figure 5.36). To do this, the amount of displacements must be divided by the maximum indentation depth (Table 5.4).

$$\Delta^* = \frac{\Delta}{\Delta_{max}} \tag{5.2}$$

From Figure 5.36, it can be concluded that the Al5086 specimens are more anisotropic than the St37 specimens.

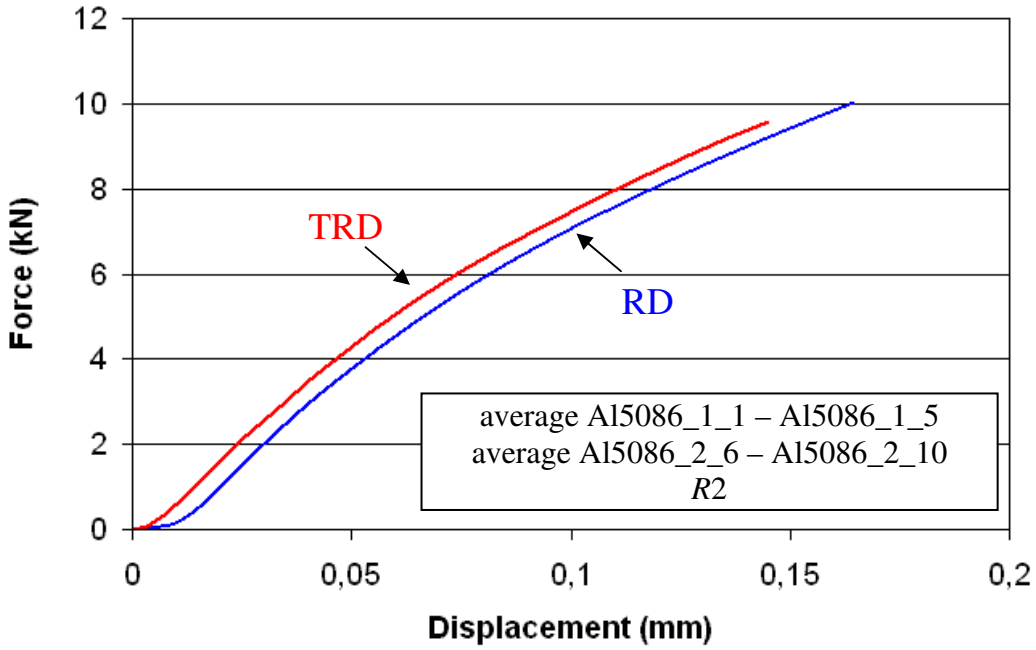

Figure 5.34 Comparison of force-displacement curves obtained from indentations on Al5086 specimens in RD and TRD

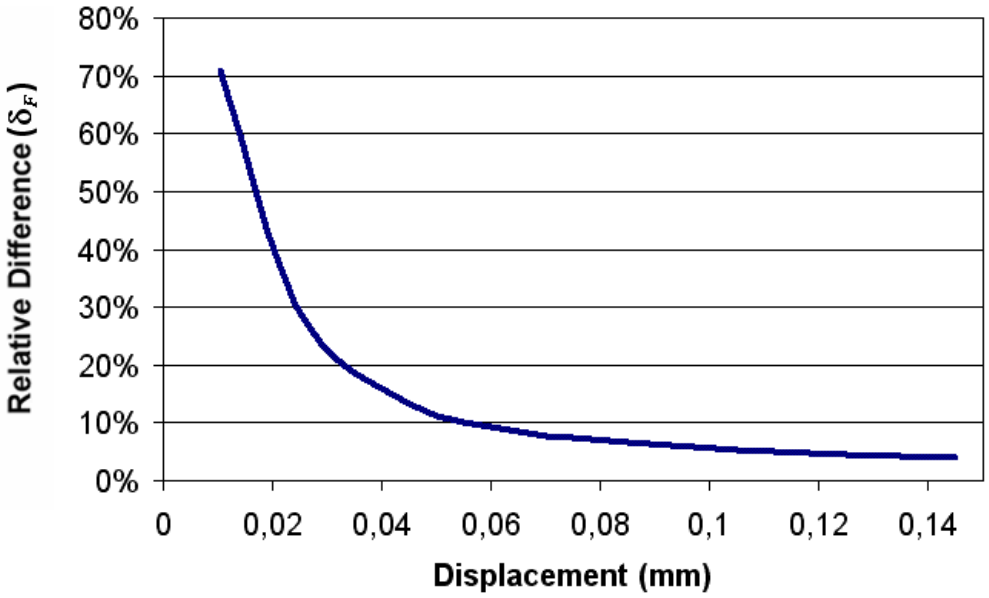

Figure 5.35 Relative difference of force-displacement curves obtained from indentations on Al5086 specimens in RD and TRD

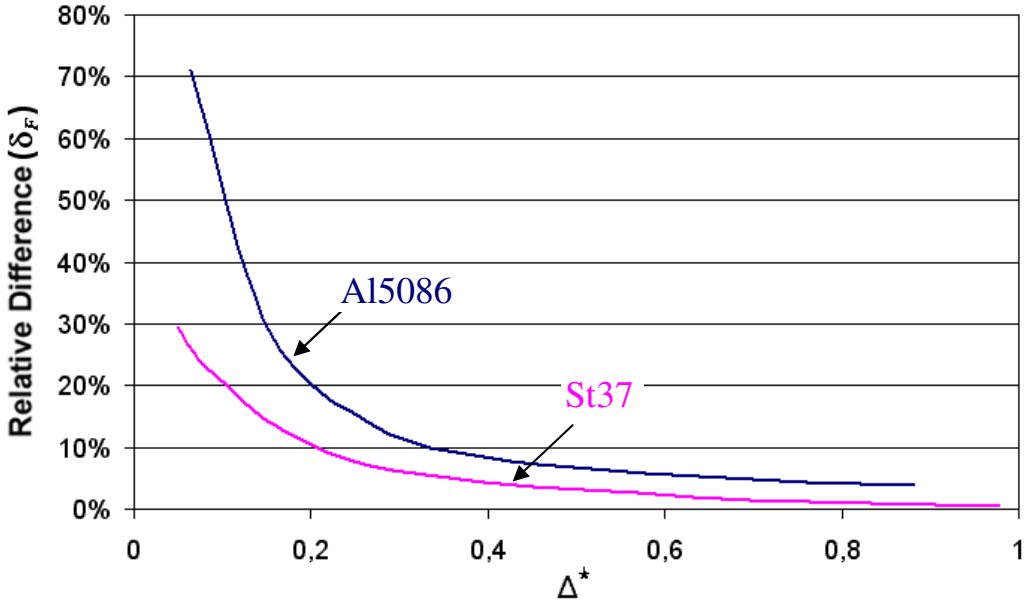

Figure 5.36 Comparison of the relative difference curves obtained from indentations on St37 and Al5086 specimens

Table 5.4 Maximum indentation depths for St37 and Al5086 specimens

	Max. Indentation Depth (mm)
St37	0,105
Al5086	0,160

5.3.4 Verification Of Finite Element Results On Specimen Dimensions

It desired to verify the specimen width and specimen thickness effects on the force-displacement curves observed in finite element simulations in Chapter 4. For this reason indentation tests are conducted on specimens with different width (Figure 5.37) and thickness (Figure 5.38) values. It is not possible to verify length effect as it is not possible to clamp specimens with lengths smaller than 32 mm.

Indentation tests on specimens with different width values resulted force-displacement curves similar to the finite element results (Figure 4.16). By increasing widths, forces increase (5.37).

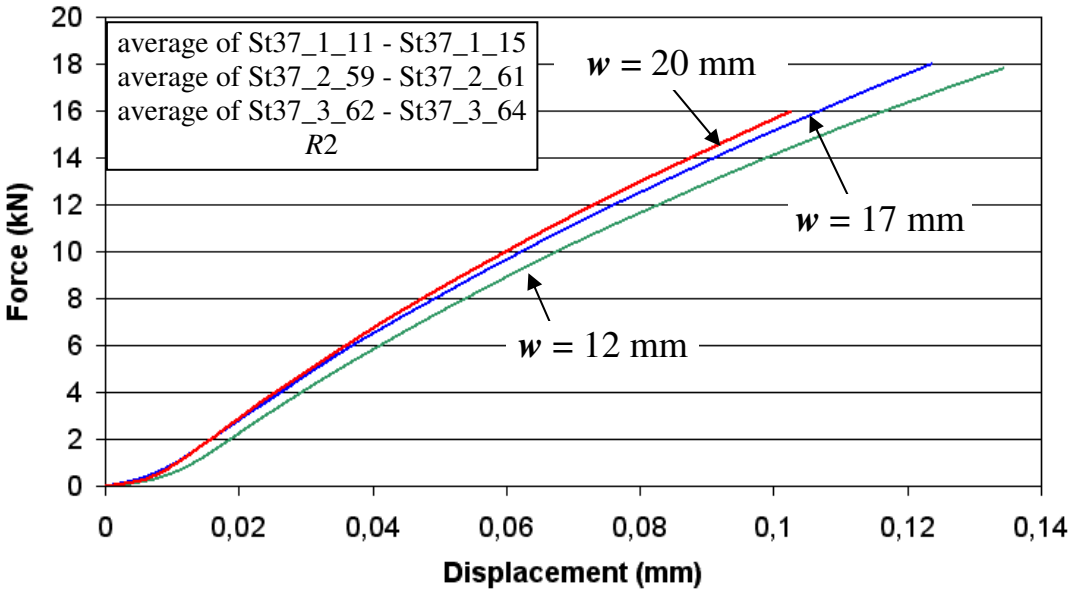

Figure 5.37 Comparison of averages of force-displacement curves obtained from indentations on specimens with different widths

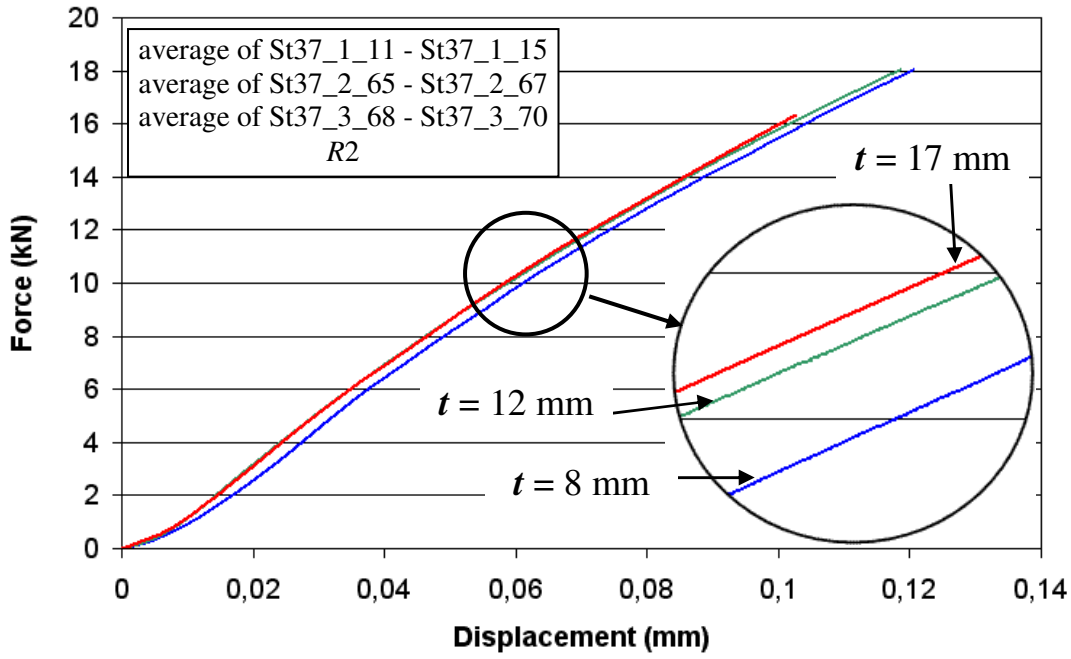

Figure 5.38 Comparison of averages of force-displacement curves obtained from indentations on specimens with different thicknesses

Thickness affect analyzed by finite element simulations (Figure 4.21) is also verified by tests. Three specimen sets with different thicknesses are indented. Results clearly show the saturation region and the increase of forces by increasing thicknesses (Figure 5.38).

CHAPTER 6

COMPRESSION TESTS

In this chapter the specimens and the results of the compression tests are supplied and the results are evaluated. Main aim of the compression test is to determine the flow curves of the St37 material used in the indentation tests. Then by comparing the flow curves obtained by compression tests in different directions, the amount of anisotropy will be found out.

Also compression tests are made on materials whose flow properties are known to verify the capabilities of the setup.

6.1 Experimental Setup

The experimental setup used in the indentations is also used for the compression tests with one tool change. The indenter is replaced with a flat punch (Figure 6.1).

This compression punch consists of two parts (Figure 6.2). First one is the steel casing, which has an extension at the bottom to be mounted to the measurement system. The second part is made of hardened steel. It is in contact with the specimens during the compression. This hardened steel part is mounted to the steel casing.

Punch speed is selected to be 1 mm/min.

Figure 6.1 Compression punch

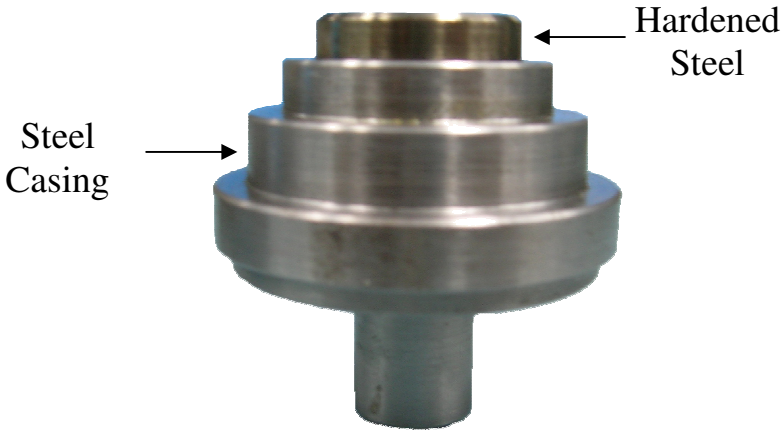

Figure 6.2 Parts of the compression punch

6.2 Specimens

Two different materials are compressed in order to determine their flow curves;

- St37
- 100Cr6

6.2.1 St37 Specimens

Main aim of the compression tests is to determine the anisotropy of the St37 specimens used in the indentation tests. As it can be seen in Section 5.3.1, force-displacement curves, obtained from indentations made in the three orthogonal directions, are not significantly different than each other. Although the desire to learn the flow characteristics of the St37 plate has started before the indentations took place, because of the unexpected indentation results the importance of the compression tests increased greatly. By these tests, also information about the sensitivity of the measurement system and the method are gained.

In the compression tests of St37, two types of specimens are used (Figure 6.3);

- Square prismatic specimens
- Cylindrical specimens.

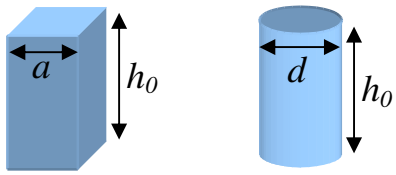

Figure 6.3 Sketches of the prismatic and the cylindrical specimens

Dimensions of these specimens are decided according to the load limits of the Zwick press. The press has a maximum loading capability of 2 tons. In order to protect the press maximum load used in the experiments is 18 kN. It is wanted to see maximum amount of flow. It is decided to have plastic deformation for 10 kN so the yielding must start at 8 kN. Taking initial yield stress as 300 MPa, the area needed will be 26.67 mm^2. According to this, specimen dimensions are decided as follows;

- For square cross sectioned specimens: $a = 5$ mm, $h_0 = 8$ mm^2
- For circular cross sectioned specimens: $d = 5$ mm, $h_0 = 5$ mm^2

To manufacture the compression test specimens firstly steel strips are cut from the St37 plate in three orthogonal directions. Two surfaces, which will contact the dies of the press, are ground. Then in the machine shop square specimens are cut from steel strip. For the cylindrical specimens, these strips are turned to the final dimensions.

6.2.2 100Cr6 Specimens

After completing the compression tests on prismatic St37 specimens, it is wanted to verify the compression test results and the method with a material with a know flow curve. Therefore, 100Cr6 specimens are manufactured at ORS Bearing Company, which has an extensive flow curve data for this material.

For 100Cr6, only cylindrical specimens (Figure 6.4) are made with the diameters specified for St37 specimens. Heights of the specimens are selected to be 8 mm.

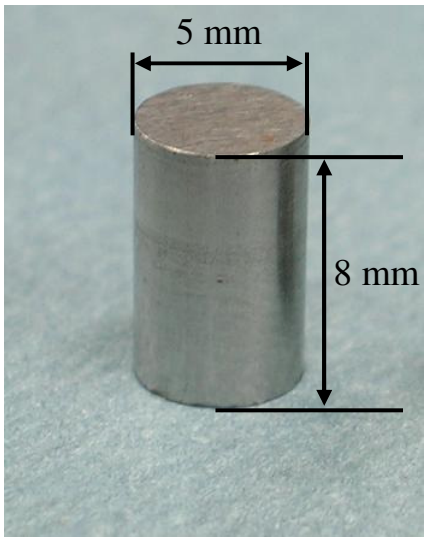

Figure 6.4 Picture of a 100Cr6 specimen

6.3 Compression Test Results for Prismatic St37 Specimens

The procedure to evaluate the compression test results starts with plotting the force-displacement curves. The curves are corrected with the extrapolation method, explained in Section 5.2.2, (Figure 6.5). Then it is followed by the calculation of the engineering stress-strain values and the true stress-strain values.

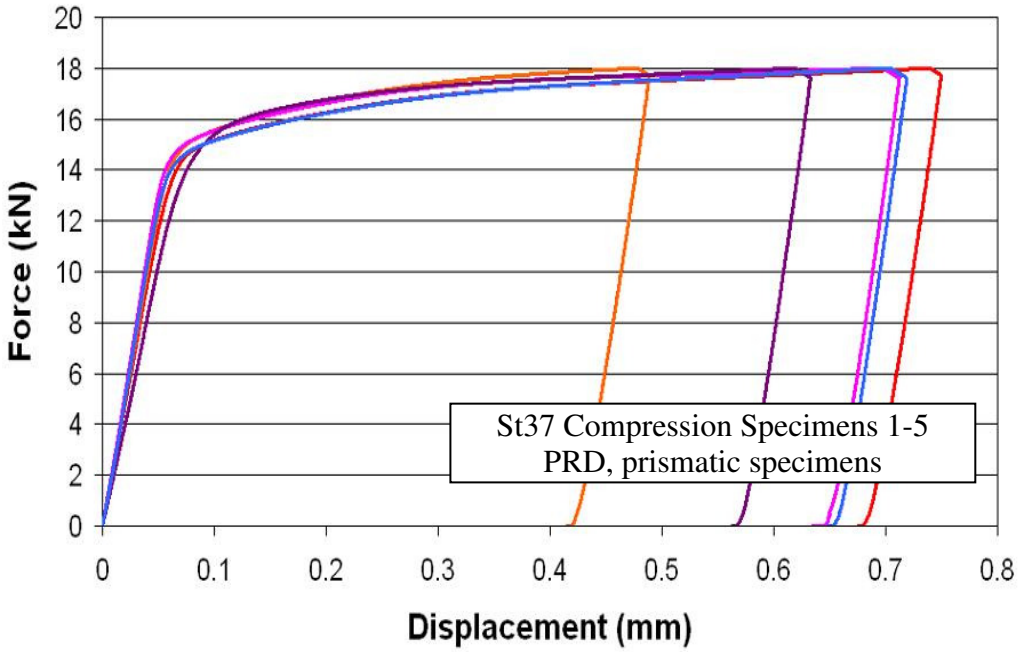

Figure 6.5 Force-displacement curves, corrected by extrapolation method, obtained from compression tests of St37 specimens in PRD

6.3.1 Engineering Stress-Strain Curves for Prismatic St37 Specimens

Firstly, engineering stress- strain values are calculated using the initial dimensions.

$$\varepsilon_{eng}(\Delta) = \frac{\Delta}{h_0} \tag{6.1}$$

$$\sigma_{eng}(\Delta) = \frac{F(\Delta)}{A_0} \tag{6.2}$$

where h_0 and A_0 are the initial height and the area of the specimens respectively.

Then the elastic moduli (E) of the curves are determined by computing the slope of the linear part of the curves. Determination of E is very important as it is the only mechanical property that is almost constant for any St37 batch. So by checking E value, overall experiment might also be verified, at least the elastic part. After the first tests on the St37 specimens, it is seen that the E values, obtained from the engineering stress-strain curves, are very small when compared to expected E values (~200 GPa), (Figure 6.6).

This might have two possible reasons. Either the forces are measured low or the displacements are measured high. As the load cell is calibrated and there is no reason for it to display lower forces, it is decided that the displacements are measured wrong. Mainly elastic deformations of the system cause this problem.

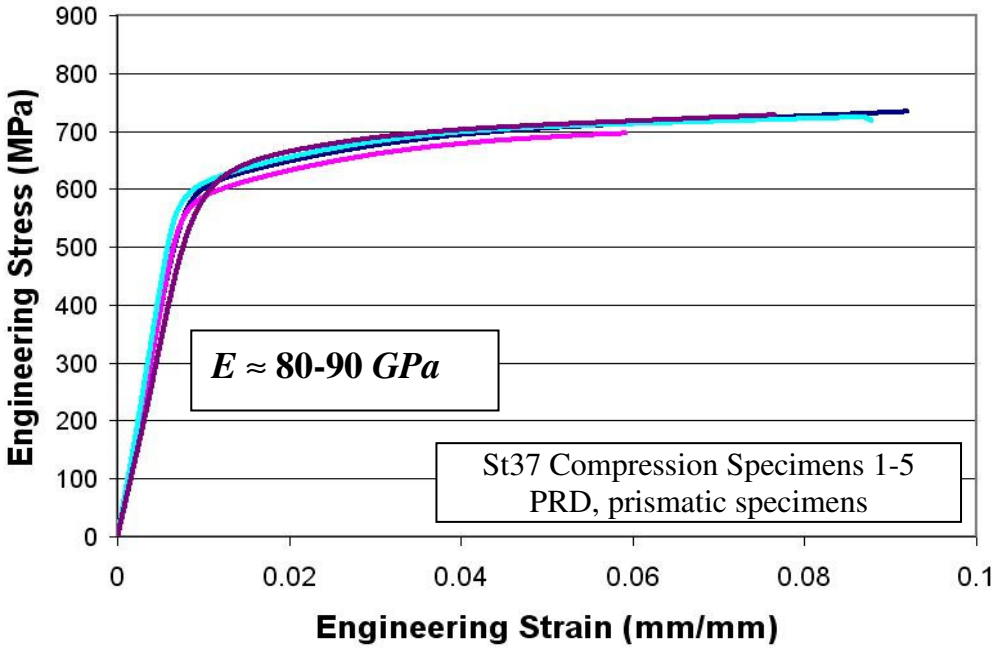

Figure 6.6 Engineering stress-strain curves calculated from the compression tests of St37 specimens in PRD

6.3.1.1 Stiffness of the System

In order to determine the stiffness of the setup (k_s), compression tests are repeated without putting any specimen between the punch and the base anvil. So the system compresses itself and it's deformation of is recorded (Figure 6.7). Figure 6.7 shows the force-displacement curves for three compressions. As the places of the transducers are changed before the third compression test, results of this test is away from the others. However when a linear line is fitted to these force-displacement curves, stiffness of the setup is calculated as k_s = 408 kN/mm for the curves (regression coefficient for the fitted lines is approximately 0.994).

Displacement values, measured in the compression tests, are then corrected with this k_s value.

$$\Delta_{corr} = \Delta - \frac{F}{k_s} \tag{6.3}$$

where Δ is the measured displacement and F is the measured force. When the corrected force displacement curves are analyzed, it is seen that the new E values are as expected (Figure 6.8).

6.3.2 True Stress-Strain Curves for Prismatic St37 Specimens

After obtaining the correct engineering stress-strain curves, true stress-strain values are calculated using Eq.(2.17) and (2.20), Figure 6.9. When the curves are plotted and analyzed on a larger scale, it is seen that calculated flow stresses are decreasing after some point (Figure 6.10). This is not something expected for such a steel at room temperature.

This unexpected drop is discussed in details. First it is thought that this might be because of a systematical error. However, no trace of such an error is found in the investigations.

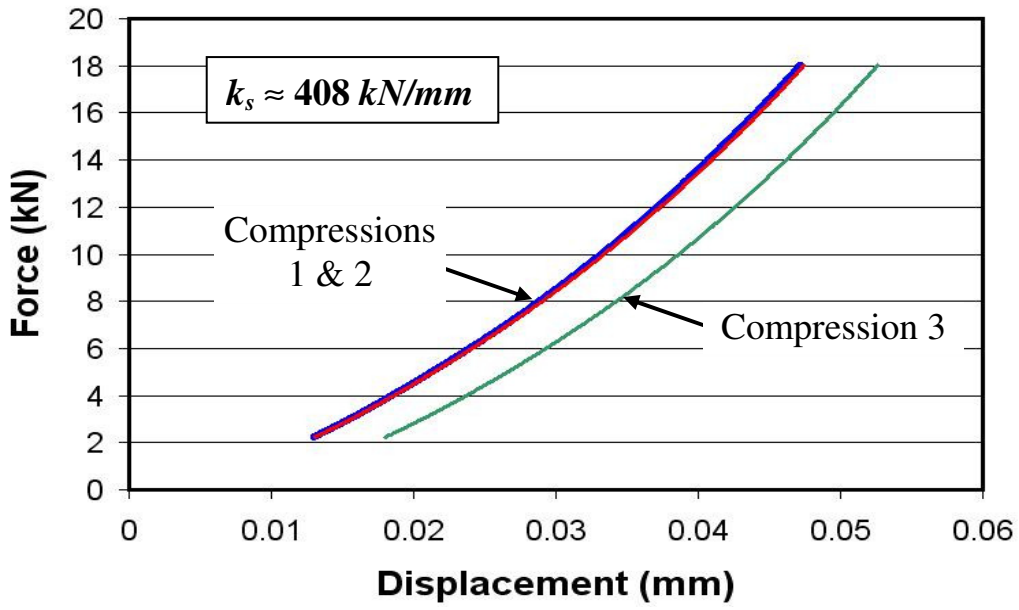

Figure 6.7 Stiffness of the system

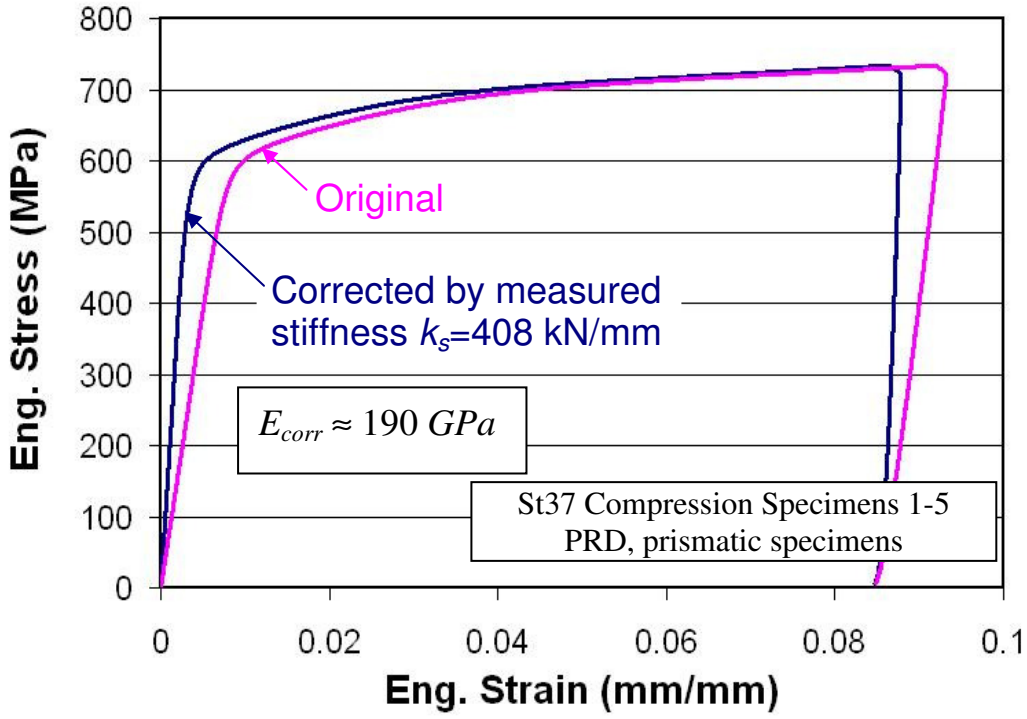

Figure 6.8 Corrected engineering stress-strain curves for St37 in PRD

Then effect of friction and geometrical uncertainties are analyzed in Chapter 5 of [42]. However, none of them causes such drops in the true stresses.

At this point it is decided not to go on with the specimens in other directions but to make tests on a material whose flow curves are known.

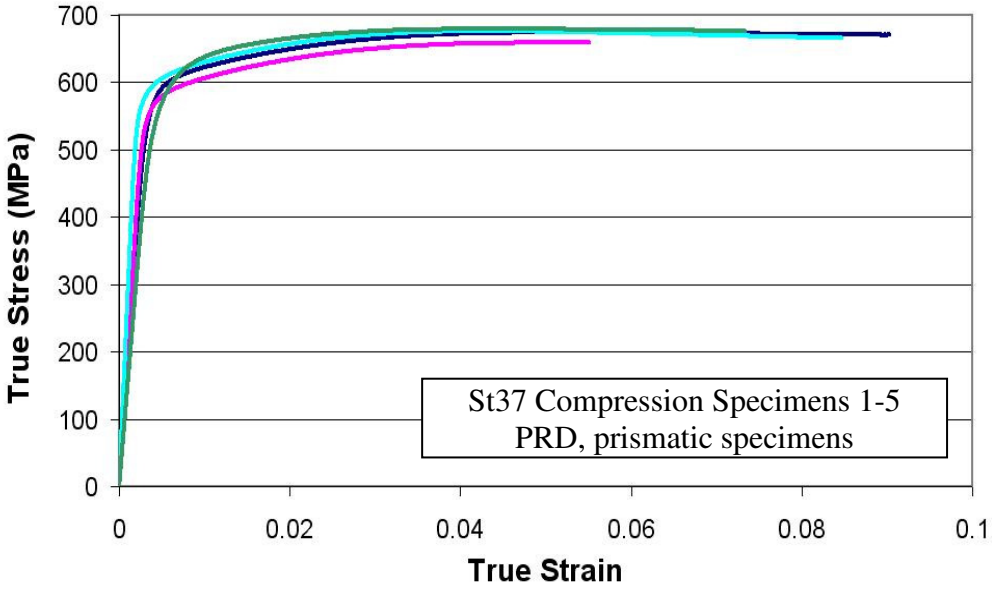

Figure 6.9 True stress-strain curves for prismatic St37 specimens in PRD

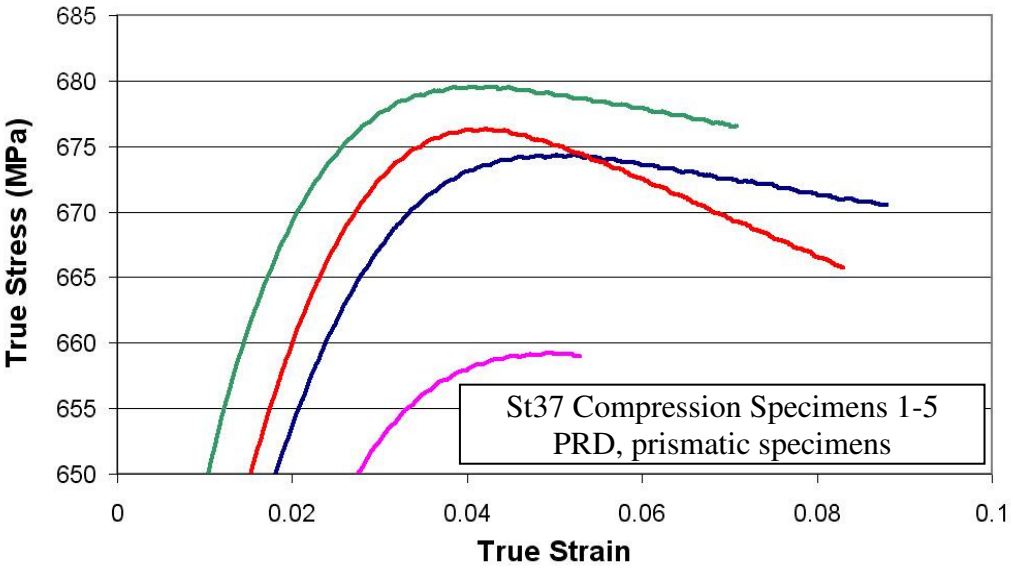

Figure 6.10 Drop of true stresses for prismatic St37 specimens in PRD

6.4 Compression Test Results for Cylindrical 100Cr6 Specimens

The need for verifying the system and the method used in the compression tests aroused after the observation of the drops in the true stresses. For this reason 100Cr6 specimens are manufactured in ORS Bearing Company. ORS also supplied flow data for the material.

6.4.1 Engineering Stress-Strain Curves for Cylindrical 100Cr6 Specimens

In the evaluation of the data, the same sequence is followed. First the force-displacement curves are corrected with the extrapolation method (Figure 6.11). Then the engineering stress-strain curves are plotted and the elastic moduli (E) are computed. Again the calculated E values are small, so the displacements are corrected with the measured system stiffness k_s (Figure 6.12). It is seen that this correction also works for the 100Cr6 specimens that the E_{corr} values reached 200 GPa.

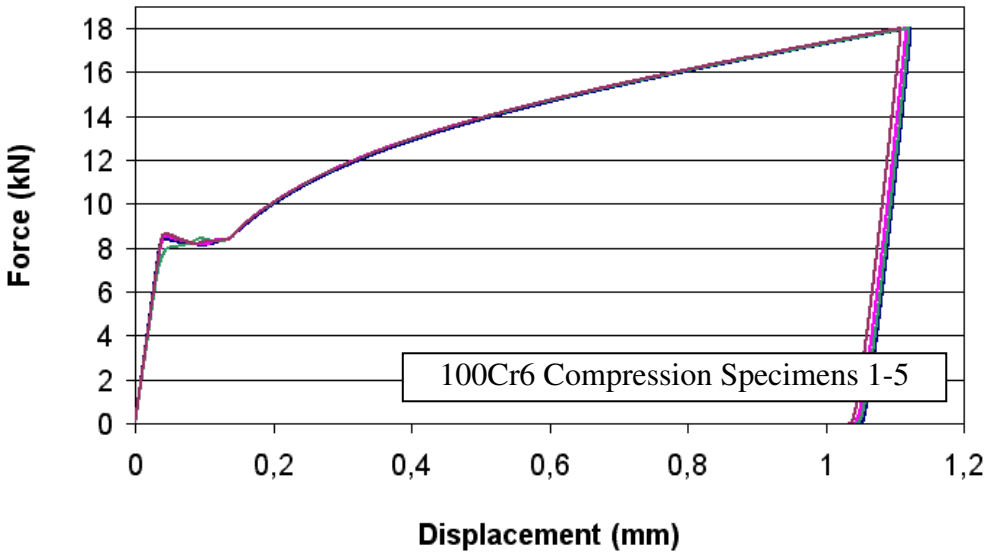

Figure 6.11 Force displacement curves, corrected by extrapolation method, for cylindrical 100Cr6 specimens

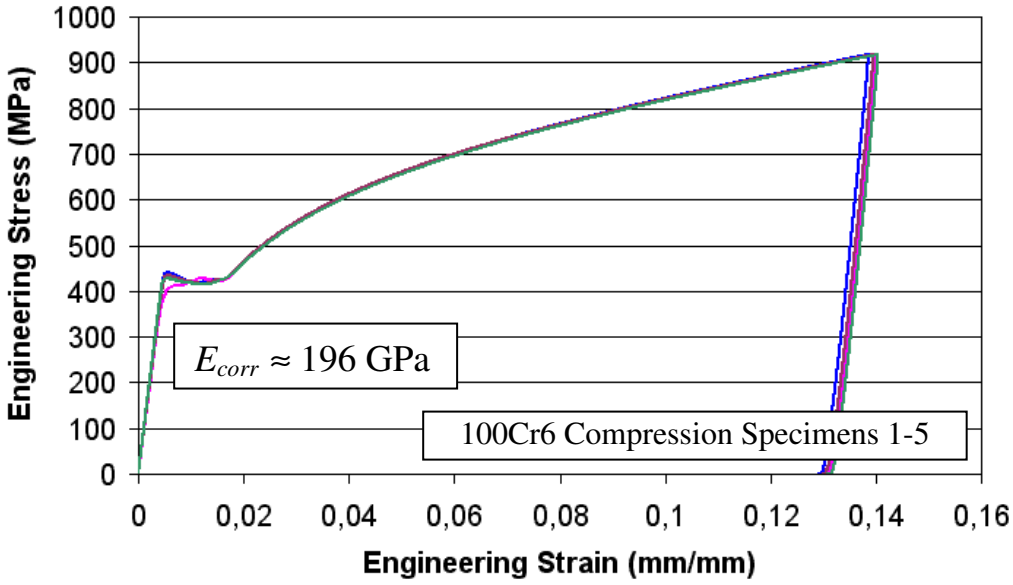

Figure 6.12 Corrected engineering stress-strain curves for 100Cr6

6.4.2 True Stress-Strain Curves for Cylindrical 100Cr6 Specimens

After the correction of the displacements, true stress-strain curves are plotted (Figure 6.13). It can be seen that there is no drop in the true stresses for cylindrical 100Cr6 specimens.

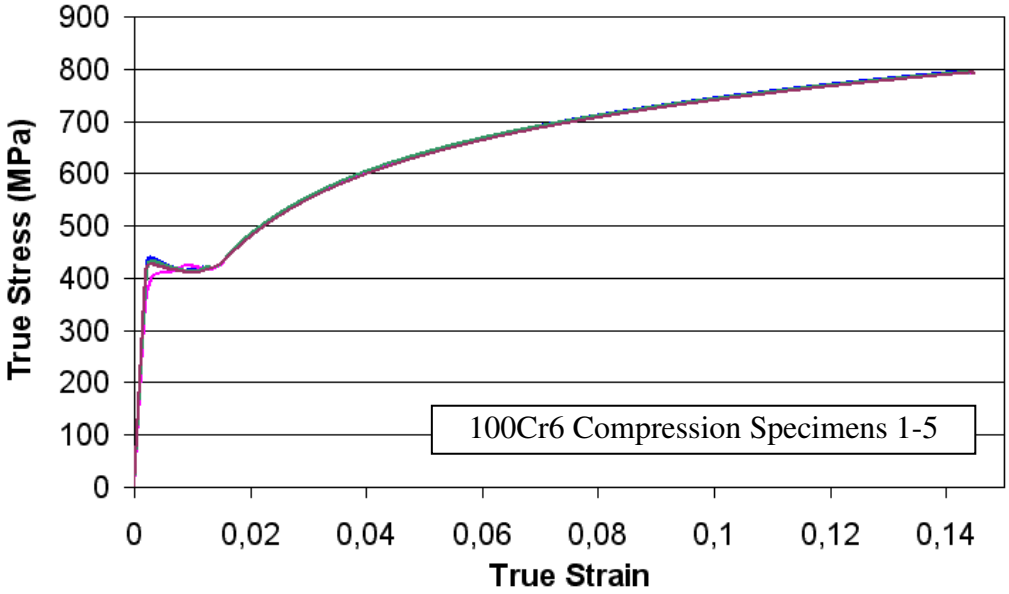

Figure 6.13 True stress-strain curves of 100Cr6 specimens

Finally, the elastic strains are subtracted from the total true strains to obtain the plastic strains by using Eq. (2.19), Figure 6.14.

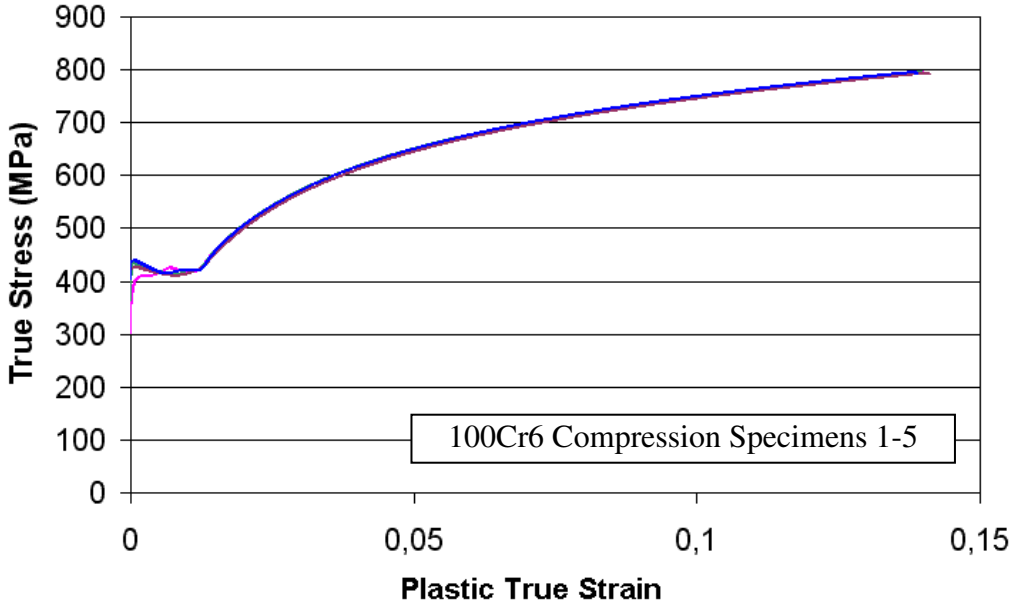

Figure 6.14 Flow curves of 100Cr6 specimens

6.4.3 Comparison of Flow Curves

Lastly, these flow curves are compared with the ones in the literature (Figure 6.15). In the literature, four flow curves are found for 100Cr6. Two of them are from the Flow Curves Atlas [46] and the other two are the results of experiments made for the thesis study of Koçak [47]. ORS company verifies that these flow curves fits the specimens they have produced.

When Figure 6.15 is analyzed on a larger scale, it is seen that the flow curves obtained fit the flow curves in the literature (Figure 6.16). Moreover, the initial yield stress found by Koçak is 443 MPa, which is very close to the one found (~426 MPa).

From these results, it can be said that there is no problem with the setup as it can successfully determine the flow curves of the cylindrical 100Cr6 specimens.

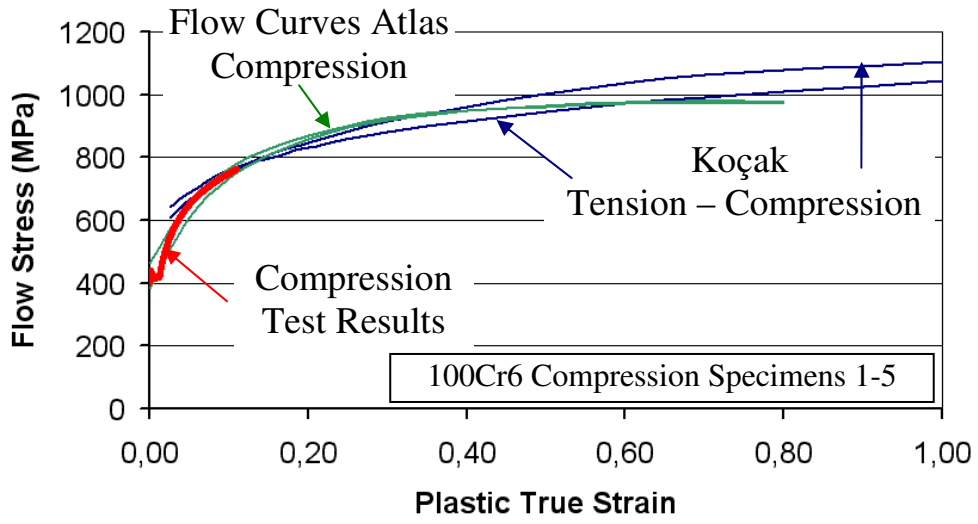

Figure 6.15 Comparison of flow curves of 100Cr6 with the ones in the literature

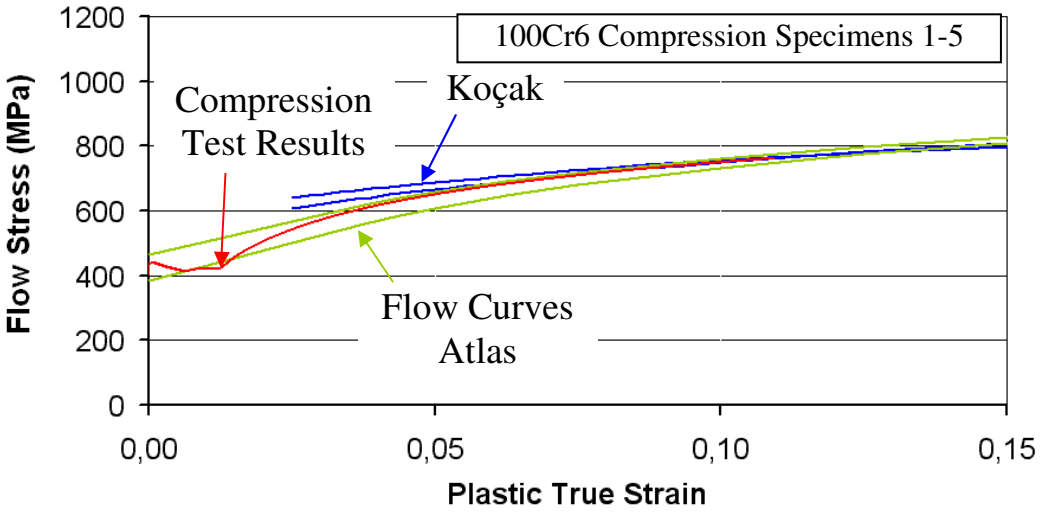

Figure 6.16 Comparison of flow curves of 100Cr6 with the ones in the literature (larger scale)

6.5 Compression Test Results for the Cylindrical St37 Specimens

As it is seen that there is no problem with the experimental setup, it is decided to make compression tests on cylindrical St37 specimens. These specimens are manufactured in lathes by turning the St37 strips.

After correcting the curves by extrapolation method, the engineering stresses and strains are computed. It is seen that the elastic moduli (E) of the curves are extremely small that they can only be corrected by a stiffness coefficient k_s = 110 kN/mm.

This is most probably because of the smaller dimensions of the specimens. During the turning operation of the steel strips in the machine shop, diameters of the specimens are made smaller than the desired ones. Because of the smaller contact area, the stresses are higher. Therefore, the specimens are probably indenting the base anvil and the punch, so that the measured deformation is wrong. However, this error is corrected by using a modified system stiffness coefficient, k_s = 110 kN/mm.

When the flow curves are plotted, it is seen that there is no drop in the stresses for these cylindrical specimens (Figure 6.17). Also, the flow stresses are significantly different than the ones obtained from tests with prismatic specimens (Figure 6.18). The flow stresses obtained from prismatic specimens are lower than the round specimens. This must be because of the imperfect contact conditions of the prismatic specimens and therefore buckling of the specimens.

6.6 Compression Test Results for the Cylindrical St37 Specimens in the Other Orthogonal Directions

As the results are successful for the cylindrical St37 specimens, compression tests are also conducted on specimens in the other orthogonal directions. Cylindrical specimens are produced only in two orthogonal directions by turning the steel strips (RD and TRD). It is not possible to produce cylindrical compression specimens in the thickness direction as no steel strip in that direction is available.

In Figure 6.19 the results of compression tests in the TRD can be seen. There is also no drop in the stresses for this direction.

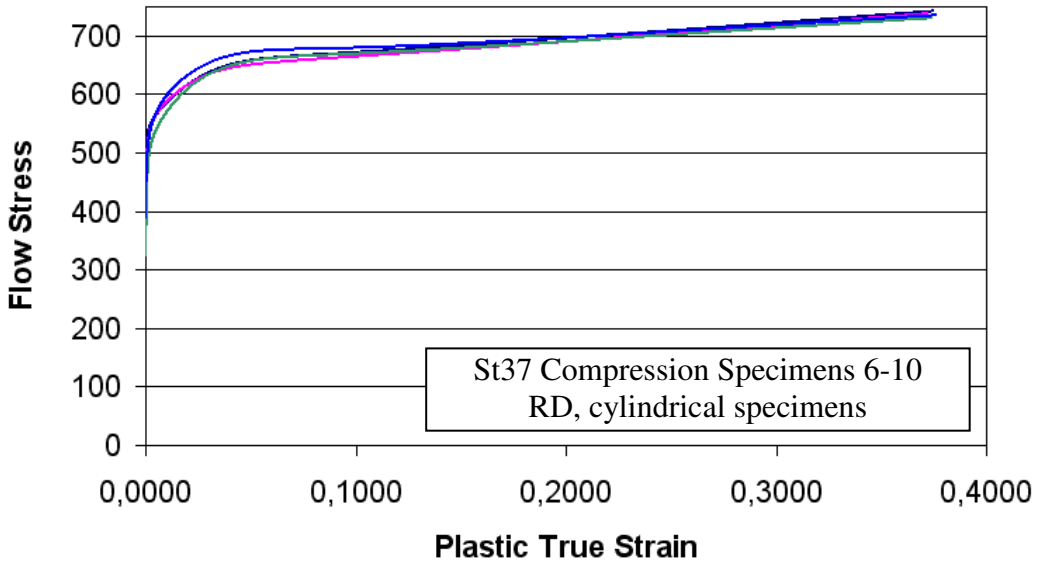

Figure 6.17 Flow curves obtained from compression tests of cylindrical St37 specimens in RD

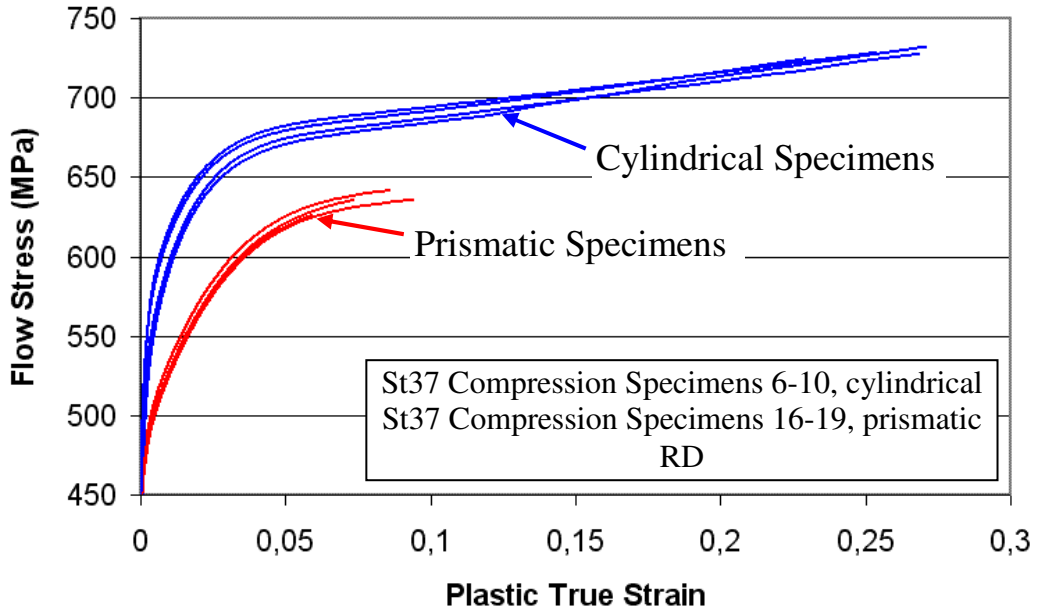

Figure 6.18 Comparison of the flow curves obtained from compression tests of cylindrical and prismatic St37 specimens in RD

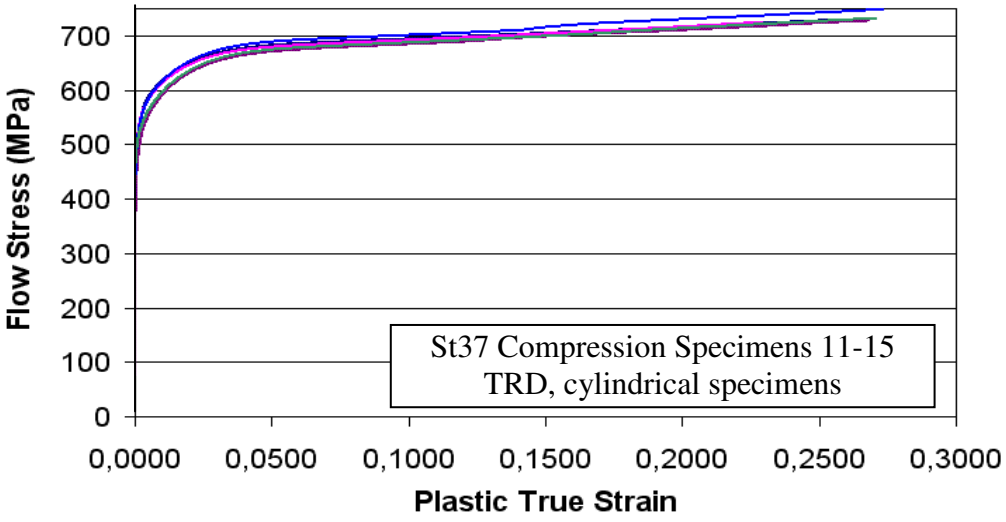

Figure 6.19 Flow curves obtained from compression tests of cylindrical St37 specimens in TRD

6.7 Comparison of the Flow Curves of St37 in RD and TRD Directions

The flow curves in the two orthogonal directions are compared in Figure 6.20. There is a clear difference but it very small. Figure 6.21 shows the flow curves on a larger stress scale.

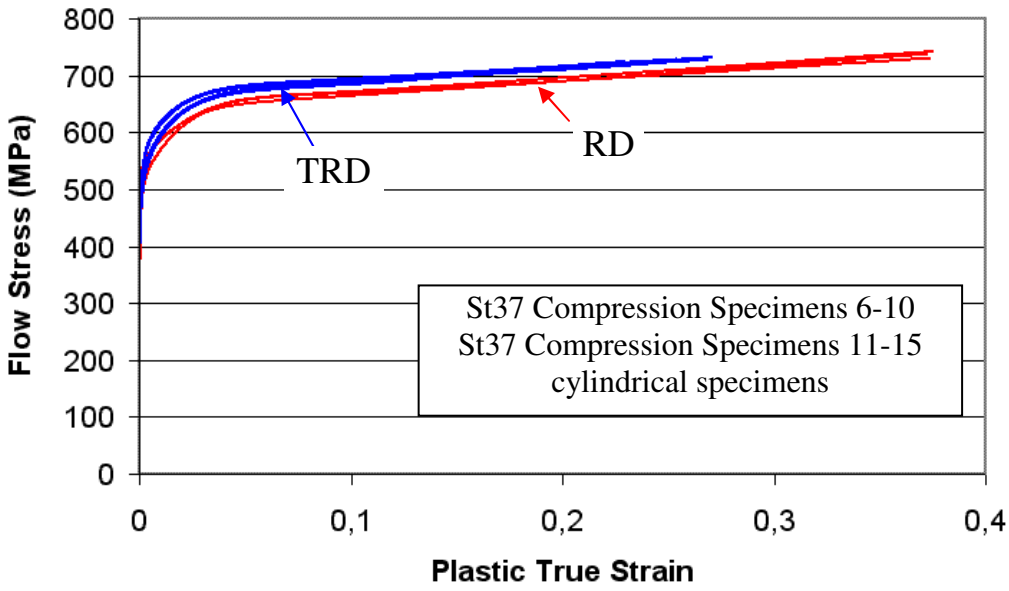

Figure 6.20 Comparison of the flow curves in RD and TRD

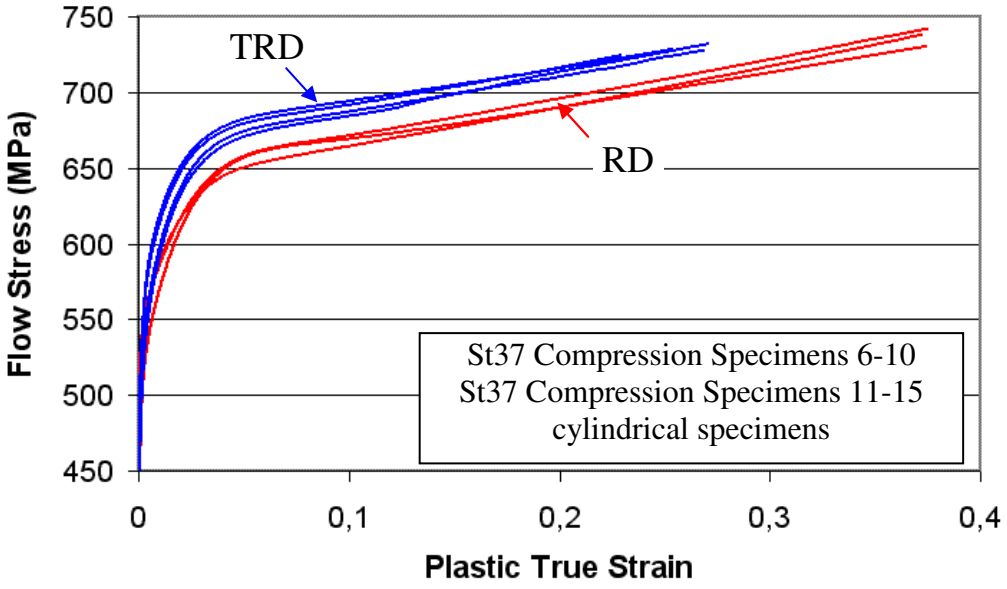

Figure 6.21 Comparison of the flow curves in RD and TRD (larger scale)

When the relative difference (δ_σ) between the flow curves of St37 are calculated and plotted against the plastic true strain values, it can be seen that the difference is very small (~3%), (Figure 6.22). This complies with the small difference (<5%) observed in the force-displacement diagrams obtained from the indentation tests (Figure 5.31). It can be said that the anisotropy in the St37 used in the experiments is very small.

$$\delta_\sigma = \frac{\sigma_{TRD} - \sigma_{RD}}{\sigma_{TRD}} \tag{6.4}$$

In Figure 6.20, it is seen that the flow stresses in TRD are higher than the stresses in RD. However, this can not be seen in the indentation results of St37 (Figure 5.30). This is most probably because of the high span seen in the results of indentations in TRD (Figure 5.28). It can be concluded that identification of anisotropy by indentation testing is not suitable for materials with low anisotropy.

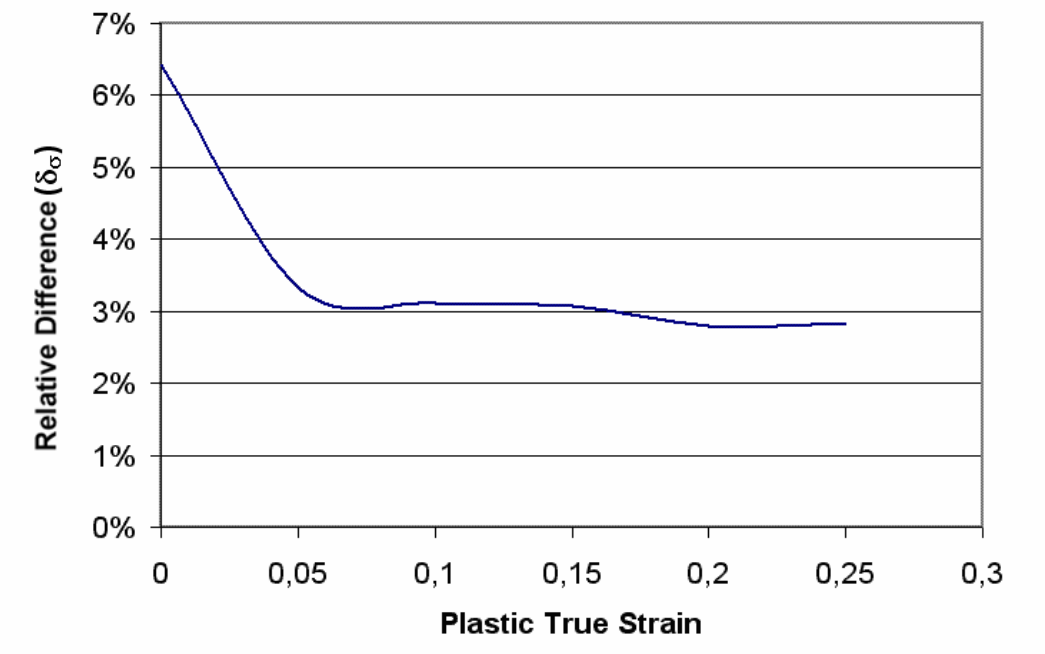

Figure 6.22 Percentage difference between the St37 flow curves in RD and TRD

CHAPTER 7

DISCUSSION AND CONCLUSION

The study aimed to analyze indentation testing whose results will be used for determination of anisotropic parameters by inverse analysis methods. As indentation force-displacement curves are going to be used by the inverse analysis procedure, the factors that influence the curves are investigated. In Chapter 4, finite element analyses of the specimen and indenter parameters are presented. In Chapter 5, the experimental factors and their influence on the results especially the repeatability of the results are determined. Then the results of indentations in different directions are shown. Following this, flow curves of the specimens are obtained by compression tests in Chapter 6.

To have reasonable amount of indentation and also suitable plastic strains indenter radius (R) is selected as 2 mm in Chapter 4. Two dimensional finite element simulations showed that friction has ignorable influence on the force-displacement curves.

By three-dimensional finite element analysis in Chapter 4, it is shown that plane-strain conditions can only be achieved by embedded indentations. Moreover specimen dimensions especially the specimen width (w) has crucial influence on

the force displacement curves. A correction factor (Eq. 4.2) is developed to correct the saturation force displacement curves to plane-strain force displacement curves.

Ideal specimen dimensions are found such that indentations in three orthogonal directions would be possible and for each indentation specimen dimensions would yield force displacement curves in saturation zones (Figure 4.23).

In Chapter 5, firstly the basics of the testing method are analyzed. Adjusting of the experimental setup is very important since by this way parallelity between the indenter and the specimen is achieved. Parallelity problems decrease the repeatability of the results. Also the orientation of the specimen after clamping should be consistent with the orthogonal directions as the force-displacement curves change by the angle to the rolling direction. Moreover, it is seen that clamping of the specimens increased the repeatability of the results significantly. Seeing the high repeatabilities of the clamped specimens, it is decided use the raw force-displacement data without making any modifications on them.

Indentation experiments are conducted on specimens with different surface qualities showed that by using ground specimens higher repeatabilities are achieved when compared to raw and milled specimens (Figure 5.20). Main reason of the spread of the results is the thickness difference, Δt (Figure 5.22). Raw and milled specimens with low Δt values supplied identical curves with the ground specimens (Figures 5.23 and 5.25).

There is no significant difference between the force-displacement curves obtained from indentations on St37 specimens in three orthogonal directions (Figures 5.29 and 5.30). However, the flow curves obtained from compression tests of the St37 specimens in rolling and transverse to rolling directions shows that actually material is not highly anisotropic (Figures 6.19 and 6.21).

Moreover indentations on Al5086 specimens yielded significant difference between the RD and TRD (Figures 5.34 and 5.35). Before indentations tensile testing is applied to this material and the anisotropy coefficient (r) – angle to rolling direction

curves are drawn (Figure 5.7). Those curves show that material is anisotropic which is consistent with the results of the indentation tests.

During the compression tests in Chapter 6, stiffness of the system is also measured. This stiffness value is used to correct the displacement measurements made in the compression tests. Also the force-displacement curves obtained from indentation tests must be corrected with this stiffness factor.

As a conclusion, this study is successful to show different parameters like friction, surface quality, clamping of the specimen, specimen dimensions, indenter geometry, contact detection methods that affect the results of indentation tests. It is seen that if the amount of anisotropy is not high in a material, this testing technique is not capable of detecting it. However, for materials with high anisotropy like sheet metals, it is an adequate technique to determine the anisotropic coefficients.

With the experience gained in this study, accurate indentation tests on anisotropic metals would be possible. Also the finite element simulation results about the affect of specimen dimensions on the force-displacement curves will help the indentation testers in the future.

The author believes that, by the help of this study, this testing method can be improved to be a standard testing method for anisotropic metals.

CHAPTER 8

FURTHER RECOMMENDATIONS

In this last chapter, further recommendations are given.

Sheet metal indentations made in this thesis aim to verify the experimental setup and the method as the inverse analysis program is only capable of identification of material parameters through three force-displacement curves obtained from indentations in three orthogonal directions. However, it is seen that metal plates usually do not have high anisotropy as the sheet ones. Moreover, the need for anisotropy parameters in the industry is mainly concentrated on the sheet metals. Therefore, indentations on sheet metals should be analyzed by finite element methods more deeply. Also the inverse analysis program should be modified so that two indentations would be enough for parameter identification of sheets.

Correction factor found in Section 4.5.2 can be improved for other indenter geometries and other materials. By this way the parameters of the correction factor might get physical explanations.

Indenter can also be analyzed by finite element simulations. As it is composed of three sections and the contact behaviour of these sections are not known, it would be useful to investigate the elastic response of the indenter during the tests. This can

not be done by indenting the specimen on the base anvil without any specimen, which is done in system stiffness analysis made in Section 6.3.1, as the base anvil will be damaged. Displacements measured would be further corrected by the results of this analysis.

Total system can be modelled including the base anvil and the lower support. Indentation simulations on the specimens placed on this deformable die setup can be compared with the indentations on the specimens placed on the rigid die.

Compression test simulations might be made with anisotropic material models to analyze the difference between the cylindrical specimens and the prismatic specimens. Moreover, friction behaviour on the circular and square contact surfaces should be analyzed in detail to clarify the drop in flow stresses in square prismatic compression test specimens.

REFERENCES

1 Banabic D., Bunge H.J., Pöhlandt K., Tekkaya A. E.: Formability of metallic materials: plastic anisotropy, formability testing, forming limits, Springer, Berlin, 123-124, (2000).

2 Tresca H.: On the yield of solids at high pressures (in French), Comptes Rendus Academie des Sciences, Paris 59, 754, (1864).

3 Mises R.: Mechanics of solids in plastic state 592 (in German), Göttinger Nachrichten Math. Phys. Klasse 1, 582, (1913).

4 Lange K.: Handbook of metal forming, Society of Manufacturing Engineers, 3.23, (1985).

5 ASTM E 517-98: Standard test method for plastic strain ratio r for sheet metal.

6 Hill R.: A theory of the yielding and the plastic flow of anisotropic metals, Proceedings of Royal Society of London A 193, 281-297, (1948).

7 Hill R.: Theoratical plasticity of textured aggregates, Mathematical Proceedings Cambridge Philosophical Society 85, 179-191, (1979).

8 Hill R.: Constitutive modeling of orthotropic plasticity in sheet metals J. Mech. Phys. Solids 38, 405–417, (1990).

9 Hill R.: A user-friendly theory of orthotropic plasticity in sheet metals Int. J. Mech. Sci. 15, 19–25, (1993).

10 Hosford W F.: A generalized isotropic yield criterion J. Appl. Mech. 39, 607–609, (1972)

11 Barlat F., Richmond O.: Prediction of tricomponent plane stress yield surfaces and associated flow and failure behaviour of strongly textured F.C.C. polycrystalline sheets, Mater. Sci. Eng. 91, 15–29, (1987)

12 Barlat F., Lian J.: Plastic behaviour and stretchability of sheet metals. Part I: A yield function for orthotropic sheets under plane stress condition, Int. J. Plasticity 5, 51–66, (1989)

13 Barlat F., Lege D. J., Brem J. C.: A six-component yield function for anisotropic materials, Int. J. Plasticity 7, 693–712, (1991)

14 Karafillis A. P., Boyce M. C.: A general anisotropic yield criterion using bounds and a transformation weighting tensor, J. Mech. Phys. Solids 41, 1859–86, (1993).

15 Banabic D., Bunge H.J., Pöhlandt K., Tekkaya A. E.: Formability of Metallic Materials, Berlin, Springer, (2000).

16 Banabic D., Comsa S. D., Balan T.: A new yield criterion for anisotropic sheet metals under plane stress conditions, Proc. Cold Metal Forming 2000 Conf. (Cluj Napoca), 217–224, (2000)

17 Paraianu L., Comsa D. S., Cosovici G., Jurco P., Banabic D.: An improvement of the BBC2000 yield criterion Proc. ESAFORM 2003 Conf., (2003)

18 Banabic D., Kuwabara T., Balan T., Comsa D. S., Julean D.: Non-quadratic yield criterion for orthotropic sheet metals under plane-stress conditions, Int. J. Mech. Sci. 45, 797–811, (2003)

19 Banabic D., Aretz H., Comsa D. S., Paraianu L.: An improved analytical description of orthotropy in metallic sheets, Int. J. Plasticity, (2003)

20 Barlat F., Brem J. C., Yoon J. W., Chung K., Dick R. E., Choi S. H., Pourboghrat F., Chu E., Lege D. J.: Plane stress yield function for aluminium alloy sheets - Part 1: Theory, Int. J. Plasticity 19, 1297–1319, (2003).

21 Bassani J. L.: Yield characterisation of metals with transversally isotropic plastic properties, Int. J. Mech. Sci., 19, 651–4, (1977).

22 Gotoh M.: A theory of plastic anisotropy based on a yield function of fourth order, Int. J. Mech. Sci. 19, 505–20, (1977).

23 Budiansky B.: Anisotropic plasticity of plane-isotropic sheets, Mechanics of Material Behaviour, Elsevier, Amsterdam, 15–29, (1984).

24 Cazacu O., Barlat F.: Generalization of Drucker's yield criterion to orthotropy, Math. Mech. Solids 6, 613–630, (2001).

25 Banabic D., Pöhlandt K.: Yield criteria for the anisotropic sheet metal, UTF Science 4, 19 - 27, (2001).

26 Tabor D.: A Simple Theory of Static and Dynamic Hardness, Proc. Roy. Society Series A, 192, pp. 247-274, (1948).

27 Tabor D.: The Hardness of Metals, Clarendon Press, Oxford Claredon Press, New York, (1951).

28 Tekkaya A. E.: Hardness Measurements on Cold-Formed Workpieces, Advanced Technology of Plasticity, Vol.II, Proceedings of the 6th ICTP, (1999).

29 Tekkaya A. E.: An Improved Relationship between Vickers Hardness and Yield Stress for Cold Formed Materials and its Experimental Verifications, Annals of the CIRP, Vol.49, (2000).

30 Tekkaya A. E.: Improved relationship between Vickers hardness and yield strength for cold formed materials, Steel Research, 72, 8, 304 – 310, (2001).

31 Chang Y., Yang J.-C.: Mechanical properties of the polypropylene copolymer measured by the impression method, Journal of Polymer Science: Part B: Polymer Physics 34, 2193 – 2200, (1996).

32 Taljat B., Zacharia T., Kosel F.: New analytical procedure to determine stress-strain curve from spherical indentation data, Int. Journal of Solids Structures 35, 4411-4426, (1996).

33 Riccardi B., Montanari R., Moreschi L.F., Sili A., Storai S.: Mechanical characterization of fusion materials by indentation test, Fusion Engineering and Design, 58-59, 755 – 759, (2001).

34 Scibetta M., Lucon E., Chaoudi R., van Walle E.: Instrumented hardness testing using flat punch, Int. Journal of Pressure Vessels and Piping 80, 345 – 349, (2003).

35 Fischer-Cripps A. C.: Nanoindentation, NJ, Springer-Verlag New York, (2002).

36 Yang F.: Thickness effect on the indentation of an elastic layer, Materials Science and Engineering A358, 226 – 232, (2003).

37 Fischer-Cripps A. C.: Analysis of instrumented indentation test data for functionally graded materials, Surface and Coatings Technology 168, 136-141, (2003).

38 Callister W.D. Jr.: Materials Science and Engineering: An Introduction, NY, John Wiley & Sons, (2000).

39 Ghouati O., Gelin J. C.: Identification of material parameters directly from metal forming processes, Journal of Materials Processing Technology 80-81, 560-564, (1998).

40 Khalfallah A., Bel Hadj Salah H., Dogui A.: Anisotropic parameter identification using inhomogeneous tensile test, European Journal of Mechanics A/Solids 21, 927-942, (2002).

41 Sasaki T., Sasaki T., Yang M., Fukushima S., Tsukano R.: Development of the CAE-assisted nano-indentation method for the evaluation of the anisotropic mechanical-properties of thin films, Journal of Materials Processing Technology 151, 263-267, (2004).

42 Topcu N.: Numerical, Analytical and Experimental Analysis of Indentation, METU, Ankara, (to appear soon).

43 Automation Creations : Aluminum 5086-H116; 5086-H32, http://www.matweb.com/search/SpecificMaterial.asp?bassnum=MA5086H116, (14.02.2005).

44 Automation Creations : Aluminum 2014-T4; 2014-T451, http://www.matweb.com/search/SpecificMaterial.asp?basnum=MA2014T4, (14.02.2005).

45 Yan Yan W.Y., Shan G.X., Kolednik O., Fischer F.D.: A numerical simulation of the crack growth in a smooth CT specimen, Key Engineering Materials 145-149, 179-184, (1998).

46 Doege E., Meyer-Noelkemper H., Saeed I.: Fließkurvenatlas metallischer Werkstoffe, Hanser Fachbuch, München, (1986).

47 Koçak Ö.: Analysis of the Formability of Metals, METU, Ankara, (2003).

APPENDIX A

DIMENSIONS OF THE SPECIMENS

Table A.1 Dimensions of the St37 indentation test specimens

	orientation	***w*** **(mm)**	***t*** **(mm)**	***l*** **(mm)**
St37_1_2	RD	20,52	18,09	45,00
St37_1_3	RD	20,66	18,04	45,04
St37_1_4	RD	20,80	18,04	45,02
St37_1_5	RD	20,54	18,03	45,10
St37_1_6	RD	20,48	18,05	45,12
St37_1_11	RD	20,52	18,04	45,02
St37_1_12	RD	20,32	18,04	45,02
St37_1_13	RD	20,58	18,04	45,02
St37_1_14	RD	20,54	18,04	45,00
St37_1_15	RD	20,50	18,04	45,08
St37_1_21	RD	20,36	19,95	45,08
St37_1_22	RD	20,48	19,97	45,04
St37_1_23	RD	20,48	19,98	45,06
St37_1_24	RD	20,46	19,96	45,18
St37_1_25	RD	20,46	19,98	45,12
St37_1_31	RD	20,50	18,04	45,08
St37_1_32	RD	20,52	18,05	45,02
St37_1_33	RD	20,58	18,03	45,06
St37_1_34	RD	20,54	18,04	45,04
St37_1_35	RD	20,53	18,06	45,03
St37_3_36	PRD	19,97	17,55	45,48
St37_3_37	PRD	19,97	17,56	45,06
St37_3_38	PRD	19,96	17,58	44,98
St37_3_39	PRD	19,96	17,56	45,42

Table A.1 Dimensions of the St37 indentation test specimens (Continued)

	orientation	***w*** **(mm)**	***t*** **(mm)**	***l*** **(mm)**
St37_3_40	PRD	19,94	17,56	45,44
St37_2_46	TRD	19,99	17,57	45,24
St37_2_47	TRD	20,03	17,56	45,20
St37_2_48	TRD	20,01	17,53	45,06
St37_2_49	TRD	20,07	17,53	45,42
St37_2_50	TRD	19,97	17,55	45,54
St37_1_59	RD	17,11	17,58	45,04
St37_1_60	RD	17,05	17,58	45,16
St37_1_61	RD	16,98	17,58	45,08
St37_1_62	RD	12,06	17,55	45,04
St37_1_63	RD	11,93	17,58	45,08
St37_1_64	RD	12,11	17,56	45,08
St37_1_65	RD	20,71	8,05	45,08
St37_1_66	RD	20,71	8,07	45,00
St37_1_67	RD	21,05	8,06	45,06
St37_1_68	RD	20,94	11,96	45,18
St37_1_69	RD	20,75	11,96	45,14
St37_1_70	RD	20,89	11,99	45,14

Table A.2 Dimensions of the Al5086 indentation test specimens

	orientation	***w*** **(mm)**	***t*** **(mm)**	***l*** **(mm)**
Al5086_1_1	RD	20,50	3,20	45,50
Al5086_1_2	RD	20,15	3,22	45,10
Al5086_1_3	RD	19,75	3,22	46,00
Al5086_1_4	RD	20,48	3,21	45,26
Al5086_1_5	RD	19,76	3,23	46,20
Al5086_2_6	TRD	19,61	3,22	45,40
Al5086_2_7	TRD	20,10	3,20	45,20
Al5086_2_8	TRD	20,10	3,24	46,00
Al5086_2_9	TRD	20,12	3,24	46,00
Al5086_2_10	TRD	20,25	3,24	45,88

Table A.3 Dimensions of the Al2014 indentation test specimens

	Orientation	***w***	***t***	***l***
Al2014_1_12	RD	18,98	15,92	45
Al2014_1_13	RD	19,42	15,78	45,26
Al2014_1_14	RD	19,12	15,92	45,18
Al2014_1_15	RD	19,22	15,9	45,18
Al2014_1_16	RD	19,06	15,9	44,74

Table A.4 Dimensions of the St37 compression test specimens

No	**Orientation**	**Geometry**	***a1* (mm)**	***a2* (mm)**	***d* (mm)**	***h* (mm)**
1	PRD	Prismatic	5,01	5,13	-	8,06
2	PRD	Prismatic	4,99	4,96	-	8,08
3	PRD	Prismatic	5,00	4,97	-	8,02
4	PRD	Prismatic	5,02	5,15	-	8,09
5	PRD	Prismatic	4,96	4,95	-	8,04
6	RD	Cylindrical	-	-	4,64	4,83
7	RD	Cylindrical	-	-	4,62	4,96
9	RD	Cylindrical	-	-	4,60	4,90
10	RD	Cylindrical	-	-	4,62	4,80
11	TRD	Cylindrical	-	-	4,86	4,96
12	TRD	Cylindrical	-	-	4,90	5,16
13	TRD	Cylindrical	-	-	4,90	5,12
14	TRD	Cylindrical	-	-	4,82	4,82
15	TRD	Cylindrical	-	-	4,82	5,10
16	RD	Prismatic	5,00	5,12	-	8,14
17	RD	Prismatic	5,00	5,14	-	8,04
18	RD	Prismatic	5,00	5,10	-	8,10
19	RD	Prismatic	5,00	5,08	-	8,14

Table A.5 Dimensions of the 100Cr6 compression test specimens

No	**d**	**h**
1	5,00	8,00
2	5,00	8,00
3	5,00	8,00
4	5,00	8,00
5	5,00	8,00